UNIVERSITÀ
DEGLI STUDI
DI PADOVA

Sede Amministrativa: Università degli Studi di Padova

Dipartimento di Costruzioni e trasporti
Centro di Meccanica dei Materiali Biologici

SCUOLA DI DOTTORATO DI RICERCA IN INGEGNERIA INDUSTRIALE
INDIRIZZO DI INGEGNERIA DELLA PRODUZIONE INDUSTRIALE
CICLO: XXIV

INVESTIGATION OF BIOMECHANICAL BEHAVIOUR OF FOOT CARTILAGINOUS TISSUES

Direttore della Scuola: Ch.mo Prof. Paolo Bariani
Coordinatore d'indirizzo: Ch.mo Prof. Enrico Savio
Supervisore: Ch.mo Prof. Arturo N. Natali

Dottorando: Chiara Venturato

ABSTRACT

The foot is one of the most important and complex structure of the human body. It allows a lot of movements and it is fundamental in many human activities, such as walking. The investigation of human articular cartilage biomechanical behavior is a complex problem that requires the analysis of different related aspects. In particular it is important to investigate the histological conformation of cartilaginous tissue coupled with a morphometric study of cartilage layers in the specific anatomic site of interest, such as the foot and in particular the hindfoot. Both histological and morphometric aspects should be considered with regard to the role of cartilage in the mobility of the ankle. Considering the histological characteristics observed and mechanical tests results present in literature a fiber-reinforced hyperelastic constitutive model is developed and a set of constitutive parameters is defined through *in-vitro* indentation test. A solid model of foot skeletal system is developed and in particular a detailed solid model of hindfoot joints is defined. Each joint complex is considered as a double layer structure of cartilaginous tissue enveloped in a synovial capsule. The whole structure is studied in particular physiological configuration: standing and dorsiflexion. Numerical results on tibio-talar joint for standing configuration joint are compared with *in-vivo* test on the same articular surface. The procedure developed is the base for the investigation of degraded cartilage due to osteoarthritic (OA) pathology. In particular a specific OA set of constitutive parameters is defined for the fiber-reinforced hyperelastic model considering *in-vitro* indentation experimental tests on OA cartilage. Numerical results of OA cartilage are compared with those of healthy cartilage, previously obtained for standing position.

SOMMARIO

Il piede è una delle strutture più importanti e complesse del corpo umano. Il piede permette numerosi movimenti ed è fondamentale in molte attività dell'uomo, come ad esempio la camminata. Lo studio del comportamento biomeccanico delle cartilagini articolari umane è un problema complesso che richiede lo studio di diversi aspetti tra loro correlati. In particolare è importante inizialmente un approfondito studio dell'istologia del tessuto cartilagineo associato allo studio della morfometria degli strati cartilaginei nel sito anatomico d'interesse, come ad esempio il piede ed in particolare la parte posteriore del piede. Sia l'aspetto istologico che quello morfometrico devono essere esaminati alla luce del ruolo della cartilagine nella mobilità della caviglia. Considerando le caratteristiche istologiche e i risultati di test biomeccanici presenti in letteratura è stato sviluppato un modello iperelastico fibro-rinforzato ed i parametri costitutivi sono stati definiti per mezzo di prove sperimentali di indentazione *in-vitro*. Un modello solido del sistema scheletrico del piede è stato sviluppato, con particolare attenzione per la definizione delle articolazioni del retro piede costituite da due strati di cartilagine avvolti in una capsula sinoviale. La struttura completa è stata studiata in due configurazioni fisiologiche: stazione eretta e dorsiflessione. I risultati numerici per la condizione di stazione eretta del giunto tibio-talare sono confrontati con test *in-vivo* presenti in letteratura sulla stessa superficie articolare. La procedura sviluppata è quindi alla base dello studio della cartilagine degenerata in conseguenza ad osteoartrite (OA). In particolare è stato definito un set di parametri costitutivi per il modello iperelastico fibro-rinforzato prendendo in considerazione prove sperimentali *in-vitro* di indentazione su cartilagine con OA. I risultati numerici del caso con OA sono stati confrontati con quelli ottenuti in stazione eretta per la cartilagine sana.

Ballare è la poesia dei piedi.

John Dryden

I vecchi amici sono i migliori.
Re Giacomo era solito chiedere le sue scarpe vecchie:
erano le più comode per i suoi piedi.

John Selden

INDEX

INTRODUCTION

The investigation of articular cartilage tissue is extremely important in consideration of the biomechanical functions that it performs: redistribution of stresses due to loads acting on the joint and the recreation of a near-frictionless interface between contacting bone ends. Considering the foot it is possible to find 28 bones involved in a high number of articulation, each one extremely important in the complex mobility of the foot. The most important load bearing joints are placed in the hindfoot, tibio-talar joint and sub-talar joint. Although these joints are extremely important in human motion they are and has been poorly studied in literature both experimentally and computationally to investigate cartilage biomechanics and cartilaginous tissue role. In the first chapter a morphometric and kinematic analysis is given for the whole foot, to underline its structural complexity, in particular for foot joints, and its fundamental role in human activity, such as walking. Further, a histological and morphometric analysis is developed for bones and cartilage, since cartilage is the main cushioning element between two bones in the transmission of loads during gate cycle. At first, attention is paid to the histological aspect that characterizes this specialized connective tissue from other connective tissue. This analysis lead to the definition of some important components that should be take into account when developing a constitutive model for cartilaginous tissue. In particular, the presence of an organized net of collagen fibers necessary to entrap proteoglycans those have the important function to link with water molecules. This complex microstructure is necessary to keep the right hydratation in cartilage layers, to sustain load in compression and redistribute loads. Moreover the biomechanical behavior of cartilage tissue is analyzed considering results from literature of indentation tests, confined and unconfined compression tests. Histological and biomechanical considerations lead to the definition of a fiber-reinforced hyperelastic model. To characterize the constitutive model with an appropriate set of constitutive parameters are considered experimental indentation tests in-vitro on cartilage disks with subchondral bone. A numerical model of the cartilage disk is developed to define a set of parameters that best fit the experimental results with a minimization procedure that consists in a fit between experimental data and numerical data.

For the definition of a solid model of the foot and in particular of the hindfoot high attention is paid on morphometrical aspects. For what concern bones it is fundamental to define a correct relative position between the bones involved in the articulation of interest. Whether for cartilage it is important to define a mean physiological thickness for a healthy adult and the area involved in the articulation. With appropriate software of image analysis, DICOM images are used to develop the solid model of the foot skeletal structure of a healthy adult. From DICOM images it is not possible to define a solid model of cartilage layers, so the articular interface is recreated with software of solid modeling. Differently from what is present in literature, cartilage is considered here as a double layer structure, where each layer is juxtaposed to one of the articular bony surface. Moreover to allow movements between bones a synovial capsule is also present in some important joints. Therefore, referring to anatomical atlas the articular surface of each bone of the hindfoot is reconstructed with a procedure that follows locally the irregularities present on the bone and ensures a regular and physiological thickness on each cartilage layer. The synovial capsule is reconstructed as a surface that includes both outer edges of cartilage layers involved in the articulation. Once the solid model is prepared the numerical model is developed with an adequate mash to preserve solid model details, such as cartilage layers thickness, and to give detailed results in the area of interest. Herein cartilage tissue of the hindfoot solid model is characterized with the fiber-reinforced hyperelastic model. First a neutral physiological configuration is considered: standing. Numerical results of tibio-talar joint are compared with in-vivo test on human ankle cartilage present in literature, which proposes a standing configuration of the foot comparable with the numerical one. The numerical model proposed is then used to investigate other physiological configuration and in particular dorsiflexion, even if in literature there was no experimental test as a term of comparison.

The procedure developed for healthy cartilage is then the starting point for the definition of a new specific set of parameters for osteoarthritic cartilage on the fiber-reinforced hyperelastic model. The experimental tests used for the optimization procedure of the constitutive formulation are indentation tests on OA cartilage. The parameters are not all free to change in the optimization procedure, only those

connected with OA pathology and in consideration evidence from histological study in literature on OA effects on cartilage mechanical properties degradation. The set of parameters that best fit the experimental data is used to fully characterize the constitutive model in the numerical model of the foot. Finally, a comparison is presented between standing configuration with OA cartilage and healthy cartilage.

CHAPTER ONE

1 FOOT ANATOMICAL STRUCTURE AND KINEMATIC

1.1 INTRODUCTION

In this chapter a global analysis of foot anatomical structure is proposed. The study starts from the forefoot, passing through the midfoot and ending in the rear foot. A more detailed view is given for the hindfoot and in particular of the tibio-talar joint and sub-talar joint. The foot is the terminal portion of the limb which bears weight and allows locomotion. The human foot and ankle complex are strong and complex mechanical structures containing more than 26 bones, 33 joints (20 of which are actively articulated), and more than a hundred muscles, tendons, and ligaments. A brief analysis is given for all the joints present in the foot, considering their anatomy, functions and more characterizing aspects. For what concern tibio-talar and sub-talar joints a more detailed study is proposed, since these joints have an extremely important function in foot mobility and since these articulation are the main target of this work. These articulations allow movements such as inversion/eversion, flexion/extension and abduction/adduction. In the last paragraphs an analysis of the gait cycle is given to understand the movements of the foot and the reaction force generated during walking and running.

1.2 FOOT BONES AND STRUCTURE

The musculoskeletal system is made up by the skeleton, muscles and joints. The skeleton plays an important role in supporting the body, and gives a strong structure that with the help of muscles, which bones offers an insertion site, allows the body to move and stay upright. In addition, some parts of the skeleton, such as the rib cage, enclose organs that are well protected from possible injuries or damage they may suffer. In particular, the human skeleton is structured to allow extensive use of arms and legs. The first allow a wide variety of movements, the latter, however, are used to walk and to maintain both static and dynamic balance.

This work focuses on a particular anatomical region of the leg: the foot. The organization of the skeletal foot, although similar to the one of the hand, has some important conformational differences. For example, unlike the thumb, the big toe is placed on an equal footing of the other toes and metatarsal bones and it forms a structure which has a propulsive function in the foot and with the massive tarsal bones it is a powerful lever to raise the entire body weight. In addition, the foot provides a stable basis for standing, dampens the stress and adapts to uneven ground in bare foot condition and shod. The bone skeleton of the foot with its arched shape structure provides relative rigidity and the essential lever arm mechanism required to maintain balance during standing. Moreover it facilitate propulsion and the development of a mechanism which gives more stability to the motion combining the action of the lateral arch and the medial arch allowing the transmission of the force generated on the ground in the propulsive phase of gait.

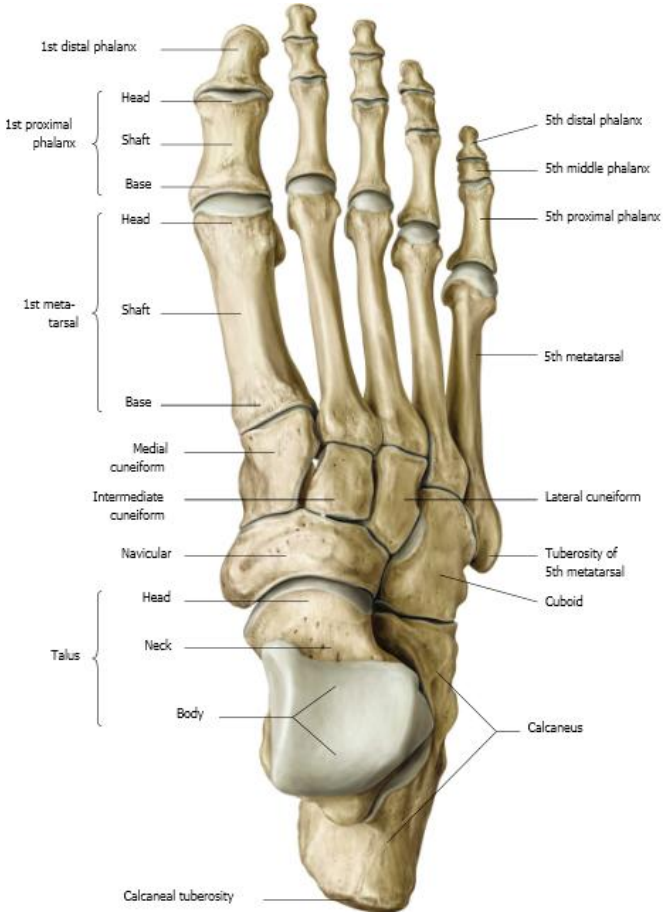

Figure 1.1: Schematic representation of foot bones, top view left foot. The different areas of the foot are defined and each bone is labeled.

In the following paragraphs the components and skeletal joints of greater importance will be analyzed in order to understand the anatomy of the foot from a functional and mechanical point of view.

The human foot skeleton includes 26 bones, which are connected in joint through cartilage layers and which are kept in a correct position during movements by a high number of muscles, tendons and ligaments.

Cartilage layers are fundamental in joints because they give flexibility and resiliency to the foot structure, whereas intrinsic and extrinsic muscles play an important role in providing support and balance to the body in standing position and stabilizing the body during gate (Abbound, 2002). Finally ligaments control movements passively and stabilize the whole bone structure. The foot can be divided into three main parts that will be described in detail in the following paragraphs.

1.2.1 Anatomy of the forefoot

In the forefoot two different areas are included: the five "metatarsal" and the fourteen "phalangeal" bones and surrounding soft tissues. The metatarsal bones are tapered distally and articulate the proximal phalanges, the bones of the toes. This part of the foot is extremely important in the last part of the gait, during the push-off phase and the toe-off phase.

A more detailed description of the bones present in the forefoot will be given in the following part of this paragraph.

1.2.1.1 The metatarsal bones

The metatarsal is a small complex of five long bones, placed between the number of distal tarsal bones and proximal phalanges of the series. Each metatarsal bone is formed by a body and two extremities. The body is shaped as a triangular prism, with the base on the back and describes a concave curved bottom. The proximal ends (or bases) are equipped with flat facets, intended to articulate with the tarsal bones of the second series (tarso-metatarsal joints) and with the metatarsal bones close (intermetatarsal joints).

The distal ends (or heads) are rounded with convex articular surfaces, like a small condyles, and exactly juxtaposed in the glenoid cavity of the proximal phalanx.

The 1st metatarsal is shorter and thicker than all the other metatarsal bones. Its proximal end has only one articular facet for the 1st cuneiform bone. The plantar surface is a ridge for the insertion of the long peroneal tendon. On either side of the ridge two depressions run where two sesamoids are positioned and connected to the tendons of the flexor muscle of the 1st ray. The inferior-lateral corner of the base is a flattened tubercle of the 1st metatarsal where the tendon of the long peroneal muscle is inserted. The 2nd metatarsal bone has a proximal end clamped between the three cuneiform bones, the 1st and 3rd metatarsal bone. The 3rd metatarsal bone articulates with its proximal end with the 3rd wedge and, laterally and medially, joins the 4th and the 2nd metatarsal, respectively. The 4th metatarsal bone is characterized by the quadrilateral surface of its proximal end by which it articulates with the cuboid bone. Medially, the same end articulates with the 3rd and 3rd metatarsal cuneiform, while the side is placed in junction with the 5th metatarsal. The 5th metatarsal bone is the thinnest. Its proximal end has a relief, the tuberosity of the 5th metatarsal, which gives insertion to the tendon of the short peroneal muscle and a large oval articular surface for the cuboid. Medially, a facet triangle connects it to the 4th metatarsal.

1.2.1.2 The phalanges

The phalanges of the foot are small long bones, corresponding in number and shape, to those of the hand, which are less developed. They decrease in volume from the 1st to the 5th finger and in length from the 2nd to the 5th. Each finger, therefore, except for the 1st (big toe) which has only two phalanges, has three phalanges, proximal, middle and distal (or second and third).

1.2.2 Anatomy of the midfoot

The midfoot includes the cuboid, navicular and three cuneiform bones (medial cuneiform, intermediate cuneiform and lateral cuneiform) and the surrounding soft tissues. The bones can be thought of as being arranged in two irregular rows, with the cuboid occupying space in both rows. The proximal row contains the navicular, on the medial side of the foot, and the cuboid, on the lateral side. The navicular, medial to the cuboid articulates anteriorly with the head of the talus and is the keystone at the top of the medial longitudinal arch. The distal row contains the three cuneiforms, medial intermediate and lateral, and the cuboid, lateral to the lateral cuneiform

(Souza, 2007). This multi-segmental configuration in conjunction with connecting ligaments and muscles contributes greatly to the stability of the midfoot (Abboud, 2002) and it's important especially in the stance phase of the gait, but also in standing position.

1.2.2.1 The cuboid

The cuboid forms a joint with the calcaneus, the calcaneo-cuboid joint, while the talo-navicular joint represents the interface between the talus and the navicular bone. These joints are the boundary between hindfoot and midfoot and their interfaces are the ones that forward loads to the midfoot and subsequently to the forefoot.

The cuboid bone is an irregularly cubical bone located on the outside of the foot in front of the heel, lateral to the scaphoid and the 3rd cuneiform bone, behind the 4th and 5th metatarsal bone.

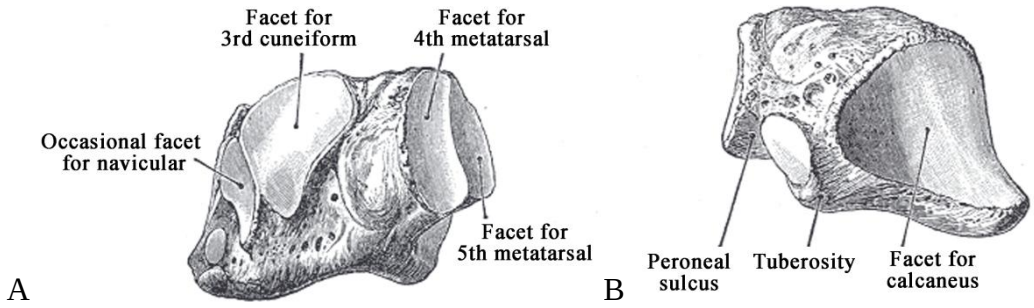

Figure 1.2: Cuboid, A) distal view, B) proximal view.

The upper surface is rough and not joint; the foot has a strong ridge to the attack of the long plantar ligament and ends with a big boss, the tuberosity of the cuboid. The face side is narrow and concave to allow the passage of the long peroneal tendon. The medial surface is larger and has a facet to host the 3rd cuneiform bone. The rear surface is articulated and corresponds to the type face of the calcaneus. The front surface is also articulated and it is divided into two facets, medial and lateral, which articulate with the bases of the 4th and 5th metatarsal bone.

1.2.2.2 The navicular

The navicular bone (or scaphoid) is a tarsal bone and it is shaped like a ship, placed in front of the talar head, behind the row of three cuneiform bones, which are medial to the cuboid.

It comprises a front face and back, two edges, the top edge and the bottom edge, and two ends, the medial and the lateral ones. On the rear side of navicular there is a glenoid cavity, which accommodates the head of the talus; the front side has three flat facets for the three cuneiform bones.

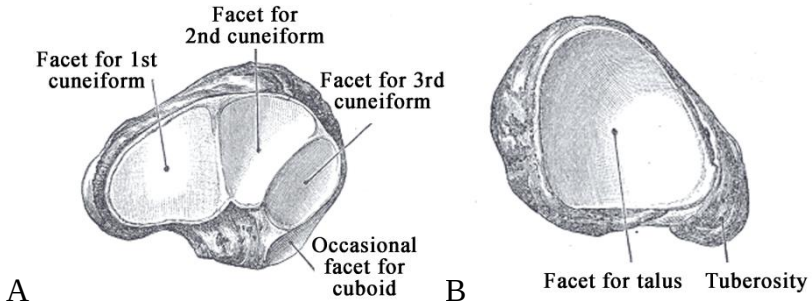

Figure 1.3: Navicular bone: A) distal view of facets for cuneiforms, B) proximal view of articular surface for talus.

The medial end is characterized by a large trial, the tuberosity of the scaphoid, which is part of the main tendon of tibialis posterior muscle.

1.2.2.3 The cuneiforms

The 3 cuneiforms are named the medial, middle, and lateral, and they are convexly shaped on their broader dorsal surfaces. The middle and the lateral cuneiforms are also wedge shaped, so that the apex of each bone points plantar ward and toward the center of the foot. The medial cuneiform is convex medially and rounded inferiorly. The medial and lateral cuneiforms project farther distally that the middle cuneiform to create a mortise for the base of the second metatarsal that articulates with the middle cuneiform. This configuration creates a keystone effect and contributes to the stability of the midfoot. See the following images.

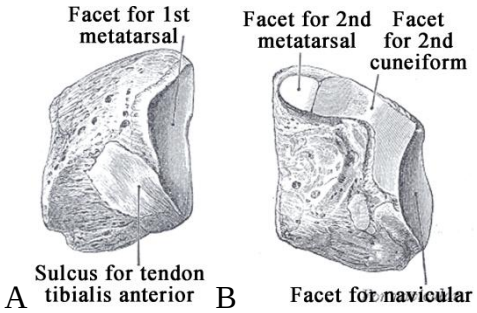

Figure 1.4: First cuneiform: A) antero-medial view, B) postero-lateral view.

The medial cuneiform (or first cuneiform) bone is the largest of the 3 cuneiforms. It is situated at the medial side of the foot, between the navicular behind and the base of the first metatarsal in front.

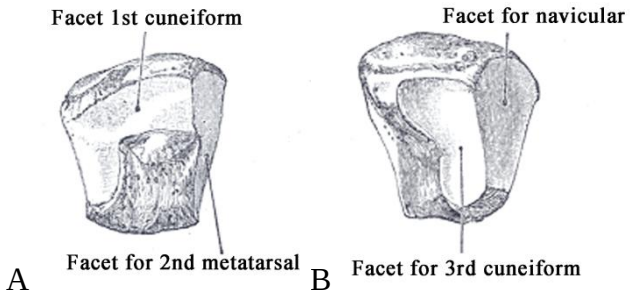

Figure 1.5: Second cuneiform: A) antero-medial view, B) postero-lateral view.

The second cuneiform bone, the smallest of the 3, is wedge shaped with a dorsal base and apex plantar. It is situated between the other 2 cuneiforms, and articulates with the navicular behind and the second metatarsal in front.

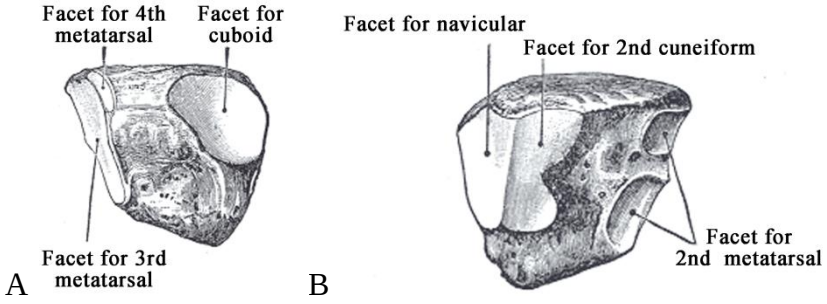

Figure 1.6: Third cuneiform: A) antero-medial view, B) postero-lateral view.

The anterior surface of the lateral cuneiform (or third cuneiform) is triangular and articulates with the third metatarsal bone. The posterior surface articulates with the lateral facet on the anterior surface of the navicular and is rough below for the attachment of ligamentous fibers.

1.2.3 Anatomy of the hindfoot

The hindfoot, also known as rearfoot, is the area in the back (rear) of the foot. The rearfoot includes the talus and calcaneus bones and surrounding soft tissues. In particular the bottom of the heel bone is cushioned by a layer of fat. For what concerns the joints present in this area of the foot, the talus forms the tibio-talar joint

with the two leg bones that are positioned on its upper side, tibia (shinbone, or shank bone) and fibula. The talus and the calcaneus form the talo-calcaneal joint (or sub-talar joint). This joint is bound together by several talo-calcaneal ligaments; it is supported by portions of the medial and lateral ligaments of the ankle, which cross over the ankle complex and the sub-talar joint. The hindfoot bears and distributes the body weight across the foot when standing or walking, in particular during the initial phases of the gate cycle.

1.2.3.1 The calcaneus

The calcaneus is the largest of the tarsal bones located in the heel of the foot and bears the weight of the body as the heel hits the ground. This bone protrudes out at the back, providing a strong lever for the triceps surae muscles of the calf and helping with plantar flexion and push off during ambulation. The calcaneus is roughly 3-dimensionally rectangular in shape, with its long axis directed anteriorly and laterally, and it has 6 surfaces.

The superior calcaneal surface of the calcaneus has 2 parts: articular and non-articular. The non-articular part extends posteriorly to form the heel; it varies in length in different individuals, is convex from side to side, is concave in the antero-posterior axis, and supports a fat pad situated anterior to the calcaneal (Achilles) tendon. The articular part that lies anterior to the non-articular part of the superior surface has an oval facet; the posterior facet faces superiorly and is also tilted anteriorly. The articular portion of the superior surface is convex in the antero-posterior axis and articulates with the posterior calcaneal facet on the undersurface of the talus.

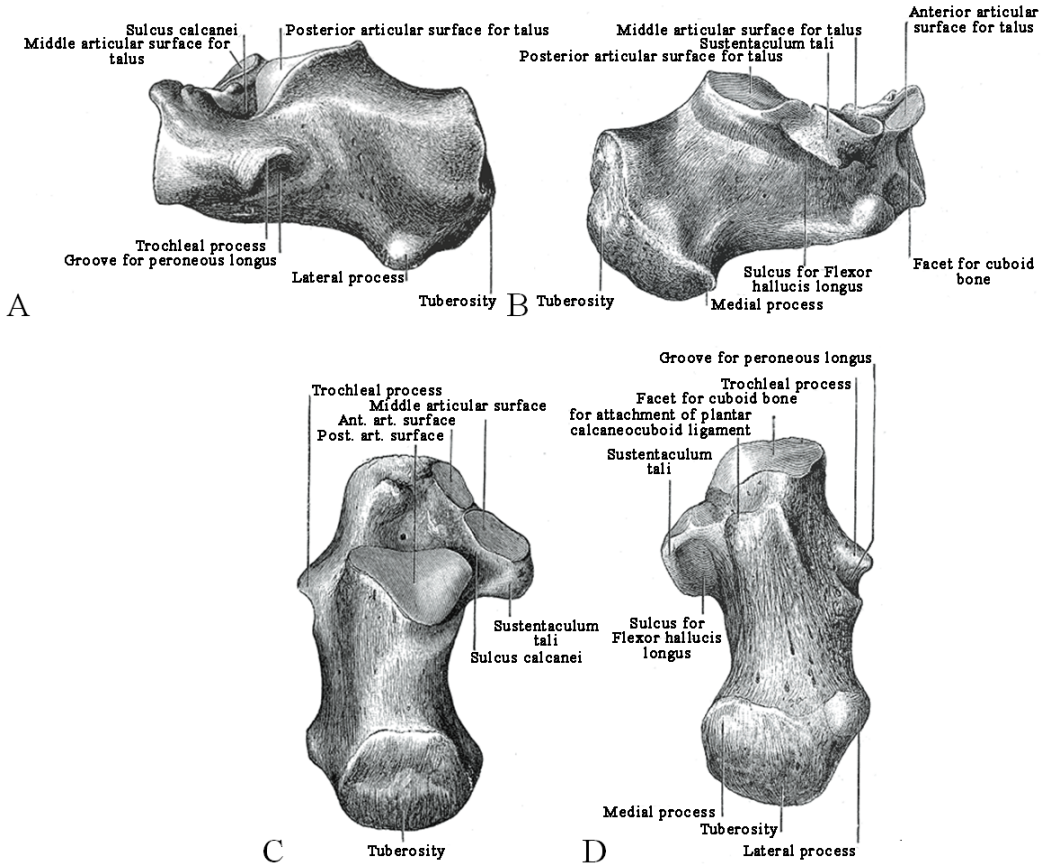

Figure 1.7: Calcaneus: A) lateral view, B) medial view, C) top view, D) bottom view.

At the anterior boundary of the posterior facet there is a deep depression, which continues postero-medial in the form of a groove. This groove is called the calcaneal sulcus. It matches the inferior similar sulcus underneath the talus, and both these grooves form a canal in the hindfoot called the sinus tarsi.

The inferior or plantar calcaneal surface is wider posteriorly and convex from side to side. It has a plantar prominence at the back, called the calcaneal tuberosity, which has a central longitudinal depression dividing it into a smaller lateral process that is the origin of a part of the abductor digiti minimi (quinti), as well as a larger broader medial process that gives attachment, by its prominent medial margin, to the abductor hallucis, and in front to the flexor digitorum brevis and the plantar aponeurosis.

The lateral calcaneal surface is broader posteriorly and becomes narrower anteriorly. It has a small tubercle in the middle, to which the calcaneo-fibular ligament is attached.

The medial calcaneal surface has a deep concavity in the antero-posterior direction in which run the neurovascular structures from the leg into the foot. Toward the upper and anterior end is a medially oriented horizontal projection, the sustentaculum tali. The sustentaculum tali has an articular surface for the middle calcaneal facet and is grooved inferiorly to house the flexor hallucis longus tendon. Its anterior margin gives attachment to the plantar calcaneo-navicular ligament, and its medial margin gives attachment to a part of the deltoid ligament of the ankle joint.

The anterior calcaneal surface provides articular surface to the calcaneo-cuboid joint and is roughly triangular. It is concave in an oblique inferior-lateral plane and convex in a plane perpendicular to this.

The posterior calcaneal surface is convex, dome shaped, wider inferiorly, and has 3 distinct areas. The lower part is rough, covered by fibrous fat tissue of the plantar heel pad. The middle part gives insertion to the calcaneal (Achilles) tendon. The upper part is smooth, slopes anteriorly, and supports a bursa, which lies between it and the calcaneal (Achilles) tendon.

1.2.3.2 The talus

The talus is the second largest tarsal bone, and it is situated above the calcaneus in the hindfoot. This bone is unique in that two thirds of the talar surface is covered with articular cartilage, and neither tendons nor muscles insert or originate from this bone. The talus has 5 articular surfaces, all of which have a weight-bearing function. The talus is composed of 3 parts (the head, neck, body) and 2 processes (the lateral and posterior).

The talar head is the portion that articulates mostly with the navicular. The body includes the dome of the talus at the ankle joint and the posterior facet at the sub-talar joint. Between the head and the body is the neck, which does not articulate with the ankle and sits over the sinus tarsi below. The body and neck of the talus are not coaxial, because in the horizontal plane the neck angles medially with a variable angle of declination.

1.2.3.2.1 Talus, head

The talar head looks forward and medial ward; its anterior articular or navicular surface is large, oval, and convex. The antero-inferior medial portion of the talar

head is quadrilateral or oval and provides articulation with the anterior facet of the calcaneus. This portion of the head is flat and continuous anteriorly with the navicular articular surface. The head of the talus nests within an articulation known as the acetabulum pedis, or foot socket, as described by Sarrafian.[2] This socket is formed by the calcaneal middle and anterior surfaces connected to the large navicular articular surface by the inferior and superior-medial calcaneo-navicular ligaments.

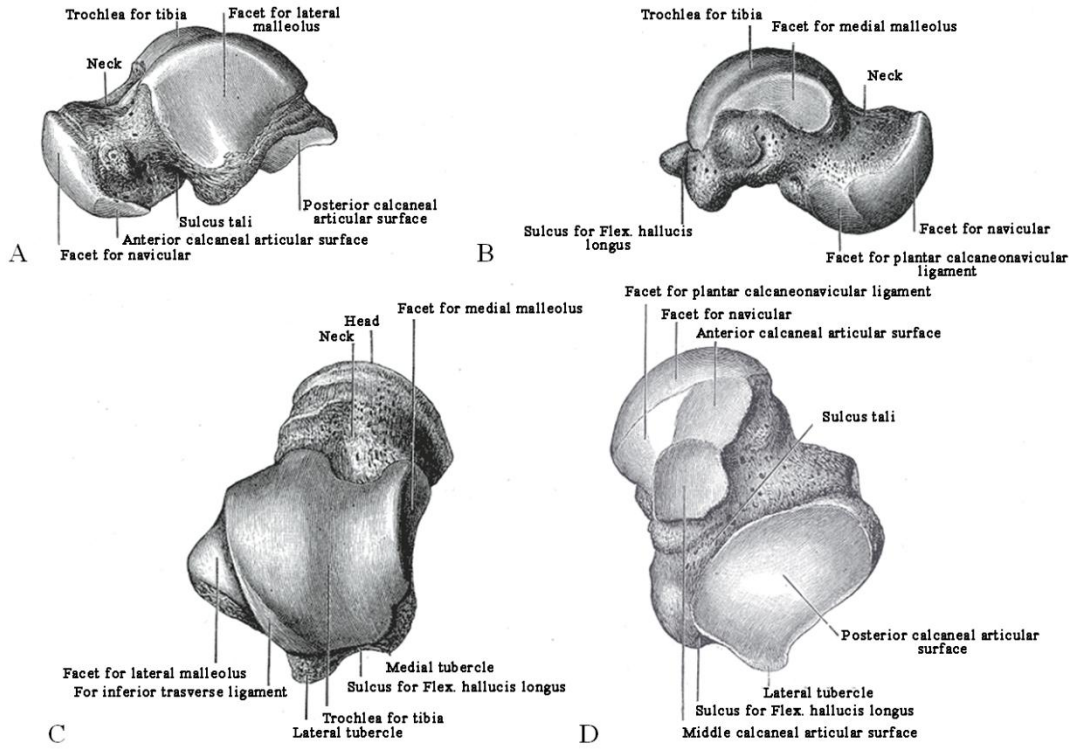

Figure 1.8: Talus: A) lateral view, B) medial view, C) upper surface, D) bottom surface, E) frontal view.

The acetabulum pedis has a variable volume capacity and adapts to the changing position of the talar head during gait. It is hinged laterally by the lateral calcaneo-navicular component of the bifurcate ligament and medially by the posterior tibial tendon and the spring ligament.

1.2.3.2.2 Talus, neck

The neck is directed forward and medial ward 15-20º and comprises the constricted portion of the bone between the body and the oval head. This portion of the talus is

most vulnerable to fracture. The neck has 4 surfaces: (1) superior, (2) lateral, (3) medial, and (4) inferior.

The superior surface of the neck is limited posteriorly by the anterior border of the trochlea of the talus (the dome or body) and anteriorly by the articular surface of the talar head. The tibio-talar capsule inserts along this superior surface just proximal to the insertion of the capsule of the talo-navicular joint. The lateral surface of the neck is concave and is continuous below with the deep groove for the interosseous talo-calcaneal ligament. It provides an insertion for the medial aspect of the inferior extensor retinaculum. The inferior surface of the neck forms the roof of the sinus tarsi and sinus canal. The medial surface provides an area for insertion of the talo-navicular ligaments.

1.2.3.2.3 Talus, body

The body of the talus is arbitrarily divided into 5 surfaces: (1) lateral, (2) medial, (3) superior, (4) inferior, and (5) posterior.

The lateral talar body surface carries a large triangular facet, concave from above downward, for articulation with the lateral malleolus. It is continuous above with the superior articular surface and in front of it is a rough depression for the attachment of the anterior talo-fibular ligament. Along the anterior, inferior, and posterior perimeter of this lateral articular surface is the lateral process, a non-articular component of the talus. The lateral talo-calcaneal ligament inserts at the inferior tip of the lateral process. Along the anterior border of the triangular lateral process are 2 tubercles for insertion of the anterior talo-fibular ligament. Along the posterior-inferior border of this lateral surface lays a groove for the attachment of the posterior talo-fibular ligament.

The medial talar body surface of the body presents 2 areas, superior and inferior. The superior portion is occupied by a pear-shaped or comma-shaped articular facet, which is broader anteriorly and is called the medial malleolar facet. It articulates with the medial malleolus of the tibia and is continuous above with the superior articular surface for tibia. The long-axis medial malleolar facet is oriented anteroposteriorly. The inferior portion is non-articular, and its anterior half is a depressed surface perforated by numerous vascular foramina. Under the tail of the medial malleolar

facet, the posterior half of the inferior portion consists of a large oval area that provides insertion for the deep component of the deltoid ligament.

The superior surface of the talar body is completely covered with articular cartilage for articulation with the tibia. It is shaped like a pulley, with the groove of the pulley termed the trochlea, closer to the medial border. The superior surface is broader in front than behind, convex antero-posterior axis, slightly concave from side to side: in front, it is continuous with the upper surface of the neck of the bone.

The inferior talar body surface presents 2 articular areas called the posterior calcaneal articular surface and the middle calcaneal articular surface. These articular surfaces, one for the posterior and the other for the middle calcaneal facets, are separated from each other by a deep groove, the sulcus tali.

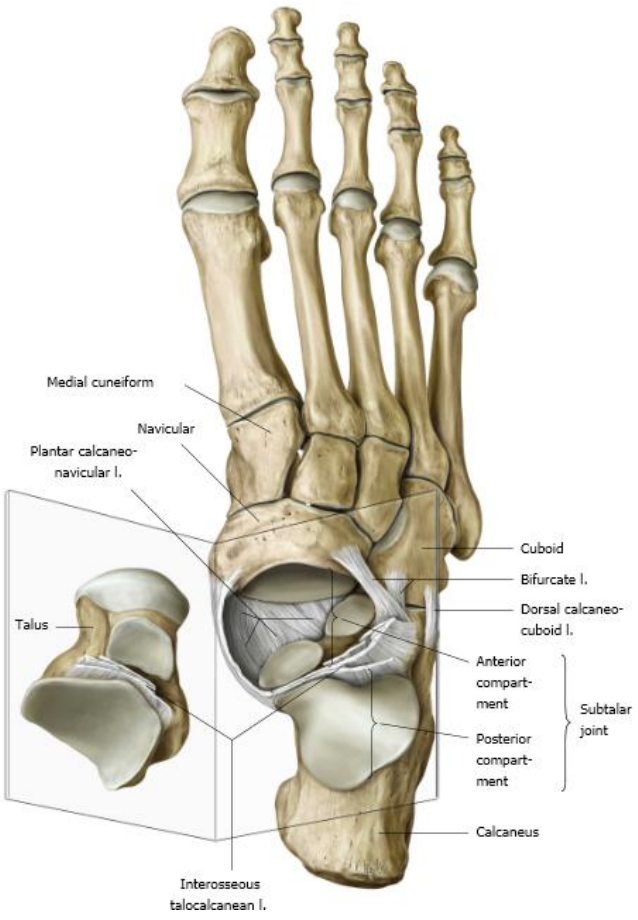

Figure 1.9: Underside of talus and its articulations.

The groove runs obliquely forward and lateral-ward, becoming gradually broader and deeper in front. In the articulated hindfoot it lies above a similar groove upon the upper surface of the calcaneus, and forms, with it, a canal termed the sinus tarsi, in which lies the interosseous talo-calcaneal ligament.

The posterior calcaneal articular surface is large and of an oval or oblong form. It articulates with the corresponding facet on the upper surface of the calcaneus and is deeply concave in the direction of its long axis, which runs forward and lateral-ward at an angle of about 45° with the median plane of the body.

The middle calcaneal articular surface is small, oval in form and slightly convex; it articulates with the upper surface of the sustentaculum tali of the calcaneus. The posterior surface is narrow, and traversed by a groove running obliquely downward and medial ward and transmitting the tendon of the flexor hallucis longus.

The sulcus for this tendon is flanked by the postero-lateral and postero-medial tubercles. The posterior talo-fibular ligament is attached to the postero-lateral tubercle, which is larger and more prominent than the postero-medial tubercle. The postero-lateral tubercle contributes an inferior articular surface that is in continuity with the postero-lateral aspect of the posterior calcaneal surface of the talus. An accessory bone, the trigonum bone, may be found in connection with the postero-lateral tubercle.

1.2.3.3 Tibia and fibula

The tibial bone is a long, massive and strong bone, located in the anterior-medial leg. It is not perfectly straight, it has an indentation that is at the top and medial side down, thus assuming an S-shape, and it also has a twist on its axis. It can be regarded as made up of a body and two extremities.

The back is smooth and convex in its whole extent, except for in its upper portion which is crossed by an oblique line (or line of the soleus muscle) that is a rough ridge directed downwards and medially. Just below this line there is the hole where nutrients flow. The front edge is chamfered at the ends, as it tends to become sharper in the center of the bone, following the winding of the shaft and at the bottom fold and medially to be terminated at the medial malleolus. The medial marginal it is not very pronounced.

The lateral margin (or interosseous) is sharp and offers attachment to the interosseous membrane of the leg. The upper end is quite developed, especially in transverse direction and expands in two masses, the tibial condyles. The top face of each of these has a shallow glenoid cavity for articulation with the femoral condyles. Between the two cavities there is a major one, developed in antero-posterior, the intercondylar eminence, formed by two tubercles. The intercondylar tubercles respectively the medial and the lateral ones divide the intercondylar area into triangular shaped front and rear portions. The glenoid rests on two strong capitals: the external one shows, on its face side, a flat articular surface, to articulate with the fibula. Finally the condyles converge on a plateau, the tibial tuberosity.

The lower end, less developed than the upper surface has a basal joint, concave antero-posterior and divided into two sides by a sagittal crest, it corresponds to the trochlea of the talus. Medially to the lower end, the bony surface expands to a four-sided projection and forms the medial malleolus. The medial malleolus is the seed coat and is furrowed by the passage of the tendons of the flexor muscles. It has a lateral facet, and sagittal plane, which is opposed to the medial talar articular surface. On the lateral side of the distal tibia there is also a small articular surface for the fibula.

The fibula (or fibula) is a long bone, thinner than the tibia and it is formed by a body and two extremities. The body has a straight and triangular prismatic form. The face side is smooth, except at the center of the bone where there is a depression to accommodate the lateral peroneal muscles. The medial surface is covered by a vertical relief, where the interosseous crest takes the interosseous membrane insertion of the leg. The back is rough for a variety of muscle insertions. The three marginal are thin and sharp. The upper end has a flat articular facet, once up and medially, in junction with the articular facet of tibia, lateral raises a pyramidal projection, the styloid process of fibula, where the insertion takes biceps femoralis. The bottom bulges in the lateral malleolus. The surface of the medial malleolus is divided up with the tibial facet, down with the articular surface of the talus. Behind this veneer there is a very sharp depression where the posterior fibulo-astragaleo ligament is set. The lateral malleolus is the seed coat of the fibula and presents a sagittal sulcus for the passage of tendons of the peroneal muscles.

1.3 ANATOMY OF FOOT JOINTS

Joints can be classified according to their mobility, through a Functional classification, or according to the interaction between the different structures involved, through the Structural classification.
The Functional Classification is divided into synarthrosis, amphiarthroses, and diarthroses, as reported in the following table

Type of category	Movements allowed
Synarthroses	no movements at all
Amphiarthroses	Slight movements
Diarthroses	Freely movable

Table 1.1: Functional classification.

While considering a Structural Classification the following classes are considered.

Type of interaction	Type of category	Movements allowed	Example
Fibrous joints (bones joined by fibrous tissue)	Sutures	No movements	skull bones
	Syndesmoses	Slight movements	inferior tibio-fibular joint
	Composes	No movements	tooth sockets
Cartilaginous joints (bones joined by cartilage)	Synchondroses (Primary)	No movements	Epiphyseal plate (hyaline cartilage)
	Symphyses (Secondary)	Slight movements	Intervertebral discs
Synovial joint (bones separated by a cavity containing fluid)	Diarthroses	Freely movable	Knee , Elbow

Table 1.2: Structural classification.

Some additional information about synovial joint are important to be given, since ankle joint (or tibio-talar joint) is a synovial joint and it is one of the most important joints for the foot mobility. Moreover this is the joint that will be studied more in

detail in this Thesis. There are different synovial joints as the following table shortly describes.

Type of synovial joints	**Movement(s) allowed**	**Example**	
Plane joint	gliding movement non-axial	intercarpal joint	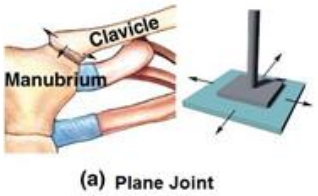
Hinge joint	extend and flex only uniaxial	elbow joint ankle joint	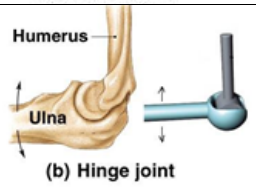
Pivot joint	rotation uniaxial	proximal radio-ulna joint	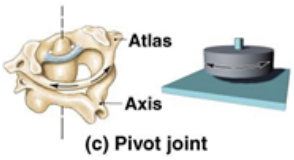
Condyloid joint	biaxial	metacarpus-phalangeal joint	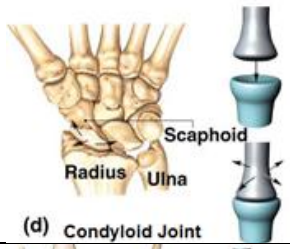
Saddle joint	only in thumb biaxial	carpo-metacarpal joint	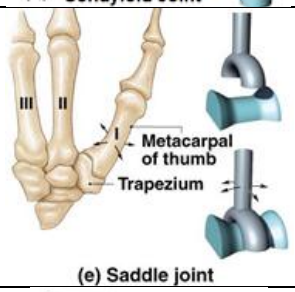
Ball & Socket joint	all movements multi-axial	shoulder joint	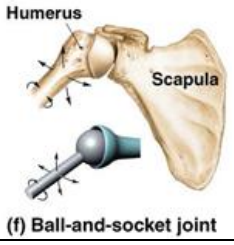

Table 1.3: Schematic representation of synovial joints.

In the previous table non-axial movement means that only slipping is possible, uniaxial means that movements are possible in 1 plane; biaxial refers to junctions that allow movements in 2 planes and multi-axial in 3 planes.

Synovial joints contain an articular cartilage, and in particular hyaline cartilage, which covers the surfaces of the bones involved in the joint. Additionally there is a joint cavity filled with synovial fluid, an articular capsule, which consists in a fibrous capsule with a synovial membrane, and there are reinforcing ligaments, which have a stabilizing function.

After a brief introduction to joints, in the following paragraphs a more detailed analysis is developed for each joint of the foot starting from the forefoot joints and ending in ankle complex joints. An overview of the high number of joint and their definition will be schematically given in the following figure.

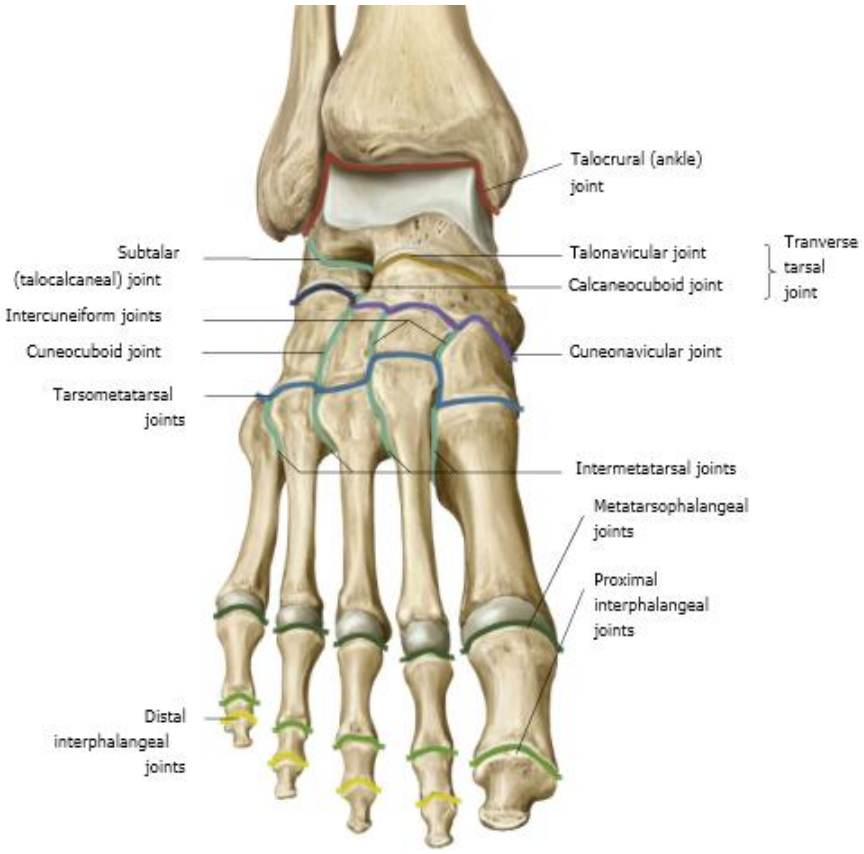

Figure 1.10: Foot joints highlighted and labelled in a schematic front view of right foot.

1.3.1 The metatarso-phalangeal and interphalangeal joints

The metatarso-phalangeal joints are condyles joint, similar to the metacarpo-phalangeal joints of the hand. In particular they are ellipsoidal joints, and allow many

movements: extension, flexion, abduction, adduction. The interphalangeal joints of the foot joints are angular shaped ganglion. They are hinge joints and their peculiar shape is necessary to allow flexion/extension movements.

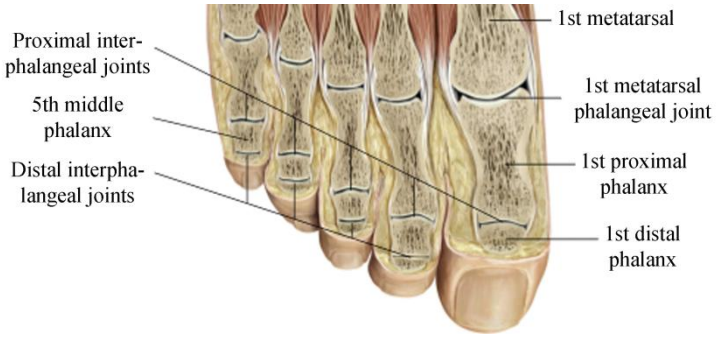

Figure 1.11: Foot trasversal section view with most important articulation of forefoot in evidence.

Each item is surrounded by a capsule, strengthened by a plantar ligament and collateral ligaments. In detail a 3D representation of the anatomic structures at the 2nd - 4th metatarso-phalangeal joints is given in the following figure. It is easy to observe the static stabilizing structures which include the plantar plate (PP), proper collateral ligament (PCL), accessory collateral ligament (ACL), fibrous capsule (C), and deep transverse metatarsal ligament (DTML). The additional structures depicted include the intermetatarsal bursae (B), dorsal interosseous tendon (D), extensor digitorum brevis (EDB), extensor digitorum longus (EDL), extensor expansion (EE), Flexor digitorum brevis (FDB), flexor digitorum longus (FDL), neurovascular bundle (NVB), lumbrical tendon (L), plantar interosseous tendon (P), superficial transverse metatarsal ligament (STML).

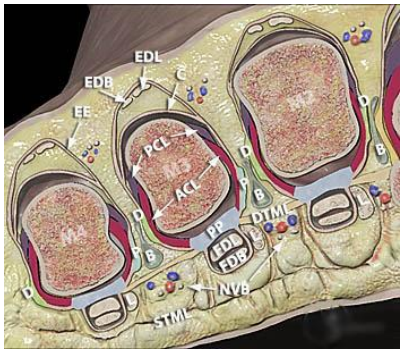

Figure 1.12: Sagittal section of the metatarsal area with anatomical structures in evidence, with particular regard to ligaments and tendons.

More over the following image shows a detail of a metarso-phalangeal joint (true image (A) and 3D reconstruction (B)), and in particular of the medial side of the 2nd metatarso-phalangeal joint. It depicts the accessory collateral ligament (ACL), proper collateral ligament (PCL), and plantar plate (PP).

A  B 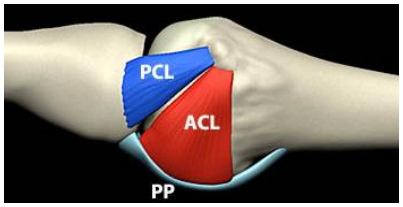

Figure 1.13: True matatarso-phalangeal joint sagital section A) and a 3D recontruction of a metatarso-phalangeal joint with ligament in evidence B).

It is interesting to give some notes on sesamoid joints. They are not properly a joint, since they don't allow a particular motion between two or more bones, but they give the direction to the muscle of the tendons that are attached on them.

In the previous figure it is possible to see the dorsal view with the first metatarsal removed and the capsule and ligaments of the sesamoids and muscular attachments are highlighted. Both sesamoids are attached to the joint capsule and to the collateral ligaments of the metatarso-phalangeal joint. They are embedded in the tendons of insertion of the medial sesamoid (abductor hallucis, medial head of flexor hallucis brevis) and lateral sesamoid (lateral head of flexor hallucis brevis, transverse head of adductor hallucis, and oblique head of adductor hallucis).

1.3.2 The tarso-metatarsal joints

The tarso-metatarsal joints are artrodie that connect the three cuneiform bones, and the cuboid bone to the bases of the five metatarsal bones. The 1st metatarsal bone articulates with the medial cuneiform bone, the 2nd with the three cuneiform, the 3rd with the lateral cuneiform, the 4th and 5th with the front face of the cuboid.

The articular surfaces are covered with hyaline cartilage, also in the intermetatarsal articular surfaces thus obliquely crossing the joint spaced dorsal surface of the skeleton of the foot (Lisfranc line spacing).

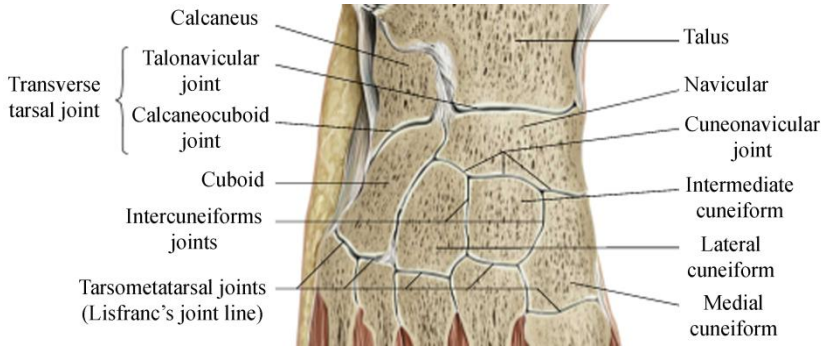

Figure 1.14: Foot trasversal section view with most important articulation of midfoot in evidence.

There is a partial joint capsule that allows communication between the tarso-metatarsal and intermetatarsal joints. The capsule has a fibrous component formed by three independent synovial membranes lined. The synovial membrane is internal to the articulation between a metatarsal bone and a cuneiform bone. Medially it corresponds to the articulation of the 2nd and 3rd metatarsal with the 1st, 2nd and 3rd cuneiform and the corresponding external articulation of the 4th and 5th metatarsal with the cuboid. The fibrous capsule is reinforced by tarso-metatarsal dorsal and plantar and interosseous ligaments.

The plantar tarso-metatarsal ligaments are formed by different layers of fibers beams, that have transverse direction, symmetrically are the dorsal tarso-metatarsal ligaments.

The interosseous ligaments, three in number, are referred to as cuneo-metatarsal interosseous ligaments. The most important is the so-called Lisfranc ligament that runs from 1st medial cuneiform to the base of the 2nd metatarsal. Further the interosseous ligament runs from 2nd to 3rd wedge at the base of the 2nd metatarsal. Finally the 3rd interosseous ligament stretches from the 3rd metatarsal to the 3rd metatarsal cuneiform and sometimes even on the 4th.

1.3.3 The tarsal joints

The tarsal joints are articulation distinguished in bones of the proximal row, the astragaleo calcaneo-fibular joint, and the joints between the bones of the distal row and the joint between the two files, namely the transverse tarsal joint (of Chopart). The joints between the bones of the distal row are: cuboideo-navicular joint, the joint cuneo-cuboid, the two wedge-navicular joints intercuneiform articulation. According

to the shapes of their articular surfaces these joints are all to be classified as artrodie. The transverse tarsal joint (of Chopart) joins the bones back to front, includes the articulation of the tarsal navicular astragalo-(medial) and the joint-calcaneal cuboid (side). The tarsal joints act simultaneously, the greater freedom of movement is achieved, however, at the transverse tarsal joint. The main changes are the internal and external rotation of the foot. The front joints allow only slight movements but they don't allow sliding.

1.3.3.1 The intercuneiform joints

The intercuneiform joints are part of the joints between the bones of the distal row of tarsus set between 1st and 2nd and between 2nd and 3rd cuneiform bones. These are artrodie. The facet joints are flat and they are placed on the lateral aspect of the 1st and 2nd cuneiform medial bone and correspond to those of the 2nd and 3rd.The bone heads are joined by a joint capsule with bones of cuneo-navicular joints and tarso-metatarsal.

The capsule is internally covered with by a synovial membrane and reinforced by dorsal and plantar intercuneiform ligaments linking the cuneiform one-another and they run across the dorsal side and, respectively, the plantar side.

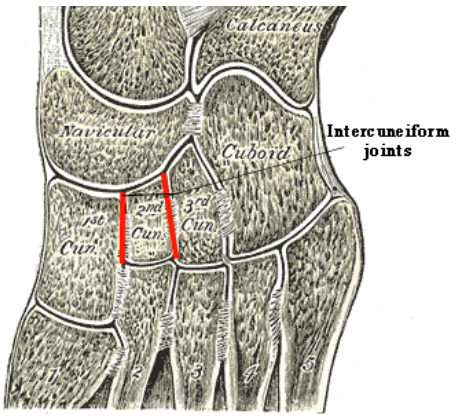

Figure 1.15: Section of a foot intercuneiform joints in evidence.

The interosseous intercuneiform ligament is located on the front of the articular surfaces. The interosseous ligament between the 1st and the 2nd cuneiform is interrupted and does communicate with the joint intercuneiform tarso-metatarsal.

1.3.3.2 The cuboideo-navicular joint

The cuboideo-navicular joint is one of the joints between the bones of the distal row of tarsus and between cuboid and scaphoid and is an artrodie. The articular surface of the scaphoid is located on the front of this bone, the medial aspect of the cuboid. The two bones are united by an incomplete fibrous capsule, and thus the articulation communicates extensively with the others in the same row, the synovial membrane has a similar behaviour. The fibrous capsule is reinforced by two cuboideo-navicolar ligaments and the two leaders joints are also held together by an interosseous ligament. The cuboideo-navicolar dorsal ligament runs from the outer contour of the scaphoid in the middle third of the dorsal surface of the cuboid. Cuboideo-navicolar plantar ligament stretches between the lower edge of the scaphoid and the plantar face of the cuboid. The cuboideo-navicolar interosseous ligament is very strong and joins the two bones posteriorly fixed on to the articular surfaces.

1.3.3.3 The cuneo-navicular joint

The cuneo-navicular joint involves the bones of the distal row and is formed by the scaphoid tarso which lays in the joining with the three cuneiform bones and forms a single articulation that is an artrodie.

The scaphoid has three facets covered with hyaline cartilage, which articulate with the corresponding posterior facet of the three cuneiform bones.

The articular ends are connected by a fibrous capsule, lined by a synovial joint, which continues with the intercuneiforms and cuboidea. The capsule is reinforced by dorsal and plantar cuneonavicular ligaments that originate respectively from the margins of the dorsal and plantar navicular, and they have on their oblique course, the dorsal and plantar surfaces of the three cuneiform to the navicular.

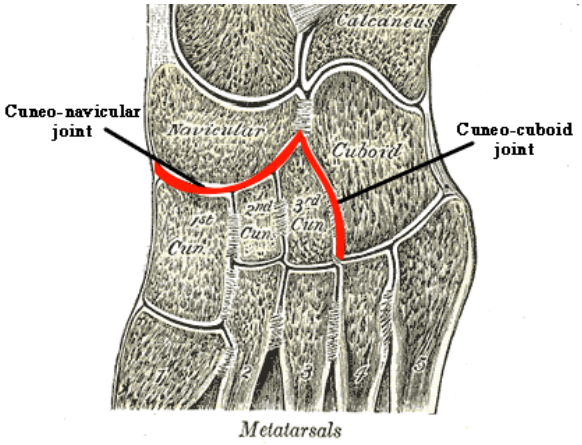

Figure 1.16: Section of a foot cuneo-cuboid and cuneo-navicular joints in evidence.

1.3.3.4 The cuneo-cuboid joint

The structure is a cuneo-cuboid joint between the bones of the distal row of tarsus and it is realized between the cuboid and the 3rd cuneiform bone; so this is an artrodia. The facet joints have a triangular shape with the base directed dorsally. The two leaders joints are held together by an incomplete fibrous capsule, covered by a synovial membrane that continues with those of nearby joints.

The fibrous capsule is reinforced by its ligaments and its articular ends are joined by an interosseous ligament.

The dorsal cuneo-cuboid ligament unites the dorsal side, assuming the two bones crosswise and behaves similarly to a cuneo-cuboid plantar ligament, the plantar side.

1.3.3.5 The talo-navicular joint

The talo-navicular joint (or astragalo-navicular joint) is one of two joints that make up the transverse tarsal joint (of Chopart) and is a typical enartrosis where there are two articular surfaces of ball-shaped segments, respectively hollow and full. The full segment is given by the head of the talus and it can be divided into three areas: the frontal, the lower and the medial. The frontal area is a convex face of the talus navicular joint, the medial lower one, corresponds to the anterior and middle calcaneal articular surfaces in direct continuity with each other and finally, a lateral surface, shaped like a triangle, which articulates with the navicular bone fibrocartilage.

There is a ball on the front of the concave surface on the scaphoid bone, it is segmented in three pieces. The joint capsule are made of fibrous part which fits the edges of the articular surfaces, except at the level where it reaches the neck of the talus bone. It is reinforced by the following ligaments: the dorsal astragalo-navicular ligament, it stretches from the neck of the upper contour of the scaphoid and the bifurcated ligament,which is made up of two parts, the calcaneo-navicular and the calcaneo-cuboid. This portion of articulation goes from the front of the heel to the side of the contour of the navicular bone. The early part of the calcaneo-cuboid merges with the former and then diverges as a V to go to the cuboid bone; the calcaneo-navicular plantar ligament stretches between the front edge of these sustentaculum and scaphoid bone and covers the head of the talus inferiorly. In its top face lays the navicular bone fibrocartilage, which spreads on the plantar side of the tarsus, between the back edge of the scaphoid bone, forward, and frontally with the sustentaculum tali.

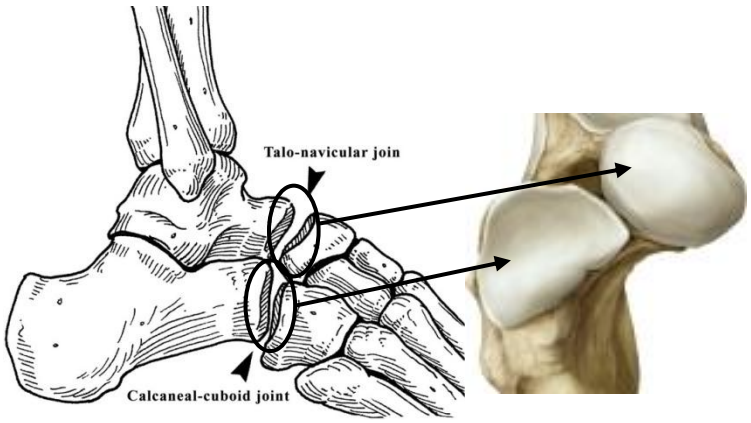

Figure 1.17: Schematic lateral view of foot with highlighted talo-navicular joint and calcaneal-cuboid joint. Frontal view of talus articulation with navicular bone and calcanues articulation with cuboid.

1.3.3.6 The calcaneal-cuboid joint

The calcaneal-cuboid joint diartrosis is the other joint that makes up the transverse tarsal joint (of Chopart). It is a saddle, whose surfaces are given by the heel, a concave face top- low-convex and the second transverse axis and, by the cuboid, a convex face and concave down crosswise.

The fibrous capsule is usually fixed on the articular margin of the two bones. Inside it is lined by a synovial membrane that rarely communicates with the talus-navicular

joint. This capsule is reinforced by its ligaments. The calcaneal-cuboid joint presents dorsal inner ligaments. The calcaneal-cuboid dorsal ligament is located on the dorsal surface of the joint capsule. The inner calcaneal-cuboid ligament is given by calcaneal-cuboid bifurcated ligament. The long plantar ligament is the ligament represented by a fibrous beam that runs from the heel to the bottom surface of the tuberosity of the cuboid, to finish with three or four digits on the distal head of the last three or four metatarsal bones.

1.3.4 The ankle complex joints

The ankle complex is commonly classified as a hinge joint, it is actually composed of several articulations that combined together allow movements such as dorsiflexion, plantarflexion, slight circumduction, inversion and eversion. The ankle complex is an articulated structure. What we normally think of as the ankle complex complex is actually made up of two joints: the subtalar joint, and the tibio-talar or talo-crural joint (or true ankle joint).

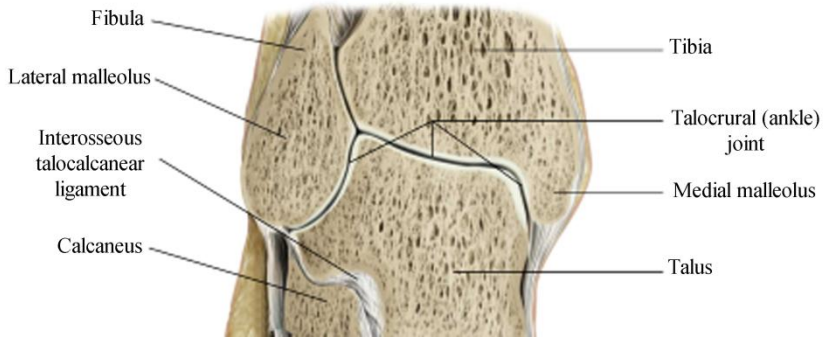

Figure 1.18: Foot trasversal section view with most important articulation of midfoot in evidence.

1.3.4.1 The astragalo-calcaneal joint

The astragalo-calcaneal joint (or subtalar joint) is an artrodie established between the talus and the calcaneus by means of the respective facet joints that are on the front and back of the sinus tarsi. Astragalus has a lower surface, the posterior calcaneal facet, and it is oval-shaped and concave along its long axis. The face of the heel joint is located behind the furrow and also has an oval shape. The joint capsule is reinforced by ligaments and a very strong peripheral astragalo-calcaneal interosseous ligament. The fibrous cap fits the contour of the articular surfaces, departing only in the posterior contour of the calcaneal area. The synovial membrane has a diverticulum that arises in communication with the cavity of the tibial-tarsal joint.

The capsule is thickened in some places where the ligaments are reinforced. These are: the anterior astragalo-calcaneal ligament, which stretches between the lower surface of the talus and the upper wall of the calcaneus, in front of the articular surfaces. Further the posterior astragalo-calcaneal ligament of square shape, ranges from the medial and lateral tubercles of the talus to the calcaneus, crossing the sides. Then the posterior medial astragalo-calcaneal ligament is thin and joins the front edge of the face lateral malleolus of the talus with the outside face of the heel. Finally the astragalo-calcaneal interosseous ligament lies between the grooves of the talus and the calcaneus and circumscribes the sinus tarsi.

1.3.4.2 The talocrural joint

The talo-crural joint (or true ankle joint, or tibio-talar joint) is composed of 3 bones as described previously: the tibia which forms the medial portion of the ankle; the fibula which forms the lateral portion of the ankle; and the talus underneath. The tibio-talar joint is responsible for up and down motion of the foot.

The second part of the ankle lays beneath the true tibio-talar joint and is formed by the subtalar joint, which consists of the talus on top and calcaneus on the bottom. The subtalar joint allows side to side motion of the foot.

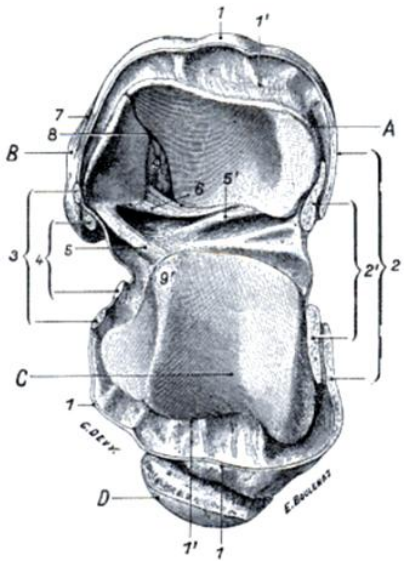

Figure 1.19: Tibio-talar joint opened view with articular surfaces and ligaments of tibia and fibula (inferior surface) and talus (upper surface).

The ends of the bones in these joints are covered by articular cartilage, tibial articular surface (A), fibular articular surface (B) and talar surface (C). The joint is enveloped in a articular capsule (1,1'). The major ligaments of the ankle complex are: the anterior tibio-fibular ligament (3), which connects the tibia to the fibula; the lateral collateral ligaments (4), which attach the fibula to the calcaneus and gives lateral stability to the ankle complex; and, on the medial side of the ankle; the posterior talofibular ligament (5), which limits the antero-posterior movement of tibia around talar dome; the deltoid ligaments (2,2'), which connect the tibia to the talus and calcaneus and provide medial stability. These components of the ankle, along with the muscles and tendons of the lower leg, work together to handle the stress the whole foot structure receives while walking, running and jumping.

In detail, the talo-crural is an articulation between the trochlea to the tibia, the fibula and the talar dome, and it is mainly responsible for the plantar/dorsiflexion. The articular surfaces of the bones of the leg form a joint mortar to the talar trochlea.

The mortar tibio-fibular is wider anteriorly and it has the largest transverse diameter. Its rear wall is formed by the lower face of the tibia and the lateral malleolus on the medial surface of the fibular side of the medial articular tibial malleolus. From the side of the tarsus, the articular surface is provided by the trochlea and the medial and lateral sides of ankle complex talus. The trochlea astragalea is strongly convex from front to back and has a central groove and two slightly convex lips. The medial and lateral faces of the ankle joint corresponding to the faces of the talus have a lower triangular apex and are separated from the trochlea astragalea by two salient edges.

There is a union joint capsule reinforced by ligaments. The fibrous part of the joint capsule is inserted on the edges of the mortar and tibial-fibular articular surface of the talus. It is thin in the front and back sides and thickened by the presence of medial and lateral ligaments.

The medial ligament (or deltoid) has a triangular shape and is separated from the apex of the malleolus, expanding into four beams, two front, one medium and one rear beam, which all represent distinct ligaments. The two frontal beams are the tibio-naviculare and tibio-astragaleal front ligaments.

The tibio-navicular ligament is superficial and is inserted on the dorsal and internal faces of the scaphoid whereas the anterior ligament tibio-astragaleal is deep and fits

in the inner surface of the talar neck. The beam is the average tibio-calcaneal ligament, located medially, which attaches to the heel of these sustentaculum.

The posterior tibio-astragaleal ligament represents the back of the deltoid ligament and is fitted on the medial facet of the talus, below and behind the articular facet for the medial malleolus. The lateral ligament, on the whole less strong than the medial, consists of three separate beams: in the front, middle and posterior ones.

The front fascia, front fibulo-astragaleal ligament, extends from the front edge of the lateral malleolus to the outer surface of the talus, in front of the articular surface to interact with the lateral malleolus. The intermediate beam of the fibulo-calcaneal ligament, runs from the lateral malleolus, near the apex to the outer face of the heel. The posterior beam connects with the fibulo-astragaleal, is strong and often arises from the posterior third of the lateral malleolus and goes back to the process of the talus.

The synovial membrane lies under the fibrous capsule along the contour of the articular cartilage. Frontally and posteriorly, the capsule is lax and it braches out diverticula; it also spreads upward between the opposing surfaces of the tibia and fibula and the interosseous ligament at the tibial-fibular sinartrosi.

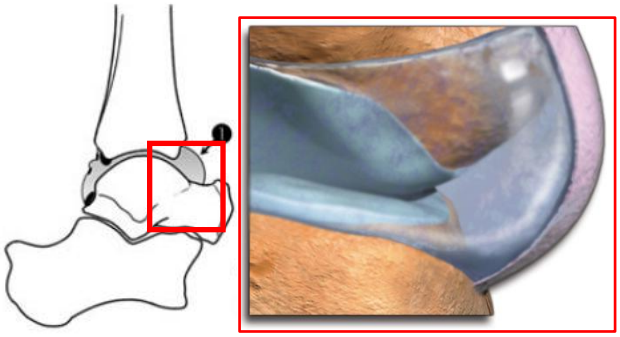

Figure 1.20: Schematic rappresentation of ankle synovial capsule.

The peculiar kind of tibio-talar joint permits only flexion and extension. The side portions of the mortar prevent any lateral movement. It should be noted that the astragalar trochlea is wider at the very frontal area and on the posterior area, thus stretching movements of the tibio-fibular complex involve the widest part of the mortar, those in flexion involve the narrowest part. The foot extension is so firmly wedged between the two malleoli that the lateral movements are close to zero.

Eventually, however, the block is operated by the ankles and the movements are smaller than possible.

1.3.5 Relevant foot structures

The arch is a complex architectural structure that combines elements of bones and joints, ligaments and muscles of the foot. It can be defined as a system of arches resting on the ground on three points (A, B, C) arranged at the vertices of a triangle.

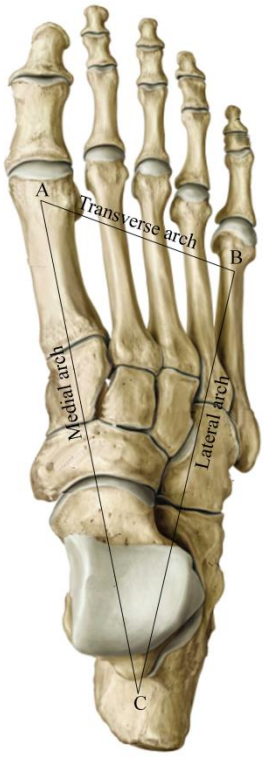

Figure 1.21: Scheme of foot bones with trasverse, medial and lateral arches in evidence, top-view.

Point A corresponds to the 1st metatarsal head, point B to the head of the 5th metatarsal and finally point C to the tuberosity of the calcaneus. Each bearing point is shared by two adjacent arches. Between A and B is bent the front arch, the arch between B and C and between A and C are outside the arch.

The body weight transmitted to the lower limb is applied to the tarsus at the rear of the talar pulley, hence the forces are divided into three areas in order to:

- support the forefoot medial load (A), through the neck of the talus, in the front pillar inner arch;
- support the forefoot lateral load (B), through the head of the talus and the calcaneus apophysis large, along the front pillar outer arch.

- to support the rear load of the body (C), through the body of the talus, the talocalcaneal joint and the body of the calcaneus in the rear pillars and arches together inside and outside.

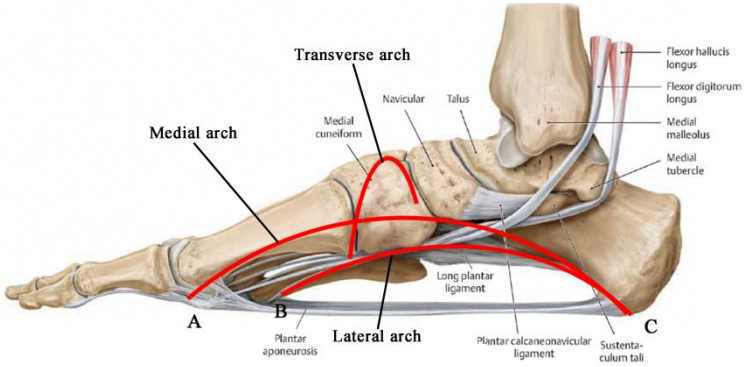

Figure 1.22: Scheme of foot bones with trasverse, medial and lateral arches in evidence from a medial view.

In the standing position, however, the talus and the calcaneus bear the main effort as it is transferred along their axis over half of the weight applied.

1.3.5.1 The medial longitudinal arch (A - C)

This arch extends from the heel to the head of the first metatarsal bone and it comprises seven segments: the first three metatarsal bones resting on the ground only through their heads, completely suspending the first cuneiform, the navicular, the keystone of this arch, is only 15 - 18 mm distant from the ground plane where the heel is resting on.

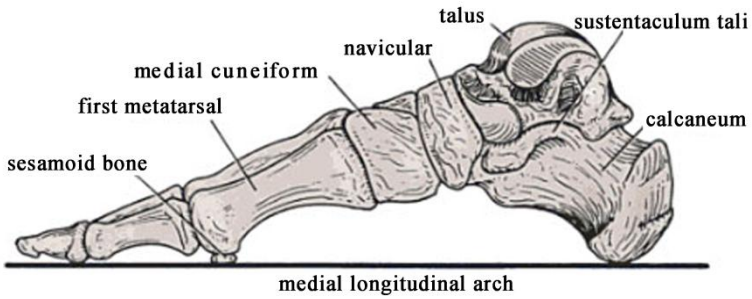

Figure 1.23: Medial longitudinal arch with the bones involved in the structure.

This arch, more mobile and flexible than the external one, behaves like a spring as it absorbs and reduces stresses and shocks. In load conditions, such as the weight of the body, talus moves on the heel thereby bringing the great apophysis of 4 mm and the posterior calcaneal tuberosity of about 1.5 mm, otherwise distant from the ground 7 to 10 mm. The navicular on the talar head back, while lower than the ground-navicular joints and wedge-wedge metatarsal is seprate downwards, decreasing the angle formed by the first metatarsal, the heel recedes, while the sesamoids move forward slightly.

1.3.5.2 The lateral longitudinal arch (B - C)

The lateral longitudinal arch extends from the front of the heel to the head of the last two metatarsal bone segment through only four: the fourth and fifth metatarsal, whose heads are at the front supporting the arch and external front, the cuboid entirely suspended the ground and the heel, which constitute the posterior tubercle of posterior arch support.

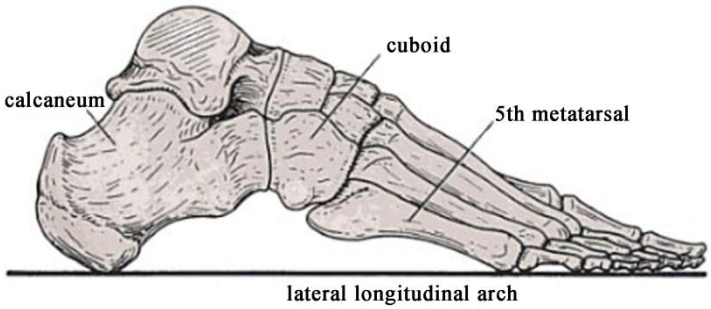

Figure 1.24: Lateral longitudinal arch with the bones involved in the structure.

This arch, unlike most, of the internal high above the ground, it is small (3-5 mm), and make contact with this through the soft parts. While the arch is elastic due to the mobility of the talus on the heel, the arch is much more rigid external transmitting the weight and pushing directly on the ground rather than absorb these forces. This follows easily by observing the typical footprint left by a foot that shows how the side is in contact with soil, in contrast to media which is rather more relieved.

Under load the calcaneus undergoes the same movement used for the vertical arch, the cuboid is lowered by 4 mm, the styloid of the fifth metatarsal of 3.5 mm. Furthermore, a joint diastasis down cuboidee and calcaneal-cuboid-metatarsal, a retreat of the heel and an advancement of the head of the fifth metatarsal.

1.3.5.3 The trasversal arch (A - B)

The arch is stretched between the front of the first metatarsal head, resting on the two sesamoid bones, and fifth, both at 6 mm above the ground. This arch passes through the front of the other metatarsal head: the second head, the higher (9 mm from the ground), form the cornerstone of the third (8.5 mm) and fourth (7 mm) are in an intermediate position.

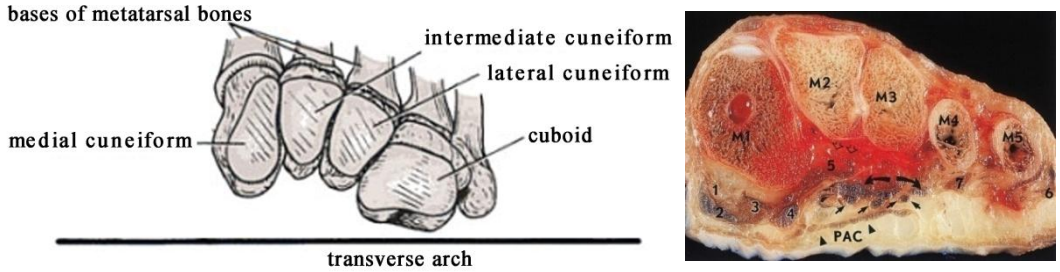

Figure 1.25: Schematic view of trasverse arch and a true image of trasverse arch.

The concavity of this arch is not very pronounced and supports to the ground by means of the heads of the five metatarsals.

Under load the anterior arch flattens and spreads out from both sides of the foot. The distance between the first and second metatarsal increases by 5 mm, 2 mm between the second and third, to 4 mm between the third and fourth, 1.5 mm between the fourth and fifth, so a total load the forefoot extends about 12.5 mm.

1.4 MOVEMENTS OF THE FOOT AND ANKLE COMPLEX

During stance phase the foot is in contact with the ground for its full length. In this phase the Body Weight (BW) load is spread for 25% to the forefoot and 75% to the rear-foot. According to Kapandji (1970) the forefoot is involved for 2/3 of the load on the first ray and 1/3 on the fifth ray.

It is possible to examine what forces are acting in the sagittal plane on a specific articulation. For example on the first two rays of the foot, first and second metatarsal and phalanx during the boost phase and derive the equilibrium conditions of the joints involved. Considering only these two rays as a together toe, they bear in this phase about 64% of the load applied to the forefoot. We understand how these rays

are those most subjecedt to stress and, consequently, to be considered when analyzing the foot.

	Mean	SD	Range of values
1st metatarsal head	29.1	8.7	6.7–52.6
2nd metatarsal head	28.3	6.9	3.3–30.2
3rd metatarsal head	22.3	7.5	0.8–36.5
4th metatarsal head	10.3	6	0.1–30.2
5th metatarsal head	3.5	3.5	0–21.0
Allucis - First ray of the foot	23.8	8.3	6.1–44.5
Second ray of the foot	5.0	2.6	0.4–14.2
Third - fifth phalanx	4.6	3.5	0.1–14.6

Table 1.4: distribution of forces in the forefoot in % of body weight during walking.

The movement of the body is defined by reference to a plane. The sagittal plane is a vertical plane which passes from front to rear dividing the body into right and left sections, the term medial and lateral is related to this plane. The frontal or coronal plane passes from side to side at right angles to the sagittal plane which divide the body into a anterior and posterior section. The transverse plane is parallel to the flat surface of the ground. Planes in this direction divide the body into an upper and lower parts. The same configuration is utilized to describe the movement of the foot.

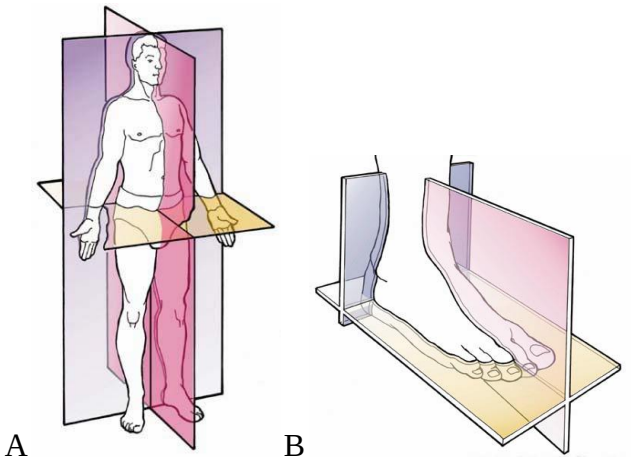

A B

Figure 1.26: the plane of the body (A) the plane of the foot (B).

In detail a discussion of mechanics of the motion of the tibio-talar joint complex requires consistent terminology. The major motions about an anatomical joint coordinate system are rotations: plantarflexion/dorsiflexion, inversion/eversion, and internal/external rotation (or abduction/adduction).

To define the movements of the ankle complex join it is useful define the coordinate system of the joint. The most utilized in the literature are represented in Figure 1.27 B (Siegler et al., 2005). The points A1, A2, A3 illustrated in the figure are the lateral malleolus, medial malleolus, and the centroid of the tibial cross-section respectively. These three points define an anatomical frame for the tibia as follows. The line A2A1 is the Z-axis of the tibia. The perpendicular to the plane containing A1, A2, A3 is the X-axis of the tibia, and the common perpendicular is the Y-axis. The origin is located at the mid-point between A1 and A2

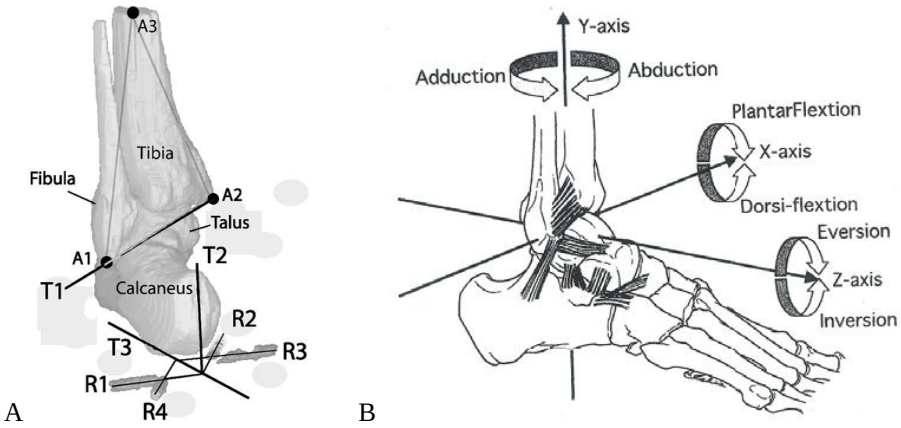

Figure 1.27: Definition of the axis of the join ankle complex A); the movements of the foot B).

1.4.1 Flexion and extension movement

Flexion and extension are movements in the sagittal plane. Flexion movements bend the body part away from the anatomical position. Extension is the movement in the opposite direction back to the anatomical position and beyond into a reversed position. In the case of the foot the flexion and extension movements are called plantarflexion and dorsiflexion respectively and represent the rotation rotations about the X-axis.

Authors	Range of motion (deg)	
	Plantaflexion	Dorsiflexion
Allinger and Engsberg,1993	20 - 50	13 - 33
Nordin and Frankel,1989	25-35	10 - 20
Siegler et al.,1988	37.6 - 45.8	20.3 – 29.8
Kapandji, 1970	30 -50	20 -30

Table 1.5: Range of motion with regard to plantarflexion and dorsiflexion movements.

As reported in the previous table plantarflexion and dorsiflexion are the major components of the motion at the tibio-talar joint during gate. Range of motion of the tibio-talar joint varies across the literature but generally is reported to be around 70 degrees of full motion, although this number is dependent on loading conditions and measurement technique. The typical breakdown of total talocrural motion is usually around 30-40 degrees of plantarflexion, and about 20-30 degrees of dorsiflexion.
Many authors cite variable ranges of motion for the tibio-talar joint in the plantarflexion / dorsiflexion rotations.

1.4.2 Inversion / eversion movement

The inversion and eversion movement of the foot are movement that rise the medial and the lateral border of the foot respectively. This kind of motion developed with rotations along the long axis of the foot, Z-axis. Motion in this direction is thought to be primarily contributed to by the subtalar joint.
The movement of inversion is produced by any muscle that is attached to the medial side of the foot. Tibialis anterior and tibialis posterior are responsible, assisted by extensor and flexor hallucis longus on both occasion. Tibialis anterior dorsiflexes and tibialis posterior plantarflexes the foot at the ankle complex and these opposite effects cancel each othe out when the two muscles combine to produce an inversion of the foot.
The movement of eversion is produced by any muscle that is attached to the lateral side of the foot. Peroneus longus, brevis and tertius are responsible. The former two, whose tendons pass behind the lateral malleolus are plantarflexors, the last is a dorsiflexor, of the tibio-talar joint. These opposite effects cancel each other out when

the three muscles combine to produce a simple eversion of the foot. In the literature there are many works that reported the range of motion of the inversion and eversion movement.

Authors	Range of motion (deg)	
	Inversion	Eversion
Siegler et al., 2005	12.5 ± 5.8, in vivo 12.6	N/A
Sarrafian, 1993	30	20
Siegler et al., 1988	14.5 - 22	10 - 17
Cass et al., 1984	15 - 20	10 – 17
Kapandji, 1970	20	5

Table 1.6: Range of motion with regard to inversion and eversion movements.

1.4.3 Abduction / adduction movement

The abduction and adduction movement are movements in the frontal plane. Abduction movements carry a body part away from the midline. Adduction is movement in the opposite direction towards the midline. Rotations about the long axis of the tibia, Y-axis (Figure b), are external and internal rotation or abduction and adduction respectively.

These types of rotation usually do not occur by themselves but in combination with plantarflexion, dorsiflexion, inversion, and eversion. The range of motion of the abduction and adduction movement of the foot are reported in the follow table.

Authors	Range of motion (deg)	
	Abduction	Adduction
Kjaersgaard-Andersen et al., 1991	N/A	24
Siegler et al., 1988	22-36	15.4 – 25.9

Table 1.7: Range of motion with regard to abduction and adduction movements.

1.4.4 Supination and Pronation movement

Supination and pronation are a combination of the above motions. It is common to use supination and inversion interchangeably and pronation and eversion interchangeably. But, supination is actually a combination of inversion, plantarflexion and adduction. Pronation is a combination of eversion, dorsiflexion and abduction. Supination is a triplanar motion involving the foot moving down and towards the center of the body while pronation is a triplanar motion of the subtalar joint involving the foot moving up and away from the center of the body.

1.5 KINEMATIC ANALYSIS OF THE FOOT

1.5.1 The gait cycle

The movements of the foot are the basis to describe the gait cycle. The gait cycle is defined as the time between the first contact with the ground by the heel of one foot and the next heel-to-ground contact with the same foot. One single limb cycle usually is composed of two phases: stance and swing. The stance phase begins when the foot first contacts the ground, and the swing phase begins as the foot leaves the ground. On the average, the gait cycle is about one second in duration with 60 percent in stance and 40 percent in swing.

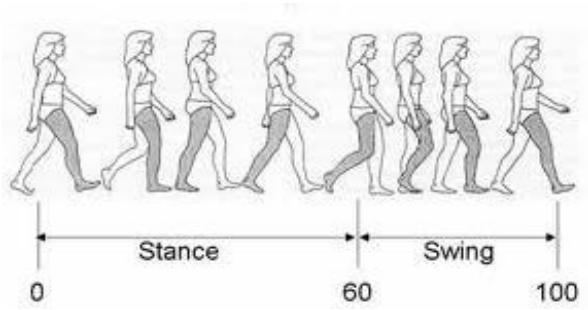

Figure 1.28: Gait cycle phases.

The stance and the swing phases of the gait can be divided in different sub-phases. With regard to the stance phase, there are five sub-phases: initial contact (heel-contact), loading response (or foot-flat) , mid stance, terminal stance and pre-swing (or toe-off).

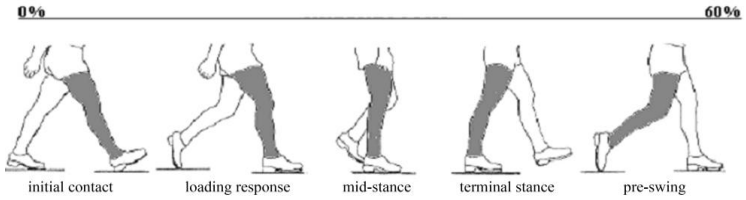

Figure 1.29: the stance phase of the gait cycle.

The first phase is the heel contact phase. This is where your heel as it goes forward hits the ground. Normal contact of the heel is on the posterior outside of the heel, not the direct back of the heel. So, normal heel wear will occur on the posterior outside of the heel. If your heels wear out directly on the back side of the heel or even the posterior inside of the heel, you do not have a normal gait. This phase continues until the foot is flat on the ground. This constitutes 20 percent of the total gait cycle. The next phase is the midstance phase. In this part of the gait cycle which represents 30 percent of the cycle, your body weight passes over your foot as the body comes forward. This is where your foot (in this case the right foot) supports your body weight. This is the part of the gait cycle where an abnormally functioning foot such as an over pronated foot (flat foot) or an over supinated foot (high arch foot) will manifest its problems. This phase ends as your body weight passes forward eventually forcing your heel to rise during the terminal stance. During the last phase the foot pushes off the ground to propel the body forward and to prepare the body to the swing phase of the gait. Most forefoot pain results in this phase of the cycle.

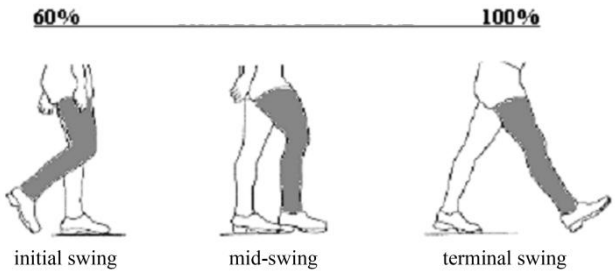

Figure 1.30: the swing phase of the gait cycle.

As shown in Figure 1.30 the swing phases of the gait can be divided in three sub-phases: initial swing, mid-swing and terminal swing. Initial swing begins at toe off

and continues until maximum knee flexion (60 degrees) occurs while the mid swing phase is the period from maximum knee flexion until the tibia is vertical or perpendicular to the ground. The swing phase ends with the terminal swing that begins when the tibia is vertical and ends at initial contact.

1.6 REFERENCES

Abbound, R. J. "Relevant foot Biomechanics" Current Orthopaedics 16, 165-179, 2002.

Aguiar de Souza V. "Design of Insole using Image Base Analysis", The University of Tokio, Master in Science, 2007.

Allinger, T.L. and J.R. Engsberg, A method to determine the range of motion of the tibio-talar joint complex, in vivo. J Biomech, 1993. 26(1): p. 69-76.

Cass, J.R., B.F. Morrey, and E.Y. Chao, Three-dimensional kinematics of ankle complex instability following serial sectioning of lateral collateral ligaments. Foot Ankle, 1984. 5(3): p. 142-9.

Fauth A. R. "Anatomiccaly based Investigation of total ankle complex arthroplasty", Pennsylvania State University, Ph.D Thesis, 2005.

Grood, E.S., Suntay, W.J., "A joint coordinate system for the clinical description of three- dimensional motions: application to the knee", 1983, Journal of Biomechanical Engineering 105, 136–144.

Kapandji, I.A., The physiology of the joints: annotated diagrams of the mechanics of the human joints. 2nd ed. 1970, London,: E. & S. Livingstone. 3 v.

Kjaersgaard-Andersen P Frich LH, Madsen F, Helmig P, Sogard P, Sojbjerg JO, "Instability of the Hindfoot After Lesion of the Lateral Ankle complex Ligaments: Investigations of the Anterior Drawer and Adduction Maneuvers in Autopsy Specimens", 1991, Clinical Orthop Rel Res, vol. 266, pp. 170-179.

Netter FH. "Atlas of Human Anatomy", 4th ed. Philadelphia, Saunders, 2006

Nordin, M. and V.H. Frankel, Basic biomechanics of the musculoskeletal system. 2nd ed. 1989, Philadelphia: Lea & Febiger. xxiii, 323 p.

Sarrafian, S.K., "Anatomy of the foot and ankle complex: Descriptive, Topographic, Functional", 1983, 1st ed; 1993, 2nd ed. , Philadelphia: Lippincott. xvii, p. 616.

Siegler S, Block J, Schneck CD, "The mechanical characteristics of the collateral ligaments of the human tibio-talar joint", 1988. Foot Ankle complex complex8:234-242.

Siegler, S., et al., Mechanics of the ankle complex complexand subtalar joints revealed through a 3D quasi-static stress MRI technique. J Biomech, 2005. 38(3): p. 567-78.

CHAPTER TWO

2 HISTOLOGICAL AND MORPHOMETRIC CONFIGURATION OF BIOLOGICAL TISSUES

2.1 INTRODUCTION

In the foot, as introduced in chapter one, there are several complex structures and the biological tissues involved have properties strictly connected to their function and the loads they stand. In this thesis the focus is on bone tissue and cartilage tissue. In particular, the investigation of biomechanical response should consider the micro-structure of the biological tissue, therefore an histological analysis is proposed in the first part of chapter two. Then a macro-structural analysis is presented through specific experimental tests from the literatureon biological tissues. These tests should be developed considering the function and the physiological loads of the specific biological tissue.

2.2 GENERAL OVERVIEW ON BIOLOGICAL TISSUES

Connective tissue is one of the four traditionally classified types of biological tissue. There are many different kinds of connective tissue. In general, they serve functions of structure and support, often connecting two other types of tissue to each other. Connective tissue usually derives from the mesoderm, the middle of three layers in an animal embryo. The characteristics of connective tissue are largely derived from the extracellular matrix, non-living material that surrounds and supports the living cells. The older classification of connective tissue had two subtypes: proper, which covered areolar and fibrous tissue; and specialized, which included bone, blood, cartilage, adipose (fat) tissue, and reticular tissue. A wider classification can be made considering the proper connective tissue, including loose connective tissue and dense connective tissue; the connective tissue with support function, including bone and cartilage; and the atypical connective tissue or fluid connective tissue, including blood.

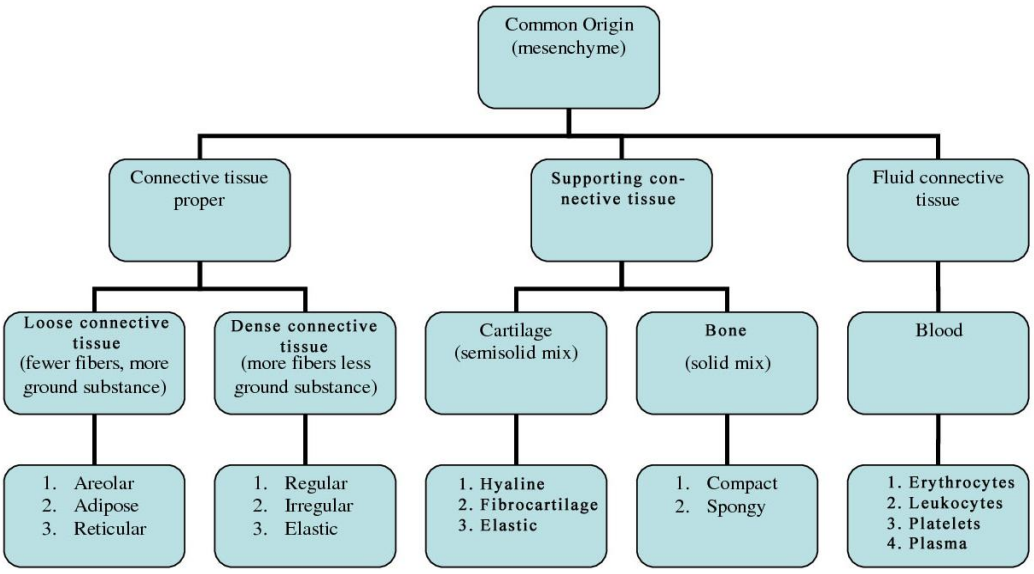

Figure 2.1: Connective tissue Classification.

2.2.1 Proper connective tissue

The classification of the proper connective tissue takes into account the components that are placed inside and in particular a further classification is made considering the percentage of amorphous substance, fibers and cells. For this reason are considered proper connective tissue several different biological tissues such as the mucosal tissue, which prevails in the amorphous substance and is found in the embryonic period eg. in cord blood (Warton jelly) or in the dental pulp of adults; fibrillary connective tissue, in it there is prevalence of one component over another, of cells, fibers and amorphous substance and can be found in the skin, in the tunica mucosa and submucosa of hollow organs, interstitium (stroma) of the organs; dense fibrillar connective tissue, that has a high prevalence of collagen and the second component of fibers can be arranged in specific direction. For dense fibrillar connective tissue a further distinction can be made between the dense fibrillar connective tissue with beam in pair (capsules coating of organs, skin, muscles, etc.), the dense fibrillar connective tissue with parallel beam (tendons) and the dense fibrillar connective tissue with crossed beam (cornea).

2.2.2 The connective tissue cells

The cells of the proper connective tissue can be divided into two categories:

- fixed cells with relatively long life that still live in the connective tissue (fibroblasts, adipocytes)
- mobile cells with short life that generally come from blood (eosinophils, lymphocytes, macrophages, plasma cells and mast cells in addition to mesenchymal cells)

Another type of cells are the mesenchymal cells: small spindle or stellate cells are the precursors of the most representative of the connective tissue pd ie fibroblast; hardly differ from fibroblasts themselves even if they have fewer organelles. They have many possibilities of growth and it is believed that all his life a certain amount of them remains to produce new connective tissue cells. The most important cells in connective tissue are fiberblasts and fat cells. Fibroblasts are responsible for the production of connective tissue components that is, fibers and amorphous substance. When they become inactive are called fibrocytes by some authors, whereas others prefer to use the term fibroblasts, they can still take action in every moment of their synthesis. They are generally arranged along the collagen fiber bundles and appear in histological sections with a form elongated, but sometimes there may be extensions or even star-shaped fibroblasts. The study of fibroblasts can benefit from the use of cell cultures which can be viewed in isolation from other tissue components. At the electron microscope show an abundant rough endoplasmic reticulum, especially when they are active and this means also, in light microscopy, in an intense basophile of their cytoplasm. Fat cells or adipocytes are specialized connective-tissue cells that synthesize and contain large globules of fat. There are two types of adipose cells: white adipose cells and brown adipose cells. Enzymes contained in adipose cells specialize in the hydrolysis of triglycerides in order to generate fatty acids and glycerol for physiological processes. The main reservoir of fat in the body is the adipose tissue beneath the skin, called the panniculus adiposus. There are also deposits of fat between the muscles, among the intestines and in their mesentery, around the heart, and elsewhere. One function of these deposits is to act as soft, elastic padding between the various organs. A brief description with information of main connective tissues cells is given in the following table.

Source of cells	Cell types	Motility	Nucleus	Cytoplasm	Function
Mesenchymal cell of the embryo or those persisting in the adult.	**Mesenchymal cell** (persists along capillaries)	Fixed	**Large**, round,euchromatic (pale staining)	**Stellate**, scanty, little differentiation of cytoplasm	**Functions for all three cell types:** **In embryo:** Loose packing between organs, Secrete ground substance; **Mesenchymal is pluripotent:** gives rise to CT cells, bone, cartilage, blood, endothelium, mesothelium. **In adult:** during wound healing; differentiates into other cell types; **Produce:** **1. Tropocollagen** for collagen and reticular fibers; **2. Tropoelastin** and microfibrils for elastic fiber formation; **3.** Ground substance containing **glycosaminoglycans;** **Fat cells** - function mainly in lipid storage (lipid droplet=mostly triglycerides). (Insulin to glucose to triglycerides)
	Fibroblast (deployed along collagen fibers)	Fixed	**active** cells: euchromatic; **inactive** cells: heterochromatic ; 1-2 nucleoli;	**Fusiform** or stellate (difficult to distinguish) Have abundant granular E.R.	
	Fat cell (singly or in clusters in loose CT, along small blood vessels, and in adipose tissue)	Fixed	Flattened, peripheral, deeply staining	**Thin**, surrounds a single lipid droplet. "Signetring shaped" in appearance.	
Lymphocytes in CT.	**Plasma cells** Uncommon in CT; abundant in: 1. Lymphoid tissues 2. Sub-epithelial CT of: **gastrointestinal** and **respiratory** tracts and mammary glands; **Size:** variable **7-20µm** in diam.	Motile (amoeboid)	E**ccentric, round;** Peripherally distributed heterochromatin resemble: a **"spoked wheel"** or a **"clock-face";**	**Ovoid,** basophilic, (extensive rough endoplasmic reticulum); **Negative Golgi** (adjacent to nucleus);	**Produce antibodies** (is localized in the endoplasmic cisternae); Functional in the humoral immune response;

Table 2.1: The table resumes some of the most important properties of each different cellular component of the proper connective tissue.

2.2.3 The amorphous ground substance

It is a highly hydrated gel in which are embedded the other components: fibers and cells. It consists of an amorphous ground substance, as well as water, minerals and vitamins, by acid mucopolysaccharides or glycosaminoglycans and glycoproteins. It is an aqueous phase in which nutrients and waste products must pass through when passing from blood to organs of the constituent cells (parenchyma).

For what concern physical properties of the ground substance it is viscous, varying from semi-fluid to jelly-like consistency and it is water soluble. Its function is to fill the space between cells and fibers in particular, thanks to its composition, it lubricates and cushions to diminish friction and wear.

The glycosaminoglycans (GAGs) or mucopolysaccharides are divided into sulfur and sulfur compounds. In the first group are the chondroitin sulfate A, B and C, keratan and eparansolfate. The second group includes acid chondroitin and hyaluronic acid. The molecular weight varies from a few hundred thousand up to several million Daltons. The main function of GAGs is to form a sort of gelatinous matrix that promotes cell cohesion and is capable of retaining water in the interstitial spaces, because the molecular negative charges. It forms chains that fit into the polysaccharide molecule made up by proteoglycans. In detail proteoglycans are molecules consisting of a single filament protein on which they occur several polysaccharide chains consisting of glycosaminoglycans (GAG). The extreme hydrophilicity gives them the ability to bind water and distribute it throughout the ground substance, thereby regulating the osmotic exchanges with the cell populations. The particular composition gives to the ground substance plasticity and at the same time a considerable resistance against compressive forces. This is particularly important in adipose tissues for example.

The set of proteoglycan molecules is to form a tangled three-dimensional network whose links are exclusively occupied by water and electrolytes and are called domains.

Glycoproteins of the ground substance are a group of molecules that, in contrast to the proteoglycans, have a low share carbohydrate. Many glycoproteins found in the ground substance are glycoproteins of the plasma passed in the extracellular matrix. In addition to these glycoproteins, which spread from the plasma in the ground

substance, there are also typical matrix glycoproteins, that can interact with various molecular constituents of the matrix. The percentage of glycoproteins is not constant but is related to the age of the subject: it tends, in fact, to increase over time thus resulting in a characteristic marker of aging.

Under the name "glycoproteins of the ground substance" are grouped the various types of molecules that perform specific functions in tissues that are present. While “structural glycoproteins” have the role to link the complex molecules of the extracellular matrix to cell populations into it. Several glycoproteins have been isolated such as:

- Fibronectin
- Laminin
- Condronectina
- Nidogeno or entactina
- Osteonectina

2.2.4 Fibers of the matrix

The fibers found in proper connective tissue are of three types: collagen, reticular and elastic. Some general details will be given in the following parts.

2.2.4.1 Collagen

Collagen fibers are highly resistant to traction (about 5 kg/cm^2), the Achilles tendon can withstand stresses of about 500 kg. In addition, the fiber elongation (deformation) is negligible, being approximately 2%. Subjected to the boil, the heat denatures protein molecules which, after cooling the mixture, giving rise to a highly viscous gel (jelly). The collagen fibers may have a diameter between 1 and 12 appear as bundles of corrugated length unquantifiable. In the connective tissue are distributed randomly and assume a wavy pattern unless they are under tension and then appear stretched. There is a faint longitudinal striations suggesting that they consist of small fibers. The longitudinal striations correspond precisely to the fibrils having a diameter between 0.2 and 0.5 μm. The fibrils are in turn composed of microfibrils of varying thickness between 20 and 150 nm. These are the Association of tropocollagen molecules. Analyzed with a specific solution they appear to be striped across light and dark bands that are repeated every 67 to 70 nm. The

existence of this period, which is the fundamental characteristic of collagen fibers, the fibers can be identified by electron microscopy. There are several types of collagen

• collagen fibrils: the most known are:

Type I (tendons, ligaments, skin and bone),

Type II (hyaline cartilage)

Type III reticular fibers (reticular stroma of organs)

• Associated Fibrillar collagens, FACIT collagens or collagen associated with collagen fibrils

Type IX to type II,

Type X and XII to the type I

• short-chain collagens, such as those typical of basement membranes:

Type IV, V and VII (basement membranes);

2.2.4.2 Reticular fibers

Reticular fibers operate in the most delicate structures (stroma) of organs such as endocrine glands, exocrine glands, etc. in the lymphoid tissue, to form a gentle support for the work on the typical cells of each organ (parenchyma). They do not form bundles as coarse collagen fibers, but are thin mesh and they are strongly PAS positive and stained black with silver nitrate (method Bielscowscky). Moreover they are composed of collagen type III.

2.2.4.3 Elastic fibers

This kind of fibers is present in connective tissue to give a degree of flexibility (wall of the arteries, ligaments and organs such as lung stretch) and in some cases (wall of the arteries) there are different orientations of elastic fibers. They are very thin and very resistant to chemical and physical, in the connective come together to form a loose mesh.

They consist of

- An amorphous component (elastine to collagen that differs from the amino acid content, there is a soluble and insoluble)

- A microfibrillar component (Fibrillin: glycoprotein that may be in a microfibrillar part of the connective tissue outside of the formation of elastic fibers, microfibrils form of 5 -10 nm)

A short resume of proper connective tissue fibers is given in the table below.

<table>
<tr><th>COLLAGEN FIBERS</th><th>RETICULAR FIBERS</th><th>ELASTIC FIBERS</th></tr>
<tr><td>Physical characteristics:

1. Subunits: fibrils= 1000-5000A diam.

2. Form fiber bundles (may branch)
bound together by matrix
= 1-10 µm diam.

3. Flexible -- not elastic; tensile strength;

4. Stain pink with H&E</td><td>Physical characteristics:

1. Subunits: fibrils= 1000-5000A diam.

2. Form network of branching fibers
bound together by matrix
= 0.2-1 µm diam.

3. Flexible -- not elastic;

4. Argyrophilic staining (affinity for reduced silver ions); also stain with PAS;</td><td>Physical characteristics:

1. Subunits: microfibrils= 110A diam.

2. Form branching fibers, = 0.5-1µm diam. bound together by elastine (a protein); or sheets bound together by elastine;

3. Highly elastic -- can stretch 150% of its length;

4. Refractive in light microscope, stains poorly with H&E, well stained with special stains.</td></tr>
<tr><td colspan="2">Chemical composition of both, COLLAGEN and RETICULAR fibers:</td><td>Chemical composition of ELASTIC Fibers & Sheets:</td></tr>
<tr><td colspan="2">1. Fibers are made up of : tropocollagen;</td><td rowspan="3">1. Microfibrils: cystine-rich protein;

2. Elastine: amorphous valine-rich protein;</td></tr>
<tr><td colspan="2">2. Tropocollagen is made up of: 3 helical polypeptide chains coiled around each other (2800 A long).</td></tr>
<tr><td colspan="2">3. Characteristic amino acids: hydroxyproline and hydroxylysine;</td></tr>
<tr><td colspan="2">Origin: Both collagen and reticular fibers are secreted by fibroblasts of CT proper</td><td>Origin: 1. Fibers secreted by fibroblasts;
2. Sheets produced by smooth muscle (e.g., aorta);</td></tr>
</table>

Table 2.2: Classification of different type of fibers and their Physical characteristics.

2.3 BONE TISSUE

2.3.1 Histological characterization of bone

The bone is a specialized form of connective tissue, characterized by mineralization of the extracellular matrix that gives the fabric a considerable hardness and durability. The bone is usually organized into defined structures, the bones. These structures can be classified according to their morphological characteristics: the long bones, short bones and flat bones

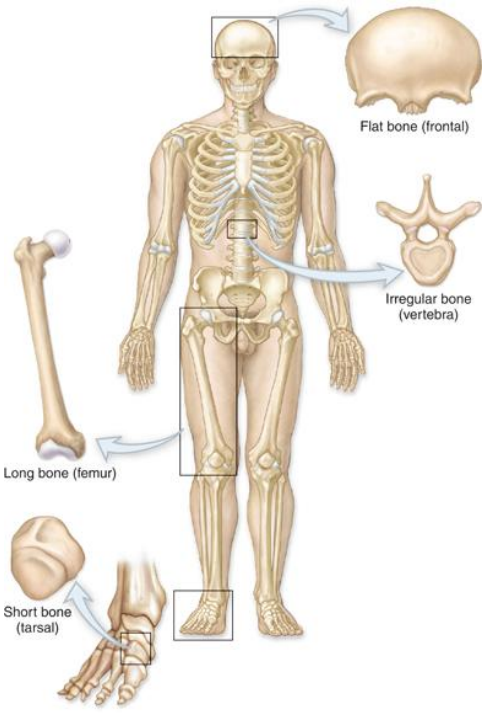

Figure 2.2: Examples of different types of bone in a schematic representation of the skeleton.

Long bones have a much greater dimension than the other two, each long bone consists of a hollow cylindrical central part consists mainly of compact bone (or cortical) said shaft, which has a large central cavity containing the longitudinal medullary bone marrow, and two rounded ends, with the largest section, called epiphyses. The epiphysis and the innermost layer of bone delimiting the medullary cavity are composed of trabecular bone (or sponge).

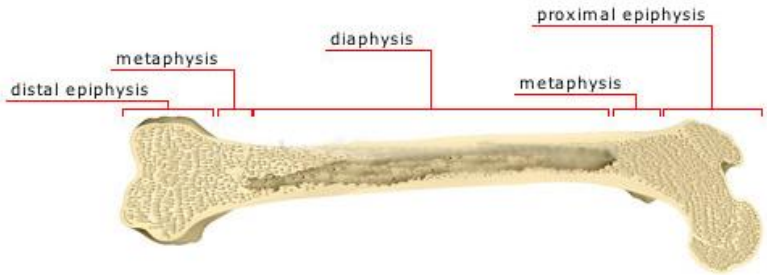

Figure 2.3: Long bone section schematically represented.

Epiphysis and diaphysis are connected together by metaphysics. Examples of long bones are the femur, homerun, and tibia. Unlike the short bones have comparable sizes in three dimensions and are mainly made up of spongy bone covered with a thin

boundary layer of compact bone. Examples are the bones of the carpus and tarsus. In the end, the flat bone width and length are much more thick, are composed of two layers of compact bone, known as internal and external boards, which contain a layer of spongy tissue in the diploe and examples are the bones of the skull and iliac bone. There are also some bones short, round or ovoid, small volume, the sesamoid bones, which develop in the vicinity of some joints of the hands and feet and a thickness of some tendons, these bones are made up predominantly of cortical tissue.

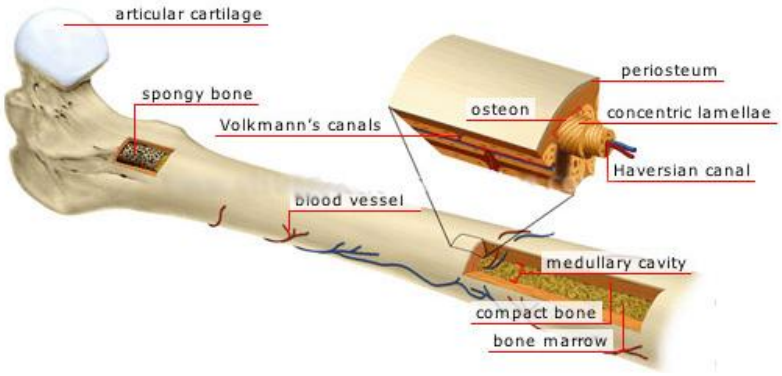

Figure 2.4: Representation of a long bone with particular details of its structure in evidence.

All bones of the skeleton are almost completely enveloped by a fibrous membrane called periosteum, consisting of an outer layer of fibrous connective tissue and an inner layer of loose connective with numerous osteoblasts. These cells form a continuous layer in contact with the bone during growth, that layer of exchange, which becomes discontinuous in the adult.

The periosteum is responsible for the increased thickness in the bone and missing parts covered with articular cartilage and at the insertion of tendons and ligaments of the bones, where bundles of connective fibers Sharpey, penetrate directly into the bone itself. The medullary cavity of the shaft is covered with a thin connective tissue, the endostio, equipped with osteogenic properties. The food is secured to bone tissue from the arteries that reach the periosteum, where they form a mesh network is very narrow. The most voluminous, the nutrient artery, enters a nutrient canal dug to reach the compact bone spongy bone where it provides branches to the bone marrow and branches that reach the Havers channels through branches usually arranged in transverse direction with respect to strip , these branches of Volkmann (or

perforating canal). There are also the lymphatic vessels, but only in the periosteum, and lymph channels are missing compact and spongy bone.

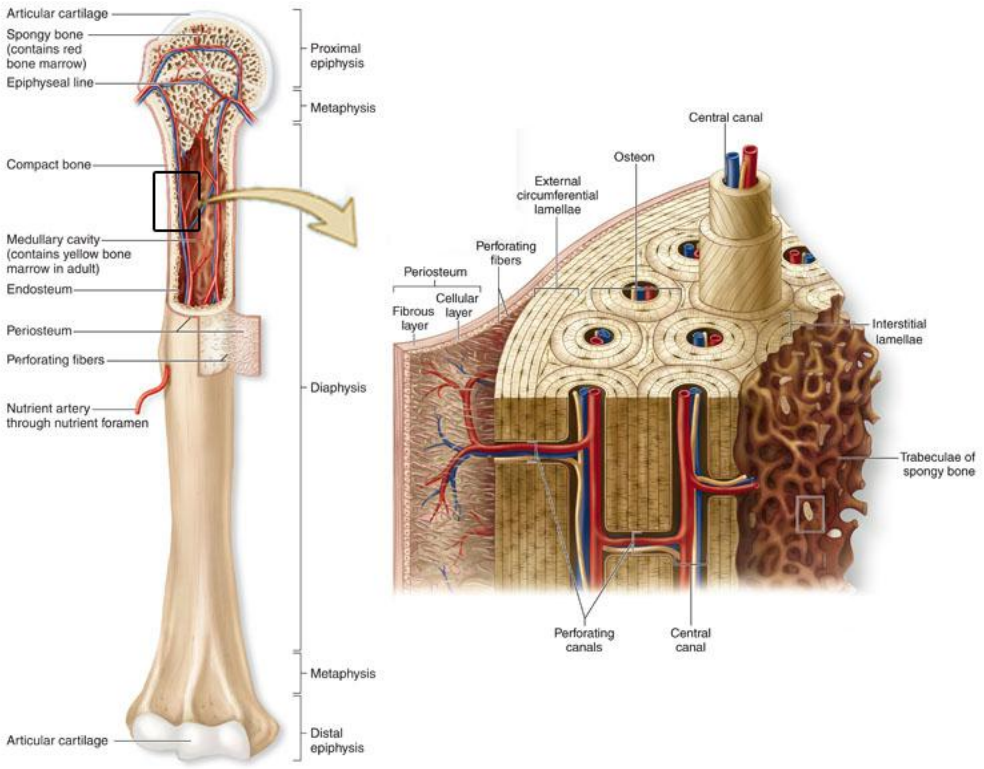

Figure 2.5: Representation of a long bone with a detailed schematic representation of cortical bone and periosteum.

The complexity of relationships in terms of biomechanical properties and structure, related to the morphology, function and physiology of bone tissue, leading to the use of a hierarchy of scale from macro to micro, in order to describe the structural organization.

The knowledge of the interactions between different levels is crucial to understand developments and changes appreciable at a macroscopic phenomenological state. It must be remembered, in fact, as the loads and the tensions that have affected the bone on bone modeling action so that, for example, the bone trabeculae are oriented along the direction of the force lines that have to endure thanks to the continuous action of regeneration and reabsorption by osteoclast and osteoblast. Each bone has a trabecular structure thus determined by its function. At the ultra structural level goes to investigate the basic components of bone matrix. This is made of a composite fiber

5 mm thick, which are in turn composed of mineralized collagen consisting in 3 microfibrils.

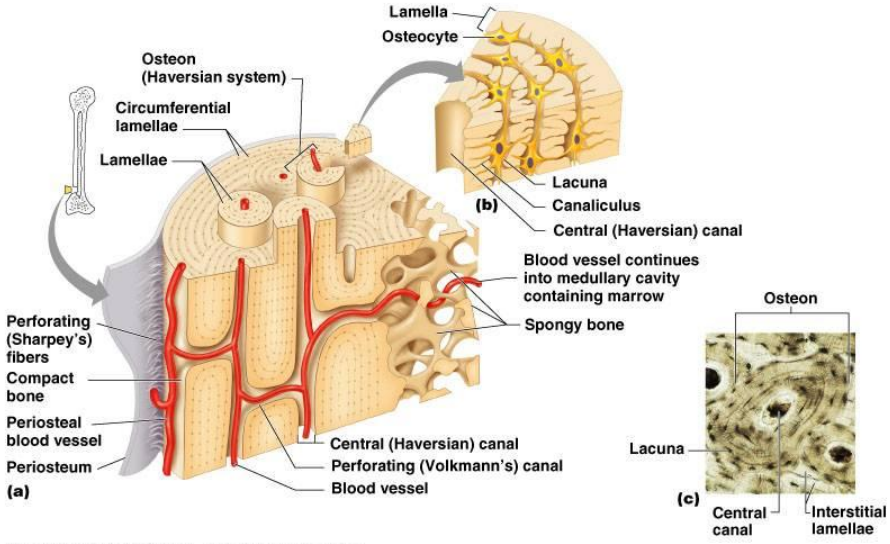

Figure 2.6: Schematic representation of cortical bone a); particular of a Haversian system section b); true image of a cortical bone with Haversian system in evidence.

At the molecular level is possible to characterize the bone matrix in its basic components, organic and inorganic.

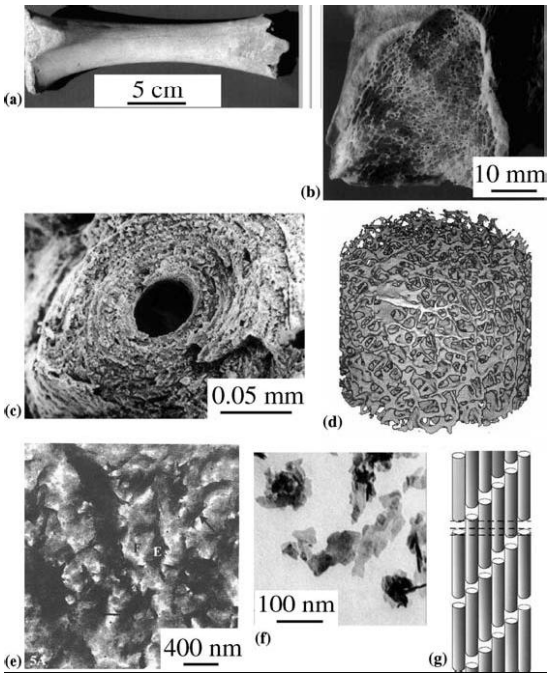

Figure 2.7: Hierarchical representation of bone: a-whole bone (macrostructure), (b) section of a long bone (macrostructure), (c) osteons (microstructure), (d) trabecular area (microstructure), (e) ultra structure, (f) hydroxyapatite crystals (building blocks), (g) of collagen molecules (building blocks).

2.3.1.1.1 Organic matrix

From the qualitative point of view, the composition of the organic matrix of bone is not very different from the cartilage. However, the two differ in how much more prominent in quantity: in the bone matrix is a low concentration of proteoglycan (0.2-1% in contrast to the cartilage which amounts to 30-40%), so the collagen becomes dominant over other constituents (about 20% of the dry weight). The distribution of collagen fibers can be observed on decalcified tissue sample must be completely free of inorganic salts. Inorganic salts are arranged neatly between the bundles of collagen fibers around the individual fibers and even within the fibrils along the microfibrils. The microfibrils are composed of three helical peptide chains laevogyrate, wrapped in a 280nm approx.), triple helix to form the tropocollagen molecule (1.5-60nm). This is related to the apatite in crystalline form. Wanting to make an analysis by depriving the tissue of calcium, it is noted that mature in the bone bundles of fibrils are arranged in an orderly manner, in parallel with each other in each slat. More specifically it is noted that the collagen fibrils starting in helical axis of the osteon in each blade, but with pitch and fiber direction very different in adjacent lamellae, while the direction and angle of the fibers are more or less regular and consistent within a single lamella.

Going down the scale in size, occurs as the architecture of the material is closely correlated with the level of cell size, i.e. with the changes induced by biological processes: the bone structure is the story of its cells. Four types of cells are identified, three of which share the same origin. Osteoclasts, osteoblasts and osteocytes, also influenced by signals such as mechanical properties of bone to respond by activating processes of functional adaptation.

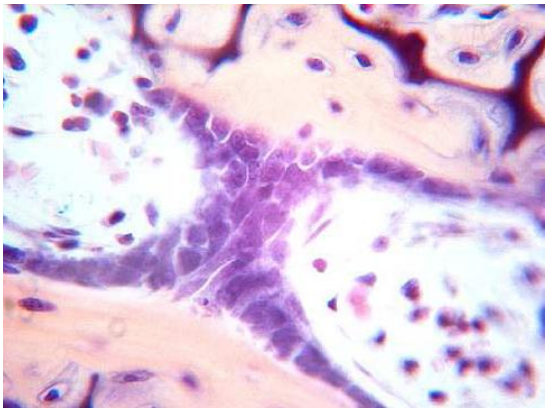

Figure 2.8: Histological picture of osteoblasts.

First, osteoblasts are the cells that synthesis of the organic matrix consists of collagen and other proteins. On cessation of the bone formation, some osteoblasts reach a dormant form and are deposited on the surface of the bone, forming a layer of cells (lining cells). Osteoblasts are separated by spaces and gaps and differentiate into osteocytes. The osteocytes are less active in osteoblasts, but able to communicate with each other through processes that take place along channels between the gaps: it is assumed that the network of osteocytes within the matrix acts as a 'mechanical sensor'. The fourth type of cells, osteoclasts, have a common origin for the white blood cells. You are in aggregate up to 10 cores and can secrete acids and enzymes capable of digesting and demineralisation of the bone matrix.

2.3.1.1.2 Inorganic part

The inorganic or mineral bone increases during growth peaking in the adult of about 30 years, which reaches around 65% of dry bone. The composition of the mineral matrix in fact varies with age, factors related to nutrition and diseases (rickets, osteoporosis, ...). Electron microscopy studies show that the mineral crystals (hydroxyapatite similar 20-40 nm long and 1.5 to 3 nm thick) are distributed as particles along the adjacent bundles of collagen fibrils but also along the individual fibrils. During the process of calcification of hydroxyapatite crystals are aligned neatly along the collagen fibrils.

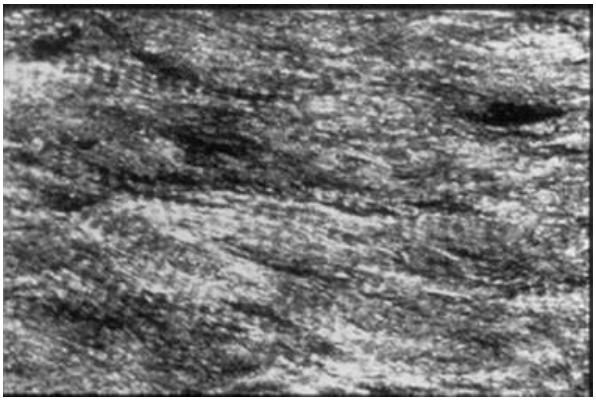

Figure 2.9: Elettronic micrography bone matrix: note the presence of microfibrils of collagen with typical cross striation and agglomerates of needle-like crystals of apatite, strongly electrondense.

It has been verified, in addition, the decalcified bone loses its hardness and rigidity, making it flexible, while retaining tensile strength, the shape of the macroscopic and

microscopic structure. When they destroyed its organic components (cells and fibers) through a process of calcination (sustained combustion with free access of air) that maintains the mineral component intact, the bone retains the shape and size but loses the original tensile strength becoming fragile. It can therefore think that the inorganic constituents of bone are responsible for the hardness and stiffness, while the tensile strength and compressive strength is related mainly to the inorganic matrix and collagen fibers. From Figure 2.9. on an electron micrograph is evident in a laminated fabric that has been produced in the micro-fractures, fractures of the rhymes run through the slats thicker, rich in mineral and therefore more fragile, and leave free the blades thin, richer in fiber collagen and therefore more plastic.

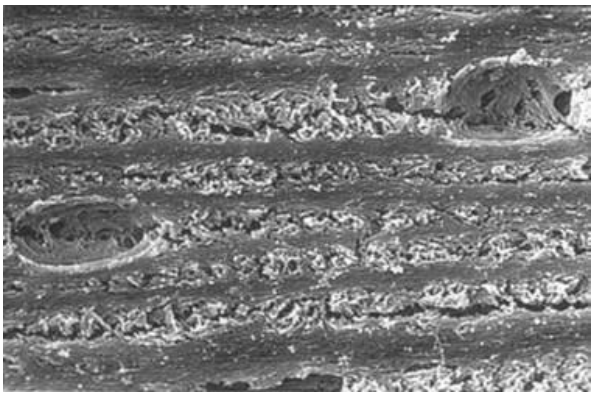

Figure 2.10: Scanning electron micrograph of lamellar bone tissue in which they were produced microfractures.

The combination of the two components of the matrix and internal architecture, continuously adapted to the type of loads and stresses, ensures maximum functional efficiency associated with low weight and suitable for many mechanical functions.

2.3.2 Cortical bone

Cortical bone tissue is a solid, compact microstructural level consists of wrapping the osteons and Haversian canals and surrounded by interstitial tissue. Each osteon, with a diameter of between 150 and 250μm, consists of a cylinder of 8-20 concentric lamellae osteon around a cavity within which they reside vascular cells (osteocytes). The bone lamellar unit is composed of layers of parallel or concentric slats, each 3 to 7μm thick and contains fine fibers that are oriented roughly in the same direction.

Each blade is made up of cells and intercellular substance. Osteocytes, are scattered at fairly regular intervals between the slats within the cavity. The microcanalicoli containing cytoplasmic processes of osteocytes form a network intercom that connects the various gaps between them and facilitate the diffusion of nutrients, hormones and products of the catabolism of osteocytes. The strips are arranged to form two different types of lamellar systems:

- internal and external circumferential lamellae: the first bound the bone marrow cavity; trabeculae of spongy bone out from this strip to the bone marrow cavity, breaking the surface layer laminated dell'endostio cironferenziale internal and the latter are located directly beneath the periosteum and their Sharpey fibers, anchoring the periosteum to the bone;

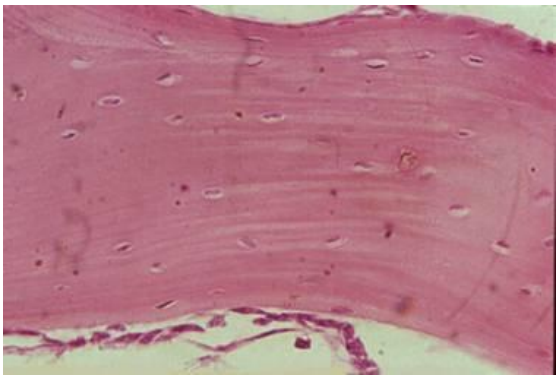

Figure 2.11: Simple lamellar bone.

- osteon lamellae: they constitute the majority of cortical bone, are organized in concentric structures, called osteons around a vascular cavity, the Haversian canal. Often the osteons may forking along its path and is bordered by a thin cementing, consisting of amorphous calcified substance with few collagen fibrils. The osteons are combined together to form long cylindrical structures with the longitudinal axis tend to arrange themselves parallel to the lines of force which the bone is subjected. When the bone undergoes remodeling, osteoclasts resorb the osteons, while osteoblasts will form new ones; residues osteons form a system of interstitial lamellae around the osteons.

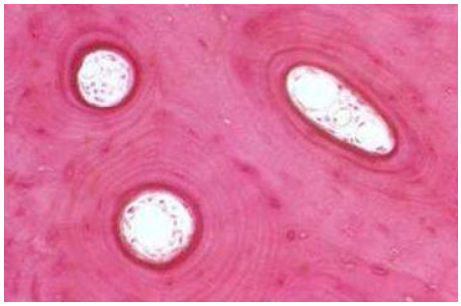

Figure 2.12: Fabric lamellar osteon, concentric lamellae are visible around the osteons.

The Haversian canal has a diameter ranging from 20 to 100μm. As previously described the Haversian canals of adjacent osteons are connected by transverse or oblique channels (channels perpendicular to the trend of Havers), the channels of Volkmann. This system of interconnected vascular channels in turn is connected with the network formed by the bone canaliculi and the lacunae of bone. Clearly the distribution and size of gaps influence the stiffness and other mechanical properties.

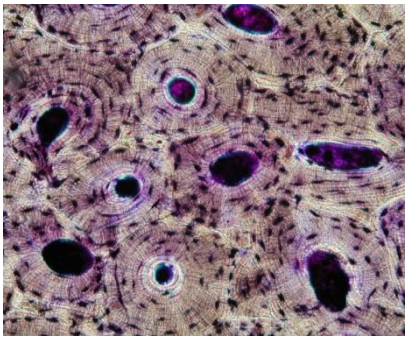

Figure 2.13: Section of compact bone tissue, chemically colored. The concentric lamellar organization around a channel of Haversian osteons is evident.

The appearance of an osteon varies depending on the section plane. In cross-section appears as a series of concentric rings arranged around a central hole (Figure 2.13), while in longitudinal sections there is a series of parallel bands arranged on either side of a slot that corresponds to the central section of the Haversian canal. The space between the osteons are occupied by groups of bone lamellae that are arranged much more irregular pore systems. Volkmann channels however, are not surrounded by concentrically arranged lamellae. Certainly, this complex structure, with a strong

preferential direction parallel to the direct bone is closely correlated with the type of stress that the bones, particularly long ones, for example, the legs must support.

2.3.3 Trabecular bone

From the engineering point of view of the trabecular bone material is classified as a composite material, anisotropic, and porous solid phone. The macroscopic structure of the trabecular bone consists of a series of interconnected trabeculae and spicules, generally devoid of osteons and a structure composed of a mosaic of angular segments of layers of lamellae preferentially aligned with the orientation of the trabeculae. The right angle of the slats separated by cementing lines, are called "packages" trabecular. Tissue remodeling takes place directly on the surface of trabecular bone tissue by removing the old and filling the cavities with new bone. Due to the high surface / volume ratio of trabecular bone remodeling is more active than that of cortical trabecular bone tissue also has a larger number of gaps have even greater extent than the cortex. The two types of bone tissue also differ in the calcium content is lower in the spongy tissue as well as the apparent density is higher while the aqueous fraction.

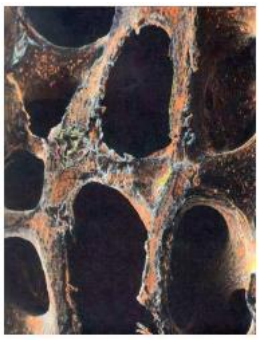

Figure 2.14: Microscopic image of trabeculae of spongy bone.

The trabecular bone is, therefore, very porous and full of water. At the micro level of the trabecular tissue containing one gate open pore space, three-dimensional and interconnected. Inside the pores and there are bone cells, making this a solid phone. The pores are the size of the order of 1 mm and the thickness of trabeculae is an order of magnitude lower. The microstructure of the trabeculae is typically oriented so that there is a direction in which stiffness and strength are

greater. This directionality gives the gate some mechanical properties of bone anisotropy.

2.3.4 Bone remodeling

When sudyng bone tissue it is important to consider also the remodeling process, since bones optimal response to load is strongly due to the lamellae conformation of cortical bone and trabecular bone. In particular trabecular bone has different trabeculae orientation and thickness in relation to loads applied on the specific bone. An example of optimization to load response is presented in the following fibures for calcaneal bone. In the figures letters from A to E distinguish different groups of lamellae. Two neutral zones are present between groups B and C, subdivided into two parts by vertical lamellae (b), which descend from the thick compact bone at the angle of Gissane (a) present in the roof of the this zone.

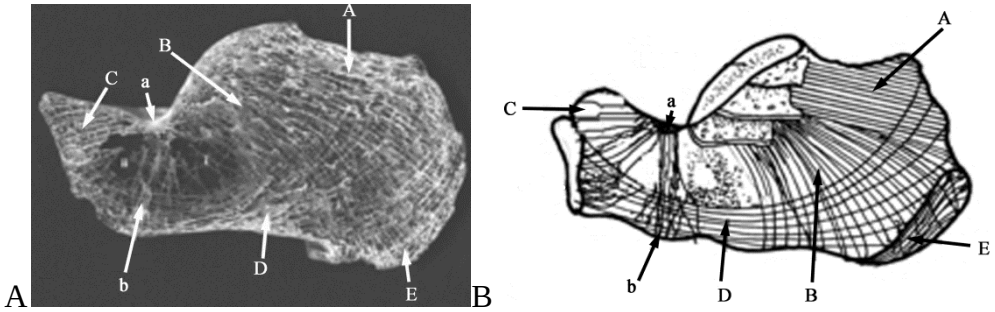

Figure 2.15: Sagittal section of the calcaneus showing various groups of lamellae from MDCT (Multidetector Computed Tomography) image A) and schematic representation B).

The process of bone formation (osteogenesis) involves three main steps:

- production of the extracellular organic matrix (osteoid);
- mineralization of the matrix to form bone;
- and bone remodeling by resorption and reformation.

The cellular activities of osteoblasts, osteocytes, and osteoclasts are essential to the process. Osteoblasts synthesize the collagenous precursors of bone matrix and also regulate its mineralization. As the process of bone formation progresses, the osteoblasts come to lie in tiny spaces (lacunae) within the surrounding mineralized matrix and are then called osteocytes. The cell processes of osteocytes occupy

minute canals (canaliculi) which permit the circulation of tissue fluids. To meet the requirements of skeletal growth and mechanical function, bone undergoes dynamic remodeling by a coupled process of bone resorption by osteoclasts and reformation by osteoblasts.

The 4 Phases of Bone Remodeling

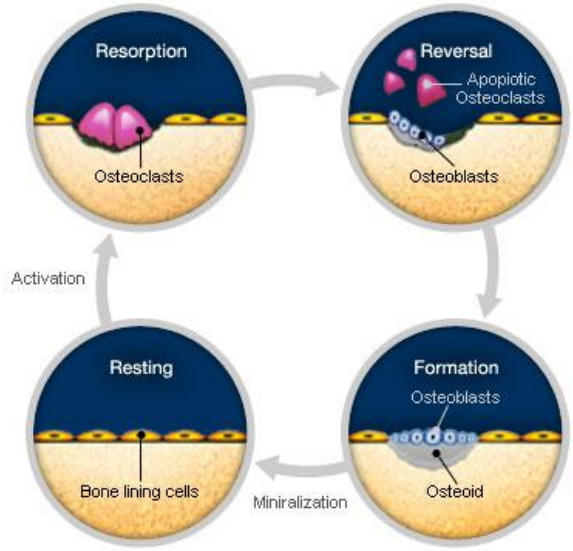

Figure 2.16: The 4 Phases of Bone remodelling process.

- Activation: Resting bone surface is converted to a remodeling surface during the activation phase. Osteoclast precursors are recruited to the bone lining cell layer where they differentiate into mature, active osteoclasts.
- Resorption: Osteoclasts remove both mineral and organic components of bone matrix by generating an acidic microenvironment between the cell and bone surface. The resorbing surface has a scalloped, eroded appearance known as Howship's or resorption lacunae.
- Reversal: Once the osteoclasts have resorbed the mineral and organic matrix, osteoblasts are recruited to the bone surface
- Formation: The removal of old bone by osteoclasts is followed by the formation of new osteoid (in the form of an unmineralized collagen matrix) by osteoblasts. During the mineralization process, hydroxyapatite crystals deposit on the collagen matrix and gradually harden, leading to the formation of new mineralized

2.3.4.1 Cellular Mechanisms of Bone Remodeling

Osteoclasts are specialized cells that resorb bone. Activated osteoclasts secrete acids and collagen-degrading enzymes onto the bone surface, resulting in bone mineral dissolution and organic matrix degradation. It is this process that creates resorption pits. After creating a resorption pit, the osteoclast will either relocate and begin resorption at another site on the bone surface (as shown below), or undergo apoptosis. Electron micrograph of osteoclast and resorption

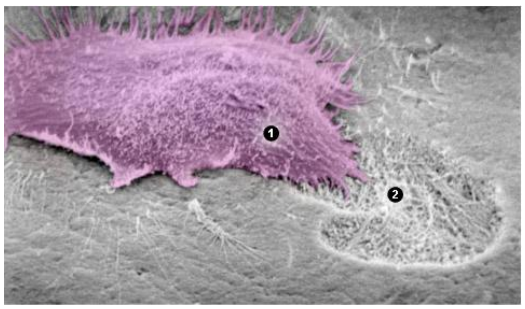

Figure 2.17: In the picture are represented 1. Osteoclast. 2. Bone surface resorbed by osteolclast.

During the reversal process, osteoblasts secrete the organic components of bone—both collagen and noncollagenous proteins—as well as alkaline phosphatase, an enzyme required for mineralization of osteoid. Upon completion of bone formation, osteoblasts either undergo apoptosis or become embedded in the bone matrix as osteocytes and contribute to the regulation of bone remodeling. Mature osteoblasts regulate osteoclasts by producing a protein that is an essential mediator for osteoclast formation, function and survival. In turn, osteoblast activity is regulated by feedback from osteoclasts. Thus, resorption and formation of bone is a carefully orchestrated sequence that involves communication between osteoblasts and osteoclasts via several important intermediaries.

2.3.4.2 The Underlying Cause of Bone Loss

The activities of specialized cells—osteoclasts and osteoblasts—define the balance between bone resorption and bone formation.6 Bone resorption and formation are tightly coupled. Conditions that favor bone resorption over formation lead to a net loss of bone and weakening of the skeleton. Increased osteoclast activity, for example, following menopause, leads to decreased bone mass with each resorption cycle. Over time, this process leads to compromised bone strength and increased risk

of fracture. Trabecular bone, which has a higher turnover as compared to cortical bone, is the most affected. About 80% of the skeletal bone mass is composed of cortical bone. The other 20% is trabecular bone. Increased bone resorption may also lead to thinning of cortical bone and increased cortical porosity. Impairment of trabecular bone architecture leads to compromised bone strength and increased risk of fracture.

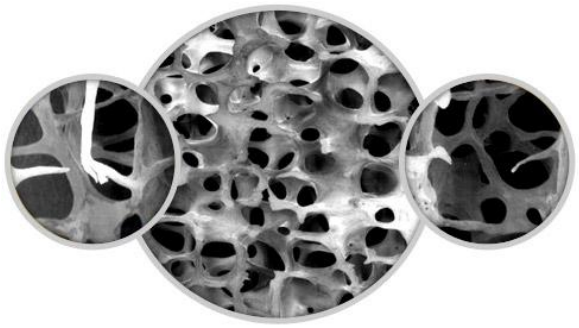

Figure 2.18: Different trabecular bone configurations: central – normal trabecular tissue; left thick trabecular tissue; right thin trabecular tissue.

The figure proposed clearly evidence some of the differences between healty and osteoarthritic trabecular bone. In particular, it is evident how trabeculae presents a reduced section and their structure is less organized and dense.

2.3.5 Biomechanical characterization of bone tissue through experimental tests

When deciding the protocol for the experimental tests is important to remember some aspects of bone tissue, such as the heterogeneity. Factors that could affect experimental results are manifold, just to name a few: the direction of withdrawal, the anatomical site of sampling, the sample preservation before test (dry, wet, frozen), bone mineral density, age of the subject from which the sample is taken. Moreover, the different structures of cortical bone and trabecular bone result in different mechanical properties. Cortical bone is an anisotropic material, meaning that its mechanical properties vary according to the direction of load. An example of how bone mechanical properties are highly variable according to age is proposed in the following table.

AGE (years)							
Property	**10-20**	**20-30**	**30-40**	**40-50**	**50-60**	**60-70**	**70-80**
Ultimate strength (MPa)							
Tension	114	123	120	112	93	86	86
Compression	-	167	167	161	155	145	-
Bending	151	173	173	162	154	139	139
Torsion	-	57	57	52	52	49	49
Ultimate strain (%)							
Tension	1.5	1.4	1.4	1.3	1.3	1.3	1.3
Compression	-	1.9	1.8	1.8	1.8	1.8	-
Torsion	-	2.8	2.8	2.5	2.5	2.5	2.7

Table 2.3: Ultimate strength (MPa) and ultimate strain (%) of cortical bone from the human femur as a function of age.

Cortical bone is often considered an orthotropic material. Orthotropic materials are a class of anisotropic materials characterized by three different Young's moduli E_1, E_2, E_3 according to the direction of load, three shear moduli G_{12}, G_{13}, G_{23} and six Poisson's ratios ν_{12}, ν_{13}, ν_{23}, ν_{21}, ν_{31}, ν_{32}.

Some value for elastic anisotropy of bone are porposed in the following table. The value reference to wet human femoral bone under mechanical testing (Reilly and Burstein, 1975) and bovine femoral bone by ultrasound (VanvBuskirk and Ashman, 1981).

Young's moduli (GPa)			**Shear moduli(GPa)**			**Poisson's ratios (dimensionless)**		
	Human	**Bovine**		**Human**	**Bovine**		**Human**	**Bovine**
$\mathbf{E_{long}}$	17	22	$\mathbf{G_{long}}$	3.6	5.3	ν_{12}	0.58	0.30
$\mathbf{E_{transv}}$	11.5	15	$\mathbf{G_{tr}}$	3.3	6.3	ν_{13}	0.31	0.11
$\mathbf{E_{transv}}$	11.5	12	$\mathbf{G_{tr}}$	3.3	7.0	ν_{23}	0.31	0.21

Table 2.4: Young's Moduli (GPa) ,Shear Moduli (GPa), Poisson's ratio of cortical bone from the human femur and bovine femur.

The stiffness of compact bone tissue depends on the bone from which it is taken. Fibular bone has a Young's modulus about 18% greater, and tibial bone about 7% greater, than that of femoral bone. The differences are associated with differences in the histology of the bone tissue. Bone is elastically anisotropic, i.e. its properties depend on direction.

The mechanical characterization of trabecular bone is even more difficult. The mechanical properties of trabecular bone as a whole are due to the mechanical characteristics of single trabecules and to its highly porous structure. Figure below shows the dependence of the Young's modulus of trabecular bone from bone density.

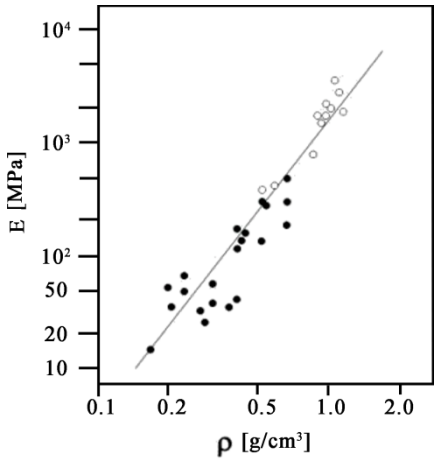

Figure 2.19: Young's modulus of trabecular bone as a function of density of bone. Bone density ρ is expressed in g/cm^3 and Young's modulus E in MPa.

Should be noted that in carrying out the tests and comparison of results is necessary to control these factors, the perspective is not easy to take a fresh sample. In other words, in order to preserve and / or freeze (without altering) the characteristics of the tissue at the time of collection, you need to minimize the time between the extraction and execution of mechanical tests. Therefore, it is appropriate for the removal of tissue are non-existent or reduced to a minimum of machining operations for obtaining the sample to be tested. Should be taken into account in order artifacts from the grip of the testing machine. For example, the clamp that holds the sample can deform causing the sample to reach the first break in the lock preventing the proper assessment of tension and breaking strain which should reach the sample as a whole.

The cortical bone, undergoing physiological stress is not higher than 0.3%, has instantaneous linear elastic mechanical behavior, then returns to the removal of the load in the deformed condition. There is a relationship of direct proportionality between applied stress and resulting deformation represented by the value of Young's modulus E. It 'been studied in the literature that the value of E for bone tissue varies depending on the liquid content of the sample, the age of the person to whom the

sample belongs, as indicated above, the direction of analysis. In addition, the tensile and compressive modulus (E = 25GPa) of the same order of magnitude, but the fabric shows better mechanical behavior in compression rather than tension in relation to its particular microstructure.

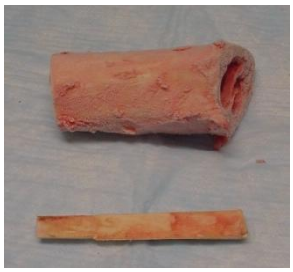

Figure 2.20: Example of a bone sample for a tensile test.

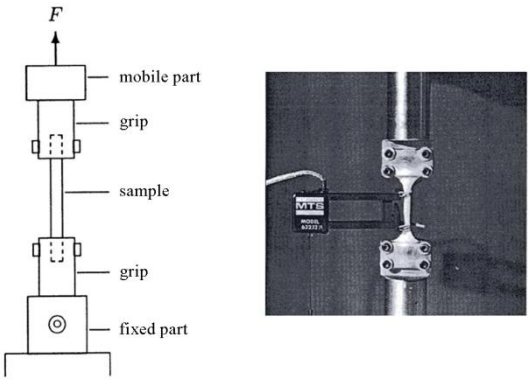

Figure 2.21: Diagram of tensile testing machine (left) and marrow tissue sample under test (right).

The characterization of the relationship between stress and strain occurs through the definition of 9 independent parameters (3 modules of elasticity, shear modules 3, 3 Poisson). Another typical mechanical test are the 3-point-bending (3PB) and the 4-point-bending (4PB).

2.3.5.1.1 Time-dependent mechanical behavior of bone tissue

Analyzing the other hand, the behavior differed over time, there is a clear answer where time-dependent phenomena of creep show, relaxation.e stress dependence of the response as a function of strain rate. Therefore, both data from tests with constant strain rate, and those from creep tests are useful for the determination of time dependent tissue. These considerations suggest that the bone, especially cortical, presents, in the range of physiological strain (lower all'0 .8%), a viscoelastic behavior: it is, however, a non-linear viscoelasticity because the time taken to

recover completely strain (unloading phase) is much broader than necessary to achieve it (loading phase). The viscoelastic behavior is highly dependent on the age of the subject, this varying with the degree of mineralization of the tissue and its component fibers of collagen.

2.3.5.1.2 Test of constant strain rate

The compression tests at constant strain rate (CSR Constant strain rate) are usually made to assess the strength of materials and indirectly reveal the viscoelastic properties, time-dependent. In this experiment, the material initially has no deformation, the deformation is then made to increase linearly over time until there is the breaking of the sample under test. For linear viscoelastic materials is (Lakes 1998):

$$\frac{d\sigma(t)}{dt} = \frac{d\varepsilon(t)}{dt} E(t)$$

So the slope of the stress-strain curve of a linear viscoelastic material is higher the more the higher the strain rate. The value of E (t) decreases over time, then the slope of a stress-strain curve decreases with the deformation. Therefore the effect of viscoelasticity is visible in the stress-strain curve for the concave down and its slope increases with increasing strain rate..

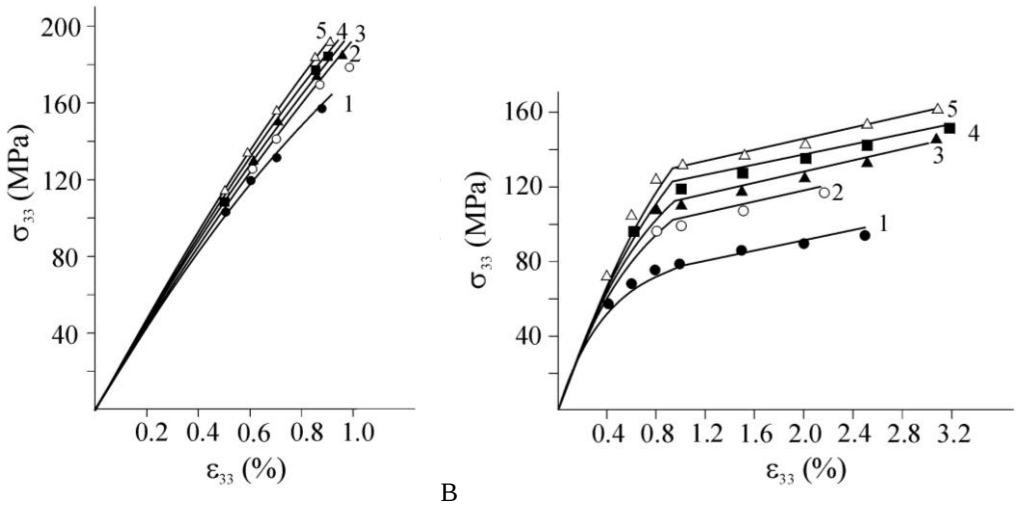

A B

Figure 2.22: stress-strain curves obtained in 2 different conditions of hydratation (2.5% (A), 10.5% (B)), for different strain rates expressed in s^{-1}*):* $\dot{\varepsilon} = 10^{-5}$ *(1),* 10^{-4} *(2),* 10^{-3} *(3),* 10^{-2} *(4),* 10^{-1} *(5).*

The stress-strain curve is nonlinear even if the material is considered to have a linear viscoelastic behavior. Although there is a linear relationship between stress and strain at a fixed time t, the experiment involves a constant strain rate deformation and time varying them simultaneously

2.3.5.1.3 Creep tests

The creep tests are carried out at constant stress in order to observe the progressive deformation of the material under test. The creep tests are used to quantify the behavior of a viscoelastic material, ie the time-dependent response of the sample. The process of creep occurs in a tissue sample when it is subjected to a load imposed so steady. In the phenomenon of creep can be defined:

$$J(t) = \frac{\varepsilon(t)}{\sigma_0}$$

Where ε(t) is the time-dependent deformation and is the applied stress.

In a creep experiment the stress is applied instantaneously to the level set and kept constant and the deformation is measured as a function of time. In linearly viscoelastic materials, the value J (t) is independent of the level of tension imposed. In these materials is seen as a linear proportionality between stress and strain for a certain time point t. The creep curves are generally divided into three regions: primary creep, secondary creep, creep services. The primary is characterized by a decreasing strain rate and follows an initial phase of elastic deformation. The secondary has a constant strain rate and strain rate to balance the structure reorganization, it is then said to create a steady state. The tertiary sector has increased strain rate until failure. The tertiary creep, always, and the secondary, at times, present the phenomenon of harm and nonlinear viscoelasticity.

Both the trabecular bone, cortical bone are subject to the phenomenon of 'creep', and may be permanently deformed beyond a certain threshold of distortion. You can also distinguish between active and creep creep passive. The active creep is achieved by keeping a constant load and measuring the amount of deformation. You can see how, after the initial elastic response, manifests a pattern of deformation increasing function of time and intensity of the applied axial stress. After removal of the load is a recovery of the deformation (creep passive) with return to the undeformed

condition. However, it is possible to observe that in the case of bone as the applied stress is close to that of failure, plus the time required to remove the strain imposed is greater than the time required to achieve this deformation. In fact, imagining to continue the curve 6 (Figure 2.23) to zero is reached for a longer time of 400 min, ie, having spent 200 minutes to cause a deformation of the material requires more than 200 minutes to recover.

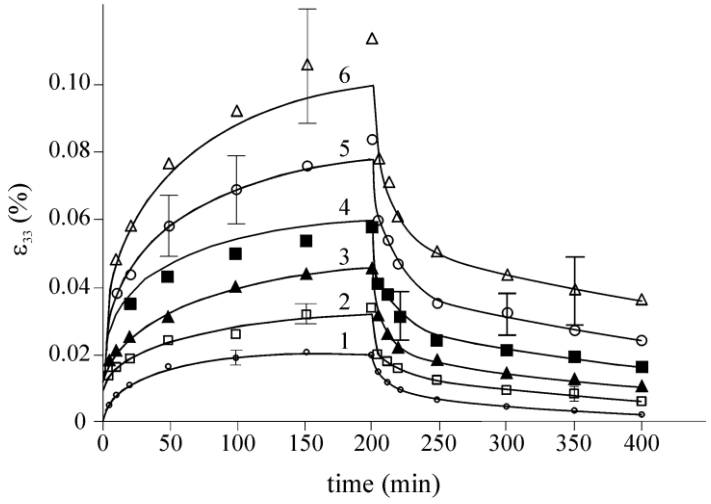

Figure 2.23: Values of active and passive creep as a function of σ / σu: 1) 0.2 2) 0.3, 3) 0.4, 4) 0.5 5) 0.6, 6) 0.7.

Therefore, applied stresss of magnitude greater than about σu / 2 (where σu represents the tensile strength of the material) leave permanent deformation (not equal to those recovered in time to load) and are due to structural damage, with loss of part of property elastic properties of the sample.

2.3.5.1.4 Stress relaxation tests

The test consists in the gradual relaxation in tension reduction of the stress applied to a sample to keep the material at a constant strain. The form of relaxation is given by:

$$E(t) = \frac{\sigma(t)}{\varepsilon_0}$$

With σ(t) time-dependent stress and ε_0 strain level held constant. This type of test is made by reaching the desired level of strain to the material and then keeping it constant, then the load is measured as a function of time. Linear elastic materials

have E(t) independent from the level of deformation and it is only a function of time and stress.

2.4 CARTILAGE TISSUE

2.4.1 Histological characterization of cartilage

Cartilage is a connective tissue with special support functions. The cartilage is a particular tissue of mesenchymal origin characterized by a cellular component surrounded by an extracellular matrix that gives texture to fabric.

The cartilage begins to develop in the fetal period, thereby supporting the first bone in the embryo to form the primitive skeletal structure. With the progress of embryo development begins the differentiation of osteoprogenitor cells that initiate the process of ossification. However, at birth, some skeletal parts are not yet ossified staying temporarily or permanently cartilaginous structures such as the period of growth and development, in the long bones is a cartilaginous region called the metaphyseal region, located between the epiphysis and diaphysis, catering to increasing the length of the bone. In adults, there are some areas of cartilage never replaced by bone tissue such as articular cartilage between the ribs, some parts of the respiratory and ear.

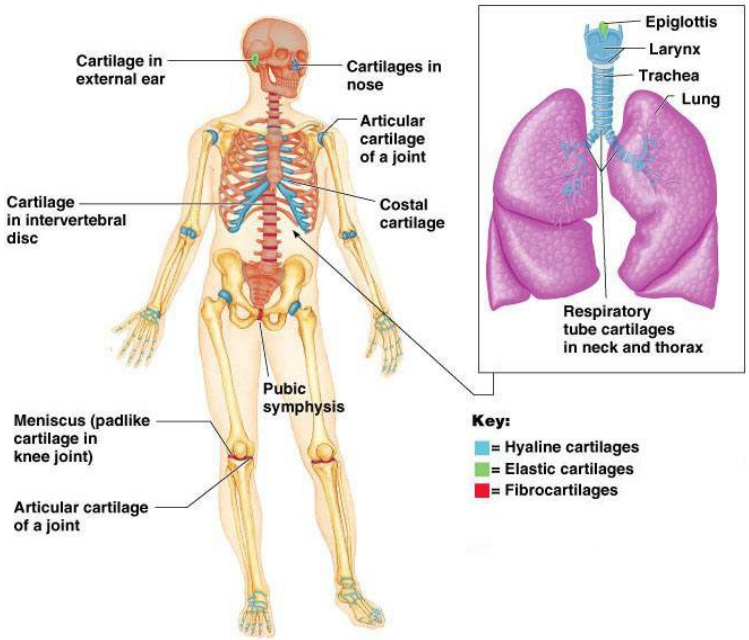

Figure 2.24: *Cartilage types in the body.*

According to the composition and texture of the amorphous component and the fibers contained in it is possible to distinguish the cartilaginous tissue in three types:

- Elastic cartilage
- Fibrous cartilage
- Hyaline cartilage

A very important role is played by the perichondrium. This is a compact layer of connective tissue that surrounds the cartilage and develops from the mesenchyme. It consists of two layers: an outer cells which form the fibrous layer and an inner one of which retain the ability chondrogenic cells still producing chondroblasts, and chondrocytes for tissue growth. Another function of this layer is to provide nourishment to the cartilage as it is not vascularized. As the nutrition of its cells is limited by the distance that nutrients and oxygen must travel to reach the chondrocytes, the cartilage does not reach a significant thickness. Please note that this layer is not present in articular cartilage that are bathed directly by the synovial fluid from which derive the necessary nourishment.

Articular cartilage itself has a hierarhical structure and is also part of a diarthroidal joint which is a composite structure. The nature of the hierarchical structure of both diarthroidal joints and articular cartilage is illustrated in the figure from your text shown below. The top row of the following figure, it illustrates the composite structure of diarthroidal joints which consist of bone, articular cartilage, ligaments, tendons, muscle and the joint capsule. The next level in this schematic figure indicates in more detail the actual bearing surface of the joint, in this case the knee joint as evidenced by the presence of meniscus, but similarly it happens also in ankle joint.

The scale is between 100 microns (.1 mm) and 1 cm. At this point the articular cartilage may be viewed as a solid homogeneous material. In the next level of structure, called the microstructure between .0001 mm (.1 microns) and .1 mm (100 microns), we see the existence of the structural features of articular cartilage including the chondrocytes (cells that make cartilage matrix) and the organization of the type II collagen fibrils.

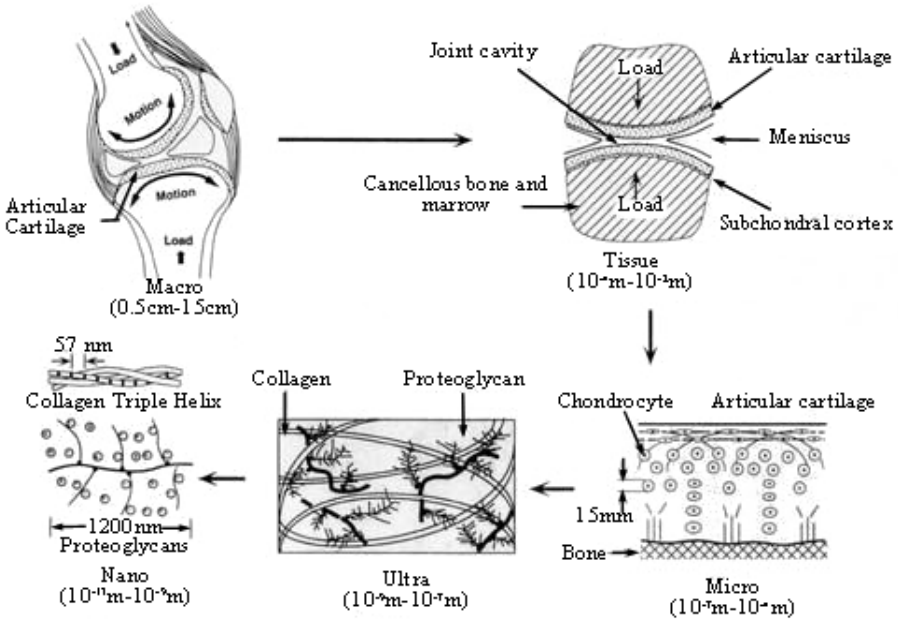

Figure 2.25: Scheme fo the structure of articular cartilage from a Macro to a Nano view considering the hyerarchical structure.

The organization at this level can actually be divided into four zones: 1) the superficial tangential zone (10-20% of the cartilage thickness, 2) the middle zone, 60% of the cartilage thickness, 3) the deep zone, 30% of the cartilage thickness, and 4) the calcified cartilage zone where the cartilage interfaces with the bone (see Figure 2.26).

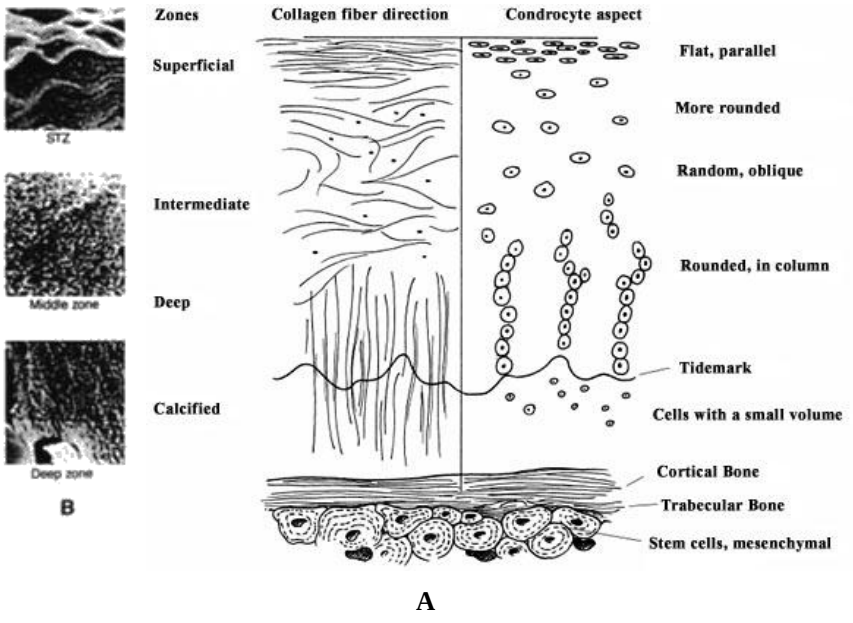

Figure 2.26: Schematic representation of collagen and condrocyte organization in cartilage.

The zones contain different collagen organization as well as different amounts of proteoglycans.

The superficial or tangential zone contains the highest collagen content, about 85% by dry weight. In addition, the collagen fibrils are oriented parallel to the joint surface, indicating that the purpose of this zone may be primarily to resist shear stresses. The amount of collagen decreases in each zone moving closer to the tidemark, dropping to 68% in the middle zone. Moreover collagen changes its configuration from a central area of a cartilage layer to a more peripheral area.

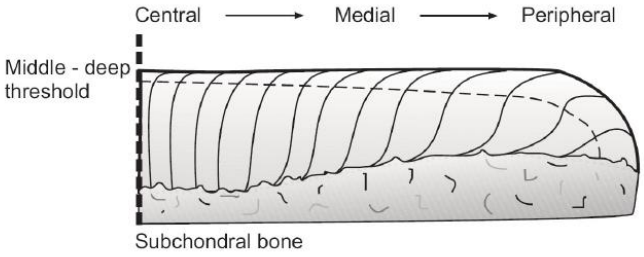

Figure 2.27: Schematic representation of a normal collagen architecture from central area to peropheal area. Additional laminae are visible depending on the location in the joint.

Collagen fibers are structural elements in articular cartilage. The structure of the collagen network is thought to be related to the mechanical stability of the tissue (Aspden and Hukins, 1981; Minns and Steven, 1977). The surface layer of cartilage is like the wall of a pressure vessel that is designed to withstand the swelling pressure in the tissue; the collagen fibers are oriented to achieve an optimal tangential stiffness of the tissue. In the deep layer, collagen fibers are oriented, likely, to optimize (a) the ties to the underlying calcified tissue and (b) the stiffness normal to the contact surface. The intermediate layer allows for a change in the orientation of the collagen fibers without discontinuity. Chondrocytes have different shapes and different volumetric concentrations in the different layers of articular cartilage. A given chondrocyte shape produces different effects on the global material properties, depending on the structure of the collagen fiber network. The shape and volumetric concentration of chondrocytes in articular cartilage appear to be related to the mechanical stability of the matrix (Wu et al. 2002).

In the following paragraphs more details are presented on biomechanical aspects related to the microstructure and the macrostructure of cartilage.

2.4.1.1 Cellular components

2.4.1.1.1 Chondrocytes

Chondrocytes are quiescent cells derived from chondroblasts, was secreting. Is contained in lacunae of the extracellular matrix such capsules basophils. Their morphology and distribution is a function of the level of depth within the cartilage. In the intermediate zone appear rounded, enclosed in capsules and isolated, moving towards the perichondrium are increasingly flattened with major axis parallel to the surface and aggregated. These groupings are made for those groups isogenic cell mitosis and are characterized by three to five cells per capsule. Moreover, since the matrix is jerky, while separating the cells completely go away.

2.4.1.2 Extracellular matrix

The extracellular matrix consists of an amorphous component (eteropolisaccaridi) or ground substance, a fibrillar component (fibrous proteins) and high amount of interstitial fluid (mainly water) that makes the matrix well hydrated. It consists of several channels that allow diffusion of nutrients, oxygen and metabolic products. Can be divided into three main areas:

- Territorial, around the capsule basophil, characterized by an abundance of proteoglycans;
- Inter-territorial, characterized by a smaller number of rich proteoglycans and collagen;
- Pericellulare capsule, surrounds and protects the chondrocyte lacunae of mechanical stress.

2.4.1.3 Amorphous components

The component or amorphous ground substance consists principally of water (80% of the total weight), mineral salts and proteoglycans.

Proteoglycans are present mainly in the territorial matrix, representing 30-40% of the dry weight of cartilage. They consist of a small part of a protein component and, in about 90%, by glycosaminoglycans (GAGs). In turn, the proteoglycan aggregate with each other m with higher$\mu$to form macromolecular complexes of approximately 4

molecular weight (108 Da). These complexes bind, via binding proteins, hyaluronic acid filaments to form aggregates such as Aggrecan.

Inter-territorial areas you may notice the presence of glycoproteins in nature saccharidic protein. These, too, along with proteoglycans, contribute to give greater strength to the cartilage.

The outstanding hydration and compressive strength of cartilage are mainly due to the presence of proteoglycans to the stage of gel. The high level of hydration is explained by the hydrophilic nature of GAGs (negatively charged). The volume that would occupy the proteoglycans in solution, in relation to their concentration in the amorphous substance, would be much higher due to the forces of repulsion between the protein linked to these GAGs. This expansion is restricted by the network of fibers and collagen that are opposed to this movement. Regarding the compressive strength, this depends on the interactions between proteoglycans, collagen and interstitial fluid. Aggrecan in covalent bonds with glycosaminoglycans on them create a high density of negative charges. These positions are reversed by the high hydration of the interstitial fluid. But when the cartilage is subjected to compression, the liquid tends to flow from the grating (similar to a sponge). The negatively charged GAGs, therefore, tend to repel against the force applied to compacting and confer rigidity to the tissue is therefore dependent on the content of GAGs themselves. Like a sponge, the stiffness should be assessed according to compression rate.

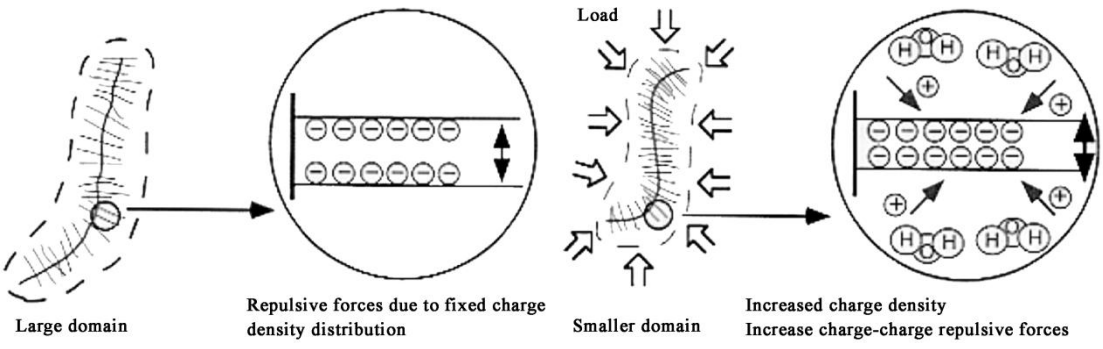

Figure 2.28: Schematic explanation og the effect of GAGs' negative charge on interstitial fluid present in the extracellular matrix.

The higher the strain rate the higher the resistance offered by the fabric as the interstitial fluid, being unable to flow faster, increases the resistance of the fabric.

2.4.1.4 Collagen components: configuration and mechanical behaviour

Collagen is the most abundant protein in the human organism. It is primarily responsible for the tensile behaviour of soft connective tissues, and in particular, tendons and ligaments. Collagen is characterised by a strongly hierarchical organization: small tropocollagen molecules link together to form fibrils, which in turn give rise to fibres and fibre bundles. The primary structure of the tropocollagen molecule consists of an uninterrupted sequence of about 300 Glycine-X-Y triplets, where X and Y are frequently represented by proline. During post-translational modification, hydroxylation, oxidation and glycosylation processes of amino acid residues usually occur (Ottani V. et al., 2002). The triplets organize themselves into a right-handed α-helix secondary structure and the conformational arrangement is defined by a left-handed helix tertiary structure. The quaternary super-structure of the tropocollagen molecule is obtained by linking three helixes by hydrogen bonds (Figure 2.29). The molecule is approximately 300 nm in length and 1.5 nm in diameter (Ottani V. et al., 2002). Tropocollagen molecules are highly reactive and undergo spontaneous fibrillogenesis. For collagen types I, II, III, V and XI, tropocollagen molecules link together by inter-molecular covalent bonds to form fibrils (Figure 2.30), that are characterised by diameter and length ranging between 20 to over 280 nm (Silver F.H. et al., 2003) and 5 μm to over 1 mm respectively (Kadler K.E. et al., 1996). Possible sites of cleavage by chemomechanical caries removal reagents by degradation of glycine or hydroxyproline are indicated by red arrows. b, triple helix. Sites of cleavage by degradation of intra-molecular cross links are shown by red arrows. c, tropocollagen molecules link together to form fibrils and inter-molecular cross links are shown by arrows in the following figure.

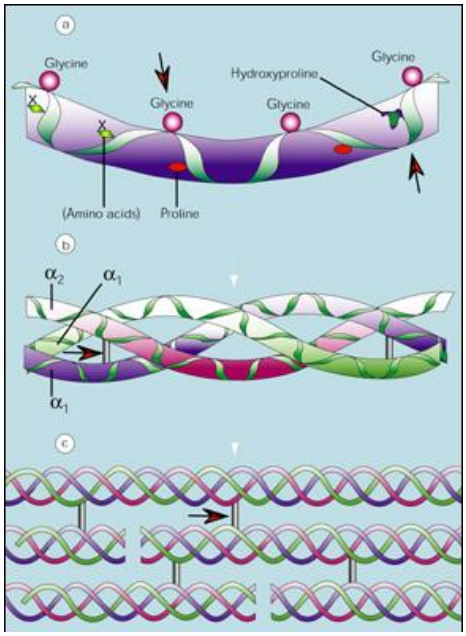

Figure 2.29: Schematic representation of polypeptide chain.

Visualization of collagen fibrils by Transmission Electron Microscopy (TEM) or Atomic Force Microscopy (AFM) shows that tropocollagen molecules organize themselves in a cross striated structure with a characteristic 67 nm repeat (Silver F.H. et al, 2003), known as the *D*-period. Adjacent repeat elements are separated by a "gap" zone (Ottani V. et al., 2002). Each repeat element is composed of parallel tropocollagen molecules linked together by covalent bonds.

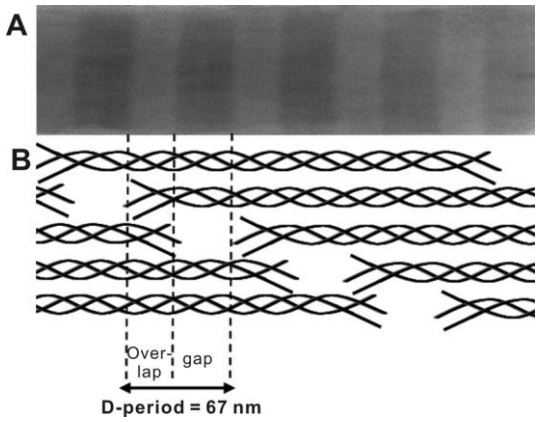

Figure 2.30: (A) Transmission electron microscopy (TEM) image of single fibrils with the 67 nm D-period visible. (B) Schematic representation of the two-dimensional axial arrangement of collagen molecules in a microfibril.

Repeat elements are joined by further covalent bonds passing through the "gap" zone (see Figure below).

This organization is known as "*D*-period structure" or the "Hodge-Petruska" model (Petruska J.A. and Hodge A.J., 1963). The D-period originates from the staggered aggregation of the collagen molecules in microfibrils.

Proteoglycans, most often decorin (Redaelli et al., 2003; Raspanti et al., 1997) and FACIT (fibril associated collagen) filaments (Eyre D.R. et al., 2004), serve to form inter-fibrillar bonds. Inter-fibrillar bonds tie adjoining fibrils together to form fibres and seem to have a definite role in guaranteeing the mechanical coupling of fibrils.

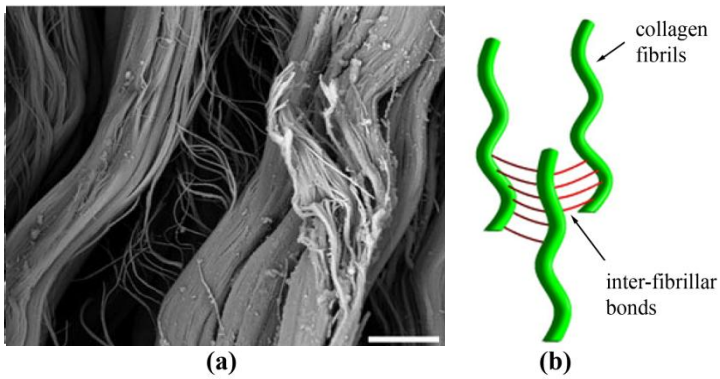

Figure 2.31: Proteoglycans and collagen filaments enable bonds between collagen fibrils. (a) SEM (the horizontal field of view spans 20 µm), from Price et al., 2009, and (b) schematic representation

As mentioned, collagen reinforcing elements can assume different arrangements, such as fibrils, fibres or fibre bundles (see Figure 2.32).

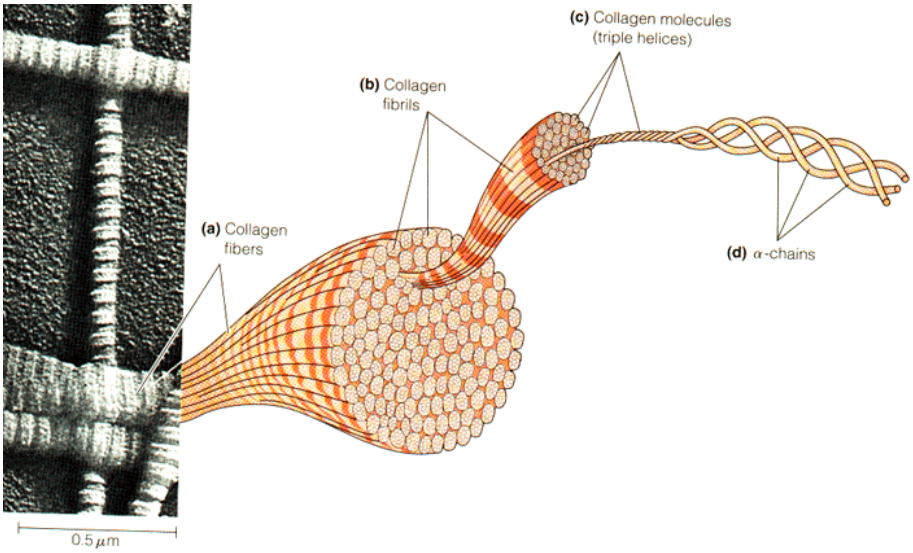

Figure 2.32: The organization of collagen in fibres bundles.

Within soft tissue, collagen fibrils show a typical crimped configuration in the unstrained state, referred to as crimped, that is characterised by helical nature with periodicity of between 10 and 100 μm, depending on the particular tissue type (Freed A.D. and Doehring T.C., 2005). Because of its hierarchical organization, collagen reinforcing elements usually show a complex mechanical response that can be evaluated by analysing the mechanical behaviour of the components and the interactions which occur when tensile loads are applied.

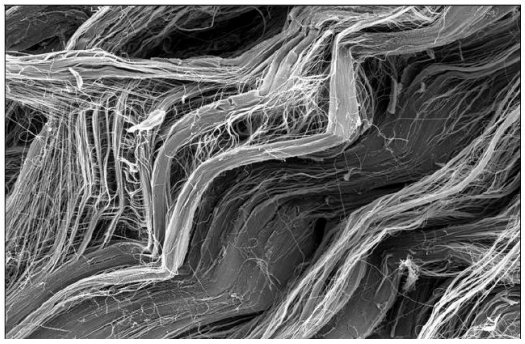

Figure 2.33: Scanning Electron Microscopy (SEM) acquisition of the typical crimped configuration of collagen fibrils in the unstrained state.

Experimental studies performed by Sasaki N. and Odajima S. (1996) on specimens from Bovine Achilles Tendon have made it possible to evaluate the stress-strain behaviour of tropocollagen molecules. Linear elastic behaviour was assessed using a 3 GPa elastic modulus. The elastic modulus of the tropocollagen molecule has been investigated by other researchers (Cusack S. and Miller A., 1979; Nestler F.H.M. et al., 1983; Hofmann H. et al., 1983), in samples from different animal species and anatomical sites, demonstrating similar results (ranging between 3 and 5 GPa).

A collagen fibril is a collection of tropocollagen molecules linked together by covalent bonds. The Hodge-Petruska model can be applied to define the micro-structural rearrangements which occur within a collagen fibril when it is stretched along its principal direction.

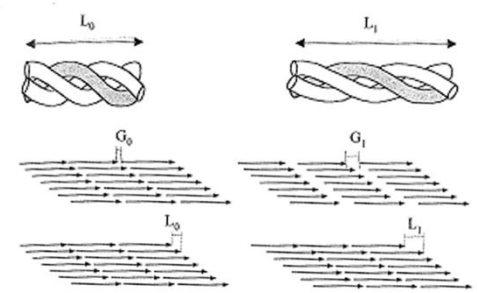

Figure 2.34: Hodge-Petruska models of a collagen fibril (a) without and (b) with strain. Stretching of a collagen fibril induces elongation of tropocollagen molecules (arrows represent arrays of molecules), increase in the length of "gap" zones and relative slippage of molecules.

Many deformation mechanisms are usually involved including elongation of tropocollagen molecules (Sasaki N. and Odajima S., 1996), increase in the length of "gap" zones and relative slippage of laterally adjoining molecules along the fibril axis (Fratzl et al., 1997) due to the stretching of the triple helixes of collagen or the cross-link between helixes (Tang et al., 2009).

The stress-strain behaviour of an uncrimped collagen fibril was investigated by Sasaki N. and Odajima S. (1996). A linear relationship between stress and strain is observed in tropocollagen molecules and uncrimped collagen fibrils and a 400 MPa elastic modulus was obtained, (Freed A.D. and Doehring T.C., 2005; Redaelli et al., 2003). The difference between the stiffness of tropocollagen molecules and collagen fibrils is determined by the larger number of deformation mechanisms acting within fibrils (Gautieri et al., 2011). In contrast to tropocollagen molecules and collagen fibrils, the tensile behaviour of collagen fibres and collagenous tissue is non-linear (see the following Figure).

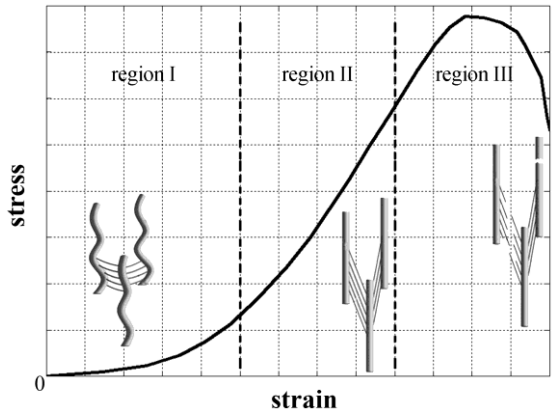

Figure 2.35: Mechanical behaviour of a collagen fibre.

The complex micro-structural arrangement of collagenous tissues is responsible for the non-linearity of the mechanical response, with regard to the crimped configuration of collagen fibrils and the orientation of inter-fibrillar bonds in the unstrained state. The stress-strain curve can be subdivided into three main regions. In the first region (the toe-region), collagen fibres extend, carrying load as an uncoiling spring. The material undergoes a progressive increase in stiffness due to the uncrimping of fibrils and re-alignment of inter-fibrillar bonds in the direction of loading. In region II (the quasi-linear region), collagen fibrils are completely uncrimped and inter-fibrillar bonds are predominantly aligned along the direction of loading (Redaelli A. et al., 2003; Reese et al., 2010). The material stiffness value is almost constant and reaches its peak. When strain exceeds a specific limit, damage phenomena develop (region III or damage region). Collagen fibrils and inter-fibrillar bonds progressively breakdown and the material stiffness value decreases until the tissue fails (Natali A.N. et al., 2004b; Natali A.N. et al., 2005). Because of the many deformation mechanisms taking place in collagen fibres, their stiffness is not constant and the value is lower then that of collagen fibrils. In the toe-region and the quasi-linear region, the elastic modulus of collagenous tissue falls in the range of 10s and 100s MPa respectively (Freed A.D. and Doehring T.C., 2005).

2.4.1.5 Elastic components: configuration and mechanical behaviour

Elastic fibers are a fibrous proteins found in large amounts in tissues such as the elastic walls of the aorta, skin, ligamentum Nuchae, etc.. The elastic components are thinner than the collagen components. they are branched and unite with one another , forming an irregular network. Elastic fibers constist of two components: an amorphous central region containing elastin suttounded by a sheath of 14nm tubular microfibrils (Yang L., 2008).

The amino acid composition of elastin resembles that of collagen in that elstin is rich in glycine (Gly) and proline (Pro). Differences include greater quantities of valine (Val) and alanine (Ala) along with small amounts of hydroxyproline and no hidroxylysine.

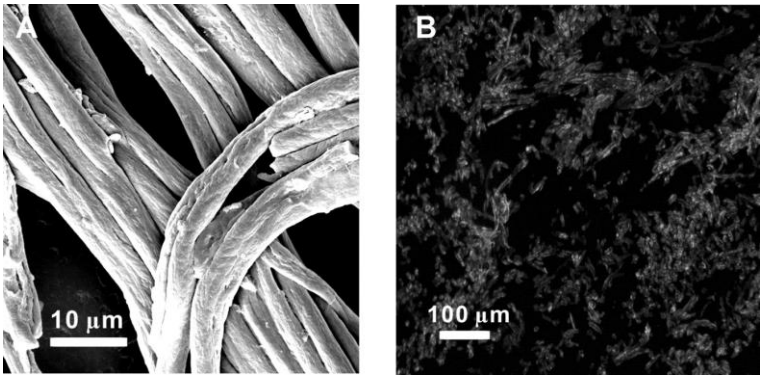

Figure 2.36: (A) SEM image of elastic fibers with diameters in the range of 3 to 5 µm. (B) Fluorescence microscope image of immunostained fibrillin-microfibrils in elastic fibers. From Yang L., 2008.

Elastin contains two unsual amino acid, desmosine and isodemsmosine, formed by covalent reactions among 4 lysine (Lys) residues (Junqueira et al., 1986). These are organized in two repetitive sequences: Val-Pro-Gly-Val-Gly and Gly-Val-Gly-Val-Gly. Desmosine and isodesmosine need to be synthesized by a particular enzyme, lysyl oxidase, that contains copper.

Elastin molecules are joined together by covalent bonds to generate an extensive cross-linked network. Because aech elastin molecule in the network can expand and contracts as a random coil, the entire network can stretch and recoil lije a rubber. The effectively cross-links elastin and is thought to account for the rubberlike qualities of this protein. Through this structure and its numerous links, elastic fibers are capable of stretching to one and one-half times their length, yield easily to very small traction forces but return to their original shape when these forces are relaxed. Looking at the tensile stress-strain diagram for elastin, it is clear its high extensibility.

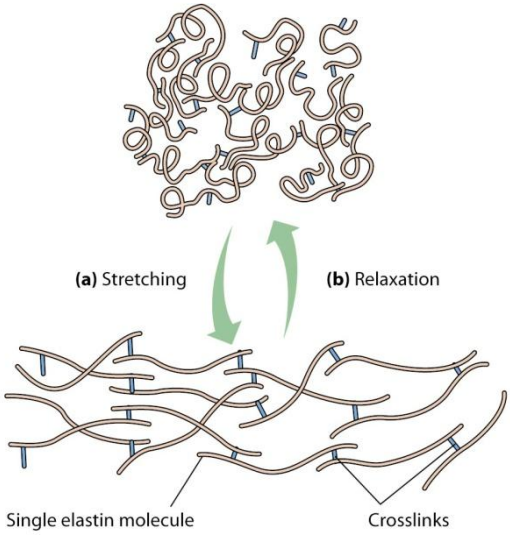

Figure 2.37: Schematic explanation of stretching and relaxation of elastin molecules.

The behavior is elastic deformation. Loading and unloading do leading to two different curves, showing the existence of an ebìnergy dissipation mechanism in the material; but the difference is small (Fung, 1993). Moreover, the elastin fibers are intermingled with the collagen fibers, with low elasticity, limiting the deformation to prevent tearing of the tissues.

2.4.1.6 Ground substance: configuration and mechanical behaviour

The amorphous intercellular ground substance is colorness, transparent and homogeneous. It fills the space between cells and fibers of the connective tissue. The ground substance is a viscous gel mainly composed of an electrolytic water solution and highly negatively charged proteoglycans (PGs). The water solution behaves as a pore fluid within the solid skeleton of the extracellular matrix and dissolved ionic species are mainly sodium Na^+ cations and chloride Cl^- anions. Proteoglycans are long molecular structures, developing along an axis made of hyaluronic acid (Figure 2.39). On that axis are laterally attached other proteins (aggregans) structured around their own axis. Along this axis are attached in turn threads of amino-acids, called glycosaminoglycans (GAGs). The basic structure of GAGs is made by disaccharide units containing a uronic acid and an amino-glycan. The uronic acid displays a negatively charged carboxyl COO^- and the amino-glycan displays at least one sulphate SO_3^-. The two main GAGs that compose proteoglycans are chondroitin-

sulphate with valence -2 and keratin-sulphate with valence -1. Because of the high water content of ground substance, proteoglycans are hydrated and electroneutrality is ensured by sodium cations (Loret B. and Simoes F.M.F., 2004).

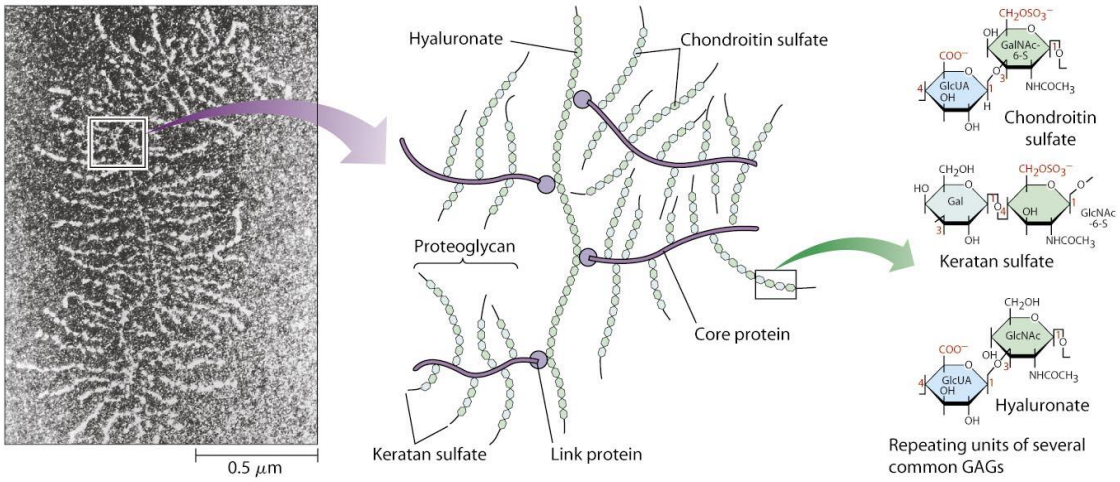

Figure 2.38: SEM micrograph and schematic representation of proteoglycans structure.

The compressive properties of cartilage are partly provided by the proteoglycans that resist compression because GAGs repulse each other due to their negative charges (Figure 2.40a). The presence of cations Na^+ shields the negative charges of the PG, and the mutual repulsive forces decrease with increasing sodium concentration (Loret B. and Simoes F.M.F., 2004). Shielding results in decreasing macroscopic compressive moduli when the salt content increases (Figure 2.40b) (Eisenberg S.R. and Grodzinsky A.J., 1985; Dean D. et al., 2006).

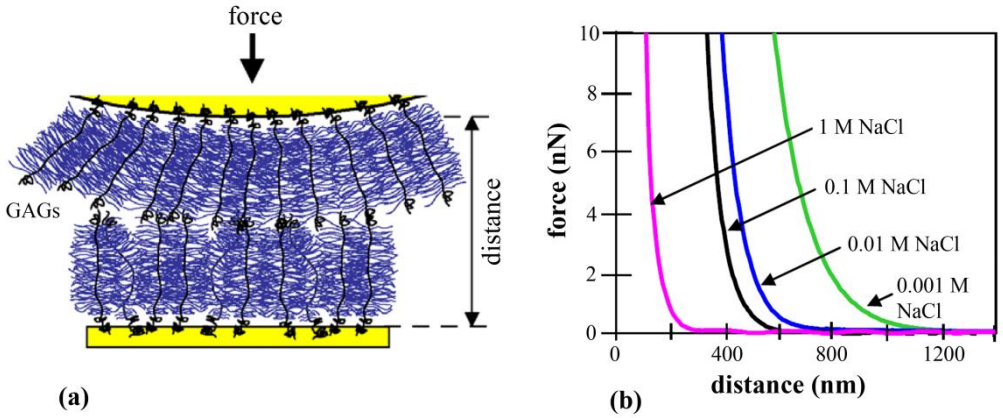

Figure 2.39: Compressive mechanical behaviour of glycosamminoglycans in NaCl solutions. (a) Schematic representation of the experimental setup and (b) experimental results for different concentrations of NaCl. From Dean D. et al., 2006.

Time-dependent mechanical properties of soft biological tissue are strongly influenced by the fluid fluxes that the ground substance undergoes when external loads are applied. Fluid flux phenomena depend on the rheological behaviour of the ground substance itself. It has been suggested (Szwajczak E., 2004) that solutions of biopolymers, such as proteoglycans, are able to organize themselves as liquid crystal polymers (LCPs).

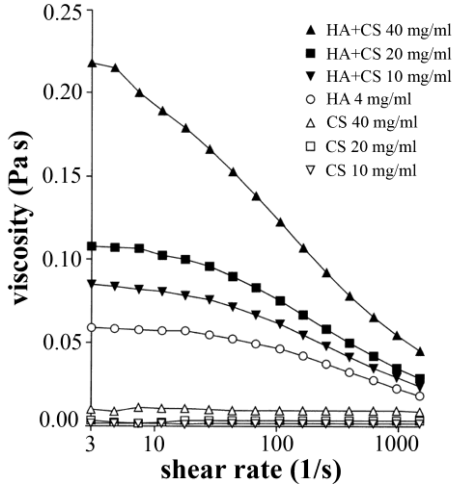

Figure 2.40: Effects of concentration of chondroitin sulphate (CS) and hyaluronic acid (HA) on the viscosity of the water solution at various shear rates. From Nishimura M. et al., 1998.

LCPs behave as non-Newtonian fluids and their viscosity depends on the strain rate (Szwajczak E., 2004). In the case of soft tissue ground substance, this behaviour is determined by the combined action of GAGs and hyaluronic acid (Nishimura M. et al., 1998).

2.4.2 Hyaline Cartilage

In general cartilage is subdivided in three cathegory in consideration of the amount of fibers, cells, liquid phase and the organization of the different components. There are: elastic cartilage, fibrous cartilage and hyaline cartilage.

The elastic cartilage has a structure similar to hyaline. The difference between the two is due to the fact that the elastic cartilage is characterized by a lower amount of intercellular substance and large amounts of elastic fibers associated with collagen II fibers, which give greater flexibility and elasticity. These fibers form a three-dimensional network and are thicker and abundant in the central portion than in the peripheric areas.

This cartilage is particularly present in the ear canal, ear, larynx and bronchioles.

Figure 2.41: cartilage, P = perichondrium, FE = elastic fibers.

The peculiarity of the fibrous cartilage is the large amount of fiber bundles of collagen. Apparently it is very similar to a dense connective tissue and is often in continuity with that. The organization of the collagen fibers depends on the anatomical site, for example, the pubic symphysis are twisted beams along different directions, forming circular rings in the intervertebral discs.

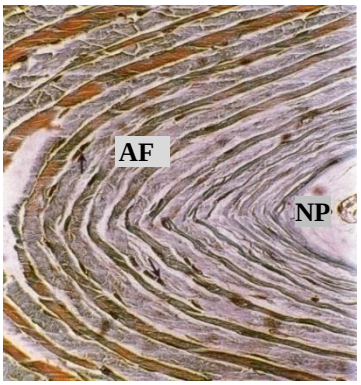

Figure 2.42: Cross section of disk inervertebrale, AF = fibrous ring, NP = nucleus pulposus.

Hyaline cartilage (from the greek hyalos, glass) is so called because it appears transparent and translucent. It is most common in the human cartilage and in the fetus, the skeleton is primitive. It is also characterized by an amorphous component and a rich proteoglycans rich in fibrillar collagen II.

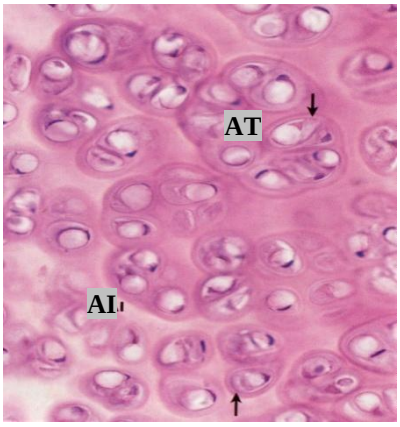

Figure 2.43: hyaline cartilage, AI = inter-territorial areas, AT = geographical areas, arrow = proteoglycan.

Articular cartilage covers the surfaces of skeletal diartrosi and is devoid of perichondrium. The trophic function is attributed to the synovial fluid in contact with it. Due to its intracellular component, the high presence of water, the surface smooth and the synovial fluid, the cartilage allows the joint to withstand pressure from various directions and to make joint movement without friction.

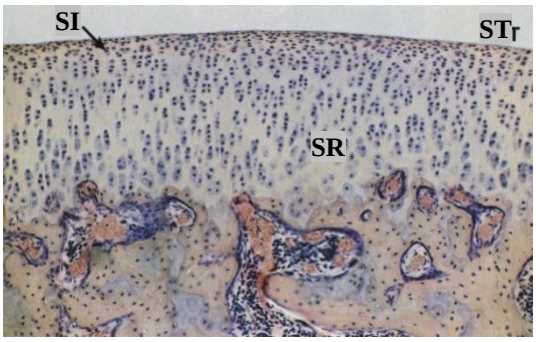

Figure 2.44: articular cartilage, ST = tangential layer, IS = intermediate, SR = radial artery.

2.4.3 Biomechanical characterization of cartilage tissue through experimental tests

Consider now the articular cartilage that lines the surfaces of skeletal joints. About 80% of the weight of articular cartilage is due to the presence of water. With regard to the weight of the dehydrated cartilage is to 30% due to proteoglycans, about 60% of collagen. The articular cartilage has a variable structure depending on the distance from the surface adjacent to the joint cavity. In particular we can identify

four areas that differ from each other in density, morphology of the cells contained, orientation of collagen fibers, proteoglycan concentration and water content. Moving from the articular surface to subchondral bone, therefore, we find a tangential zone, an intermediate zone, a deep zone and finally a zone of limestone.

The superficial zone of articular cartilage in particular may be important for engineering of layered tissues due to the unique role that superficial chondrocytes play in joint lubrication (Jay et al., 2001; Schumacher et al., 1994), its biomechanical function as a tension resisting diaphragm (Meachim and Stockwell, 1979) and its distinctive proliferative and biosynthetic response to mechanical stimuli (Lee et al., 1998, Huber et al. 2000). Studies that were undertaken to further clarify the unique role of the superficial zone thus far have concentrated on cell shape (Hunziker et al., 2002; Jadin et al., 2005), cell density (Bywaters, 1937; Hunziker et al., 2002; Jadin et al., 2005; Quinn et al., 2005; Stockwell, 1971), cytoskeletal organization (Kim and Spector, 2000), growth-related changes in the bovine chondrocyte organization (Jadin et al., 2007), single cell mechanical properties (Jurvelin et al., 1996), gene expression (Darling et al., 2004; Jay et al., 2001; Khan et al., 2001; Schumacher et al., 1994), and metabolism (Eger et al., 2002). While it is widely accepted that the organization of human chondrocytes of the radial zones occur in vertical columns and the transitional zone in small "random" groups (Aydelotte and Kuettner, 1988; Brighton et al., 1984; Kuettner et al., 1991), it remains unclear how the human chondrocytes of the superficial zone are organized.

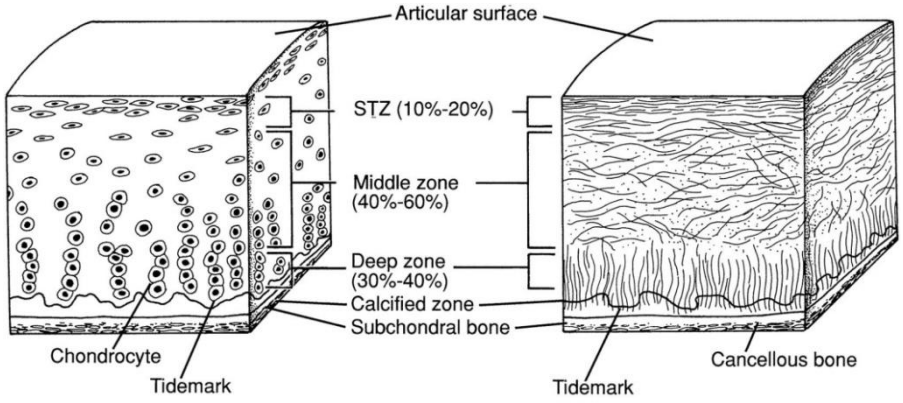

Figure 2.45: Structural zones of articular cartilage.

- Superficial zone (SZ) is the area in direct contact with the joint cavity that contains synovial fluid and represents about 10% of the total thickness. In this zone the

collagen fibers runs parallel to the surface, the proteoglycan concentration is low and the water content is the highest among the four areas.

- Middle zone (MZ) represents approximately 50% of the total thickness and consists of a high concentration of collagen, almost 70% of dry weight. Collagen fibers, in contrast to its previous state, do not grow along preferential directions. The percentage of water present is less than the area above and increases the proteoglycan. The chondrocytes are in spherical isolated and encapsulated.
- Deep layers (DZ): 30% of the total thickness. In this area the concentration of proteoglycan is high while the water content is lower than the previous layer. Contrary to the first layer, the collagen fibers in lower concentration than the previous areas, are oriented perpendicular to the bone surface.
- Calcified layer: is the most subtle and connects the cartilage subchondral bone. The dividing line between the two tissues is called the tidemark and is crossed by the collagen fibers of this layer which must be anchored directly into the bone.

cartilage zone	% water content	% collagen content (dry weight)	% proteoglycan content (dry weight)
superficial zone	80	86	15
medial zone	70	76	25
deep zone	60	67	20

Table 2.5: Distributions of cartilage components along the depth of cartilage layer.

One of the most important components of cartilage tissue are collagen fibers and water. These are the components that mostly affect biomechanical behaviour of cartilage and these should be taken into account when testing cartilaginous tissue.

2.4.3.1 Characterization of cartilage biomechanics behavior with experimental tests

Mechanical properties of articular cartilage can be characterized by determining the load-deformation behaviour of the tissue. For this purposes three different commonly accepted test procedure: indentation, unconfined and confined compression tests.

2.4.3.1.1 Indentation test

Indentation tests is one of the most used to identify mechanical properties of articular cartilage (Hayes et al., 1972) and to assess its viability (Broom and Flachsmann, 2003). There is a wide variety of indentations tests and their possible applications. First of all, indentation tests can be classified with respect to the type of indenter used (cylindrical flat-ended, spherical, etc.). In the simplest case of cylindrical indenter, the contact area is supposed to remain constant during the indentation process, and only two mechanical variables, namely, the contact force, and the indenter displacement, can be recorded as functions of time during the depth sensing indentation (Argatov and Mishuris 2011). Indentation test is possible in situ or in vivo with arthroscopic probes but it is invasive (Vasara et al. 2005).

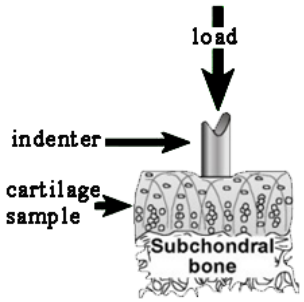

Figure 2.46: During indentation, the sample is compressed with a plane-ended or spherical ended, impermeable or permeable indenter.

In a study by Brown et al. (2007) a disk of articular cartilage from bovine patellae is tested with an indenter at different loading rate. In particular normal
bovine patellae were harvested from prime oxen within 24 hours of slaughter, wrapped in a 0.15M saline soaked cloth and stored at -20°C. Prior to treatment, the joints were thawed in saline, sectioned into 20 x 20 mm samples. The thickness of the cartilage-on-bone specimens were measured with a digital linear variable displacement transducer (LVDT), embedded in Palapress (Heraeus Kulzer GmbH & Co. Hanau, Germany) dental acrylic and mounted in stainless steel sample holders. Care was taken to ensure that the cartilage remained hydrated during this process. Each sample was then placed in saline for at least 90 minutes. Before testing, the sample height was remeasured to ensure that its thickness had recovered to that prior to preparation. Normal samples (18 samples) were subjected to compressive loading to 33% strain at loading rates of 0.1 s-1 to represent the usual rate of loading in the clinical environment (Franz et al. 2001), and compare the results to those obtained at

0.025 s-1 to provide an insight into the way that different rates of loading might determine the outcome of an indentation process. The loads were applied via a 4 mm diameter plane-ended circular indenter in the centre of the sample area.

Samples were unloaded and allowed to recover for 2 hours in saline between tests and checked to ensure that full thickness was regained. The stress-strain behaviour of cartilage was obtained from the load-displacement. By taking geometry into account we allow a more reliable parameter for cross comparison than the Reaction Force-Displacement measurement alone, as the geometry of the specimen, particularly thickness, will affect their deformation characteristic (Hayes et al. 1972; Töyräs et al. 2001; Zhang et al. 1997).

Results are reported in the following figure for the average results of normal cartilage, the stiffer normal cartilage and the softner normal cartilage in the two different loading rate.

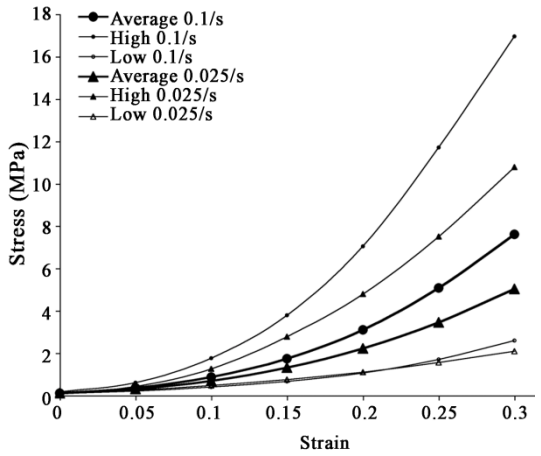

Figure 2.47: Results for indentation test of normal cartilage at different loading rate to a 33% strain.

Mechanical test results from the indentation of normal cartilage-on-bone samples showed a large variation stiffness between subject.

This has also been observed in previously published in vivo (Vasara et al. 2005) and in vitro (Broom & Flachsmann 2003; Kempson 1982) investigations.

A change in the loading rate produced a further variation in mechanical behaviour in accordance with other work by Oloyede et al (1992). In the same work by Brown et al. also degraded cartilage was tested with indentation test at two different loading rate. Results are reported below for the loading rate of 0.1/s and 0.025/s.

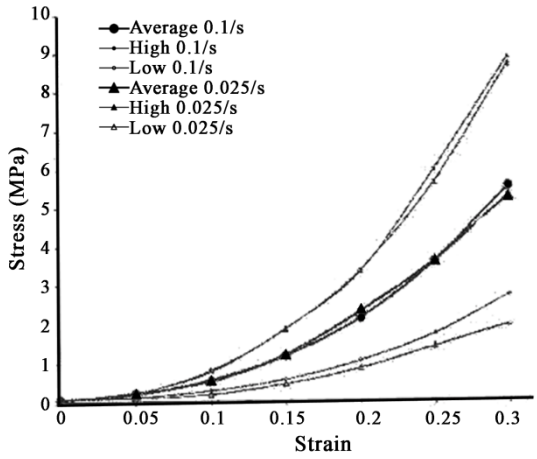

Figure 2.48: Results for indentation test of osteoarthritic cartilage at different loading rate to a 33% strain.

The osteoarthritica cartilage shows a lower sensitivity to loading rate. But comparing the results for normal and osteoartritic results at the loading rate of 0.1/s it is possible to observe a significative variation in the stress-strain response, while at the loading rate of 0.025/s the difference is reduced. In particular the average curve of OA cartilage at 0.025/s is very close to the healty cartilage one.

This lead to the conclusion that OA cartilage has a significative different mechanical response at high loading rate and than it is particularly important to study rapid loads as can happen for heel strike phase of gate cycle and running.

Although the normal and degraded group showed a large variation in their stiffness, the stress-strain behaviour maintained similar basic attributes. The osteoarthritic samples were generally characterised by slightly lower resultant stresses in the toe region and higher stresses at the later stages of deformation (Brown et al. 2007).

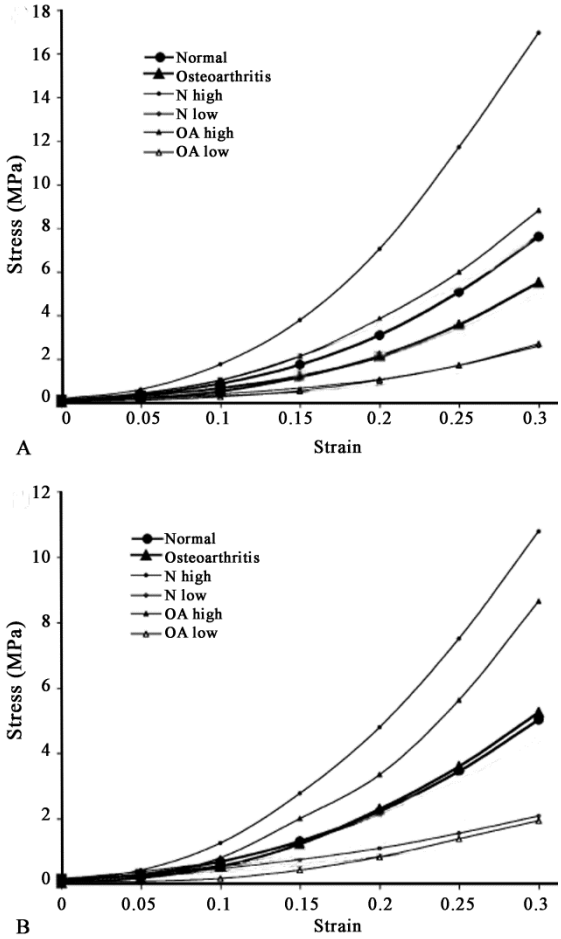

Figure 2.49: Results for indentation test of normal and osteoarthritic cartilage until a 33% strain at a loading rate of 0.1/s A) and at a loading rate of 0.025/s B).

These results will be used in chapter four to define the set of parameters for normal cartilage, while the results for osteoarthritic cartilage will be used in chapter five to define a specific set of parameters for degraded cartilage.

2.4.3.1.2 Confined compression

Confined compression tests when used in conjunction with biphasic theory, the confined compression test can be used to estimate material parameters, such as the hydraulic permeability (Armstrong and Mow, 1982; Buschmann et al., 1992). An issue which has arisen in the interpretation of confined compression experiments is the nature of the boundary conditions at the cartilage/porous-platen interface and at the radial-edge/confining-wall interface (Buschmann et al. 1998).

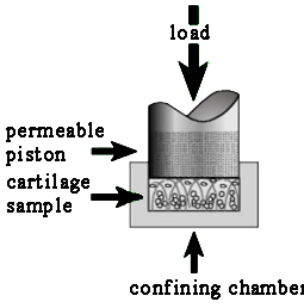

Figure 2.50: In confined compression the sample is compressed with a permeable piston. The sample is placed in a confining chamber.

The experimental procedure followed by Buschmann et al. (1998) is developed on cylindrical cartilage disks (8) from the central area of the humeral heads of 1-2 yr old cows (4) were cut using a 6 mm diameter dermal biopsy punch within 24 h of slaughter (Jurvelin et al., 1997). The final disk for testing was punched to 3.6±0.05 mm diameter. Mean individual disk thickness was 1.0-1.22 mm with a variation of ±25 lm within a disk. Disks were stored at 4°C in a humidified chamber for at most 6 h prior to testing.

A custom-built mechanical testing device was used (Jurvelin et al., 1997). Cartilage disks were placed in a 3.78±0.01 mm diameter cylindrical hole of the confined compression chamber containing PBS. A 3.70±0.01 mm diameter stainless-steel porous filter (Meyer Sintermetal AG, Studen Switzerland ~5 μm pores, 50% porosity, ~15 μm peak-peak surface roughness via TalySurf) was placed on the articular surface. An equilibrium tare load of 4-7g was applied. The elastic stiffness of the testing system, 82.7±5.5 g μm-1 (Mean±S.D. N=7), was used to correct jaw-to-jaw displacements to obtain specimen surface-to-surface displacements.

Each disk underwent tests during an ~4 h period. The disk was subjected to a sequence of 30-36 ramp compressions of 5 μm amplitude with 1 μms-1 velocity to a final 15% offset. When the slope during relaxation was less than 0.5 g min-1 the next step was executed.

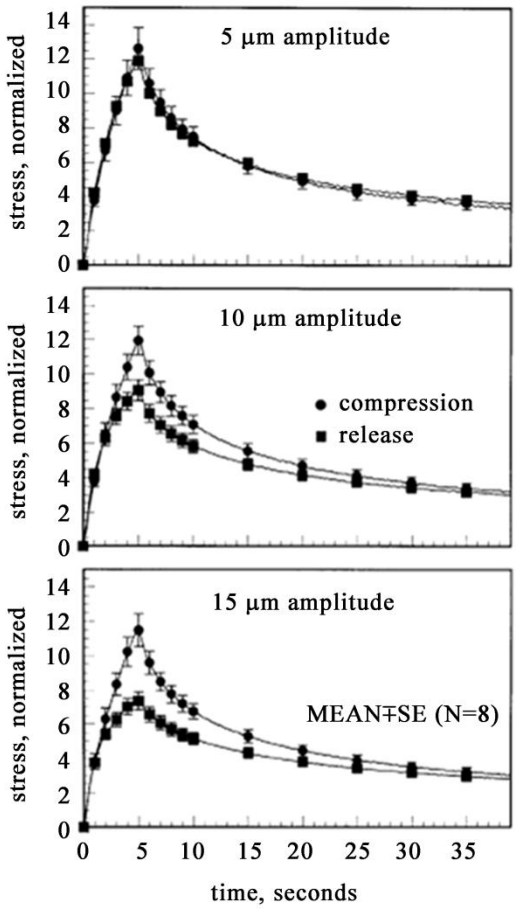

Figure 2.51: stress relaxation responses to ramp compression and ramp release displacements of 5, 10 and 15 µm in confined conditions. Results are normalized and with ε_0 the imposed surface-to-surface strain.

Normalized compression and release stress-relaxation profiles for 5 µm amplitude displacements were similar. A gradually increasing asymmetry and non-linearity appeared when increasing the displacement amplitude to 10 µm and to 15 µm, where the decrease in compressive stress for ramp release was smaller than the increase in compressive stress for ramp compression.

Normalized compression stress-relaxation profiles demonstrated linear material response while normalized release stress-relaxation profiles demonstrated higher non-linear behavior (Figure 2.52).

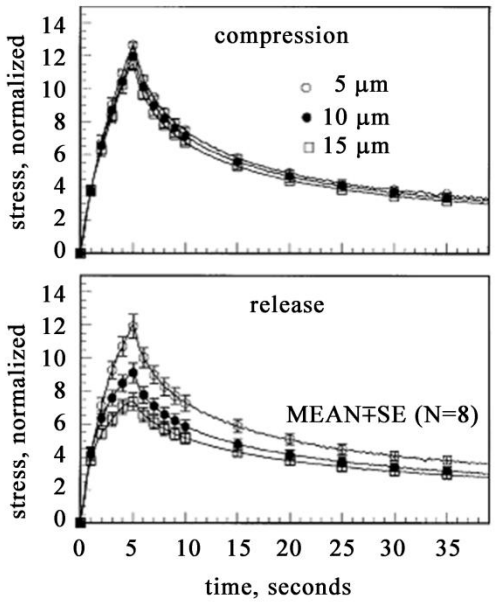

Figure 2.52: The same curves of previous figure are regrouped to illustrate an essentially linear response to small-amplitude (5-15 μm) compressive displacements and a non-linear response to small amplitude release displacements.

2.4.3.1.3 Unconfined compression

Confined compression is widely used; however, some technical issues regarding the porous interface have encouraged the use of other configurations. One such alternative is unconfined compression, where a tissue disk is compressed between two smooth impermeable surfaces. This geometry has been widely used for the study of the biological effects of load.

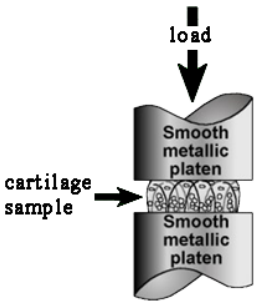

Figure 2.53: In unconfined compression the sample is compressed between two smooth frictionless impermeable platens.

In a study by Langelier et al 2003 it was demonstrated that unconfined compression of young adult articular cartilage/bone disks from a free swelling state exhibits: (i) a nonlinear transient response that stiffens significantly when compression amplitude

is increased and stiffens even more as a function of compression amplitude when strain rate is increased and (ii) an equilibrium response that can be linear or nonlinear depending on the strain rate used.

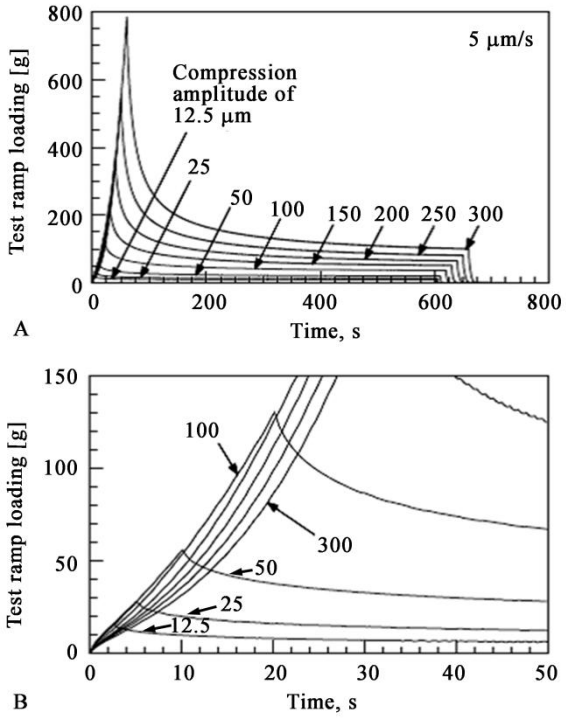

Figure 2.54: Example of stress relaxation profiles for the test ramps performed at 5μm/s (A), and magnification showing the form of the stress rise during the ramp (B).

During compression test a load can be maintained over time to investigate the influence of the biphasic composition of cartilage. The displacement is kept costant from point B to E (see following figures). Rapidly at first we have the liquid phase response and an increasing stress can be measured until the end of a compressive phase with a positive gradient of compression. In this first phase there's also an exudation of free fluid. When the compression is constant fluid redistribution allows for relaxation phase (points B to D) and matrix deformation, until the equilibrium point (E). During compression the mechanical response of cartilage is related to the rate at which fluid may be forced out of the tissue, but also the number of GAGs and the elastic properties of collagens. Articular cartilage shows nonlinear strain dependence and pressure dependence.

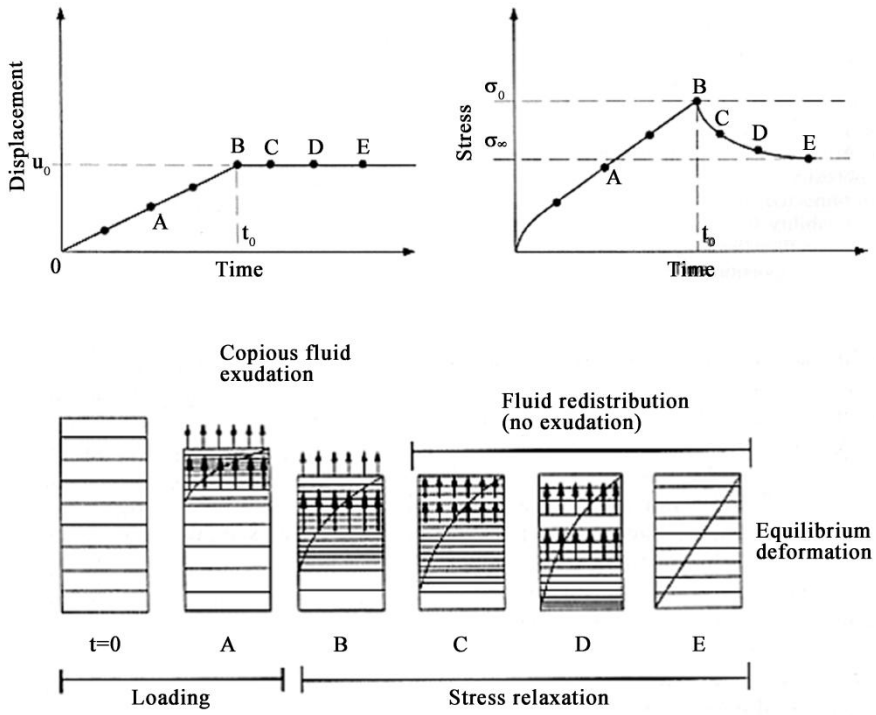

Figure 2.55: Schematic correlation between displacement and stress and fluid flow insiede cartilage sample.

This properties are foundamental, in fact the decrease of permeability with compression acts to retard rapid loss of interstitial fluid during high joint loadings.

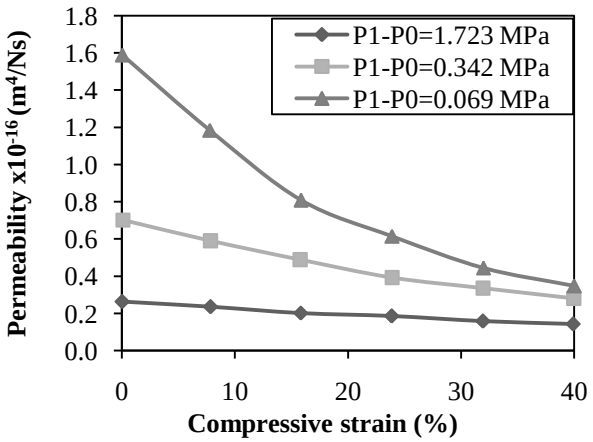

Figure 2.56: Permeability decrease with different applied pressure.

Permeability decreases in an exponential manner as function of both increasing applied compressive strains and increasing applied pressure.

Therefore from literature experimental results is possible to deduce the necessity of an hyperelastic model to define the stress-starin behavior of cartilage. In addition, the role of cartilage components, such as collagen fibers in extracellular matrix, and the strain rate dependency of these components must be take in to account in consideration of the physiological condition to be studied.

2.5 REFERENCES

Argatov I., Mishuris G., "Flat-ended rebound indentation test for assessing viability of articular cartilage: Application of the viscoelastic layer model", Mechanics Research Communications, 38 (8), pp. 565–568, 2011.

Armstrong CG, Mow VC, "Variations in the intrinsic mechanical properties of human articular cartilage with age, degeneration and water content", J Bone Joint Surg [Am], 64, pp. 88-94, 1982.

Bernd Rolauffs, James M. Williams, Alan J. Grodzinsky, Klaus E. Kuettner, and Ada A. Cole, Distinct horizontal patterns in the spatial organization of superficial zone chondrocytes of human joints, J Struct Biol. May; 162(2): 335–344, 2008.

Bloom and Fawcett, "Textbook of Histology",12th Ed, Chapman & Hall, 1994.

Broom N.D. and Flachsmann R., Physical indicators of cartilage health: the relevance of compliance, thickness, swelling and fibrillar texture. Journal of Anatomy, 202, pp. 481–494, 2003

Buschmann MD, Soulhat J, Shirazi-Adl A, Jurvelin JS, Hunziker EB, "Confined compression of articular cartilage: linearity in ramp and sinusoidal tests and the importance of interdigitation and incomplete confinement" J Biomech. 1998 Feb;31(2), pp. 171-8.

Carlo Di Bello, "Biomateriali – Introduzione allo studio dei materiali per uso biomedico", Patron Editore, 2004.

Cohen B, Lai WM, Mow VC. A transversely isotropic biphasic model for unconfined compression of growth plate and chondroepiphysis. Journal of Biomechanical Engineering 120, pp. 491-6, 1998.

Cusack S. and Miller A., 1979. Determination of the elastic constants of collagen by Brillouin light scattering, Journal of Molecular Biology, vol. 135, pp. 39-51.

Dean D., Han L., Grodzinsky A.J., Ortiz C., 2006. Compressive nanomechanics of opposing aggrecan macromolecules, Journal of Biomechanics, vol. 39, pp. 2555-2565.

Eisenberg S.R., Grodzinsky A.J., 1985. Swelling of articular cartilage and other connective tissues: electromechanical forces, Journal of Orthopaedic Research, vol. 3, pp. 148-159.

Eroschenko V. P., Di Fiore M. S. H., "Di Fiore's atlas of histology with functional correlations", Lippincott Williams & Wilkins, 2008.

Eve Langelier, Michael D. Buschmann "Increasing strain and strain rate strengthen transient stiffness but weaken the response to subsequent compression for articular cartilage in unconfined compression", Journal of Biomechanics 36 (2003), pp. 853–859

Eyre D.R., Pietka T., Weis M.A., Wu J.J., 2004. Covalent cross-linking of the NC1 domain of collagen type IX to collagen type II in cartilage, The Journal of Biological Chemistry, vol. 279, pp. 2568-2574.

Frank C.B., Shrive N.G., 1999. Biological materials, In Biomechanics of the musculo-skeletal system, Chichester, New York, pp. 107-126.

Fratzl P., Misof K., Zizak I., 1997. Fibrillar structure and mechanical properties of collagen, Journal of structural biology, vol. 122, pp. 119-122.

Freed A.D., Doehring T.C., 2005. Elastic model for crimped collagen fibrils, Journal of Biomechanical Engineering, vol. 127, pp. 587-593.

Fung Y.C., 1993. Biomechanics: mechanical properties of living tissues (second edition), Springer-Verlag, New York.

G E Kempson "Relationship between the tensile properties of articular cartilage from the human knee and age", Ann Rheum Dis 41(5), pp. 508–511, 1982.

Gautieri A., Vesentini S., Redaelli A., Buehler M.J., 2011. Hierchical structure and nanomechanics of collagen microfibrils from the atomistic scale up, Nano letters, In press.

Hofmann H., Voss T., Kuhn K., Engel J., 1983. Localization of flexible sites in thread-like molecules from electron micrograph – Comparison of interstitial, basement and intima collagen, Journal of Molecular Biology, vol. 172, pp. 325-343.

Junqueira L.C., Carneiro J., Long J.A., 1986. Basic histology (fifth edition), Prentice-Hall International, London.

Jurvelin J, Kiviranta I, Arokoski J, Tammi M and Helminen HJ. Indentation study of the biomechanical properties of articular cartilage in the canine knee. Eng Med 16, pp. 15-22, 1987.

Jurvelin J, Kiviranta I, Saamainen AM, Tammi M and Helminen HJ. Indentaion stiffness of young canine knee articular cartilage influence of strenuous joint loading. J Biomech 23, pp. 1239-1246, 1990.

Jurvelin J, Kiviranta I, Tammi M and Helminen HJ. Effect of physical exercise on indentation stiffness of articular cartilage in canine knee. Int J Sports Med 7, pp. 106-110, 1986a.

Jurvelin J, Kiviranta I, Tammi M and Helminen HJ. Softening of canine articular cartilage after immobilization of the knee joint. Clin Orthop, pp. 246-252, 1986b.

Jurvelin JS, Arokoski JP, Hunziker EB, Helminen, HJ. Topographical variation of the elastic properties of articular cartilage in canine knee, J Biomech 33, pp. 669-675, 2000.

Jurvelin JS, Räsänen T, Kolmonen P and Lyyra T. Comparison of optical, needle probe and ultrasonic techniques for the measurement of articular cartilage thickness. J Biomech 28, pp. 231-235, 1995.

Kadler K.E., Holmes D.F., Trotter J.A., Chapman J.A., 1996. Collagen fibril formation, Biochemical Journal, vol. 316, pp. 1-11.

Kerr J. B., "Atlas of Functional Histology", Elsevier Health Sciences, 1999.

Korhonen RK, Laasanen MS, Töyräs J, Helminen HJ, Jurvelin JS. Superficial collagen network modifies differently equilibrium response of articular cartilage in unconfined compression and indentation. Trans Orthop Res Soc 27, pp. 79, 2002.

Korhonen RK, Töyräs J, Nieminen MT, Rieppo J, Hirvonen J, Helminen HJ, Jurvelin, JS. Effect of ionic environment on the compression-tension nonlinearity of articular cartilage in the direction perpenticular to articular surface. Trans Orthop Res Soc 26, pp. 439, 2001.

Laasanen MS, Töyräs J, Hirvonen J, Saarakkala S, Korhonen RK, Nieminen MT, Kiviranta I, Jurvelin JS. Novel mechano-acoustic technique and instrument for diagnosis of cartilage degeneration. Physiol Meas 23, pp. 491-503, 2002.

Laasanen MS, Töyräs J, Korhonen RK, Rieppo J, Saarakkala S, Nieminen MT, Hirvonen J, Jurvelin JS. Biomechanical properties of knee articular cartilage. Biorheology 40, pp. 133-140, 2003.

Langelier Eve, Michael D. Buschmann, Increasing strain and strain rate strengthen transient stiffness but weaken the response to subsequent compression for articular cartilage in unconfined compression. Journal of Biomechanics 36(6), pp. 853–859, 2003.

Li LP, Soulhat J, Buschmann MD, Shirazi-Adl A. Nonlinear analysis of cartilage in unconfined ramp compression using a fibril reinforced poroelastic model. Clinical Biomechanics (Bristol, Avon) 14, pp. 673-82, 1999.

Li LP, Buschmann MD, Shirazi-Adl A. A fibril reinforced nonhomogeneous poroelastic model for articular cartilage: inhomogeneous response in unconfined compression. Journal of Biomechanics 33, pp. 1533-41, 2000.

Limbert G., Taylor M., 2002. On the constitutive modelling of biological soft connective tissues. A general theoretical framework and explicit forms of the tensors

of elasticity for strongly anisotropic continuum fiber-reinforced composites at finite strain, International Journal of Solids and Structures, vol.39, pp. 2343-2358.

Loret B., Simoes F.M.F., 2004. Articular cartilage with intra- and extrafibrillar waters : a chemo-mechanical model, Mechanics of Materials, vol. 36, pp. 515-541.

Lyyra T, Jurvelin J, Pitkänen P, Väätäinen U and Kiviranta I. Indentation instrument for the measurement of cartilage stiffness under arthroscopic control. Med Eng Phys 17, pp. 395-9, 1995.

Lyyra-Laitinen T, Niinimäki M, Töyräs J, Lindgren R, Kiviranta I, Jurvelin JS. Optimization of the arthroscopic indentation instrument for the measurement of thin cartilage stiffness, Phys Med Biol 44, pp. 2511-2524, 1999.

Lyyra T, Kiviranta I, Väätäinen U, Helminen HJ, Jurvelin JS., In vivo characterization of indentation stiffness of articular cartilage in the normal human knee, J Biomed Mater Res., 48(4), pp. 482-7, 1999.

Minns R.J., Soden P.D., Jackson D.S., 1973. The role of the fibrous components and ground substance in the mechanical properties of biological tissues: a preliminary investigation, Journal of Biomechanics, vol. 6, pp. 153-165.

Mow VC, Kuei SC, Lai WM, Armstrong CG. Biphasic creep and stress relaxation of articular cartilage in compression: Theory and experiments. Journal of Biomechanical Engineering 102, pp. 73-84, 1980.

Natali A.N., Pavan P.G., Carniel E.L., 2004b. Damage phenomena in anisotropic soft biological tissues: a constitutive formulation, Russian Journal of Biomechanics, vol.8, pp. 43-60.

Natali A.N., Pavan P.G., Carniel E.L., Dorow C., 2004a. Visco-elastic response of the periodontal ligament: an experimental-numerical approach, Journal of Connective Tissue Research, vol. 45, pp. 222-230.

Natali A.N., Pavan P.G., Carniel E.L., Lucisano M.E., Taglialavoro G., 2005. Anisotropic elasto-damage constitutive model for the biomechanical analysis of tendons, Medical Engineering and Physic, vol. 27, pp. 209-214.

Nestler F.H.M., Hvidt S., Ferry J.D., 1983. Flexibility of collagen determined from dilute solution viscoelastic measurements, Biopolymers, vol. 22, pp. 1747-1758.

Nishimura M., Yan W., Mukudai Y., Nakamura S., Nakamasu K., Kawata M., Kawamoto T., Noshiro M., Hamada T., Kato Y., 1998. Role of chondroitin sulphate-hyluronan interactions in the viscoelastic properties of extracellular matrices and fluids, Biochimica et Biophysica Acta, vol. 1380, pp. 1-9.

Ottani V., Martini D., Franchi M., Ruggeri A., Raspanti M., 2002. Hierarchical structures in fibrillar collagens, Micron, vol. 33, pp. 587-596.

Ottani V., Raspanti M., Ruggeri A., 2001. Collagen structure and functional implications, Micron, vol. 32, pp. 251-260.

Petruska J.A., Hodge A.J., 1963. Recent studies with the electron microscope on ordered aggregates of the tropocollagen molecule. In Ramachandran G.N. (editor), Aspects of protein structure, Academic Press, New York, pp. 289-300.

Raspanti M., Alessandrini A., Ottani V., Ruggeri A., 1997. Direct visualization of collagen-bound proteoglycans by tapping-mode atomic force microscopy, Journal of Structural Biology, vol. 119, pp. 118-122.

Raspanti M., Cesari C., De Pasquale V., Ottani V., Strocchi R., Zucchelli G., Ruggeri A., 2000. A histological and electron-microscopic study of the architecture and ultrastructure of human periodontal tissues, Archives of Oral Biology, vol. 45, pp. 185-192.

Redaelli A., Vesentini S., Soncini M., Vena P., Mantero S., Montevecchi F.M., 2003. Possible role of decorin glycosaminoglycans in fibril to fibril force transfer in relative mature tendons – a computational study from molecular to microstructural level, Journal of Biomechanics, vol. 36, pp. 1555-1569.

Reese S.P., Maas S.A., Weiss J.A., 2010. Micromechanical models of helical superstructures in ligament and tendon fibers predict large Poisson's ratios, Journal of biomechanics, vol. 43(7), pp.1396-1400.

Reilly, D.T. and Burstein, A. H., The elastic and ultimate properties of compact bone tissue, J. Biomechanics, 8, pp. 393-405, 1975.

Rieppo J, Laasanen MS, Korhonen RK, Töyräs J, Hirvonen J, Helminen HJ, Jurvelin JS. Depth-dependent mechanical properties of bovine patellar cartilage, Trans Orthop Res Soc 26: 2001.

Sasaki N., Odajima S., 1996. Stress-strain curve and Young's modulus of a collagen molecule as determined by the X-ray diffraction technique, Journal of Biomechanics, vol. 29, pp. 655-658.

Shu-xin Zhang, "An atlas of histology", Springer-Verlag,1998.

Silver F.H., Freeman J.W., Seehra G.P., 2003. Collagen self-assembly and the development of tendon mechanical properties, Journal of Biomechanics, vol. 36, pp. 1529-1553.

Soltz MA and Ateshian GA. A Conewise Linear Elasticity mixture model for the analysis of tension- compression nonlinearity in articular cartilage. Journal of Biomechanical Engineering 122, pp. 576-86, 2000.

Szwajczak E., 2004. Dependence of hyaluronan aqueous solution viscosity on external fields. Part II, Russian Journal of Biomechanics, vol. 8, pp. 89-94.

Tang Y., Ballarini R., Buehler J., Eppell J., 2009. Deformation micromechanisms of collagen fibrils under uniaxial tension, Journal of the royal society, vol. 7(46), pp. 839-850.

Töyräs J, Rieppo J, Nieminen MT, Helminen HJ, Jurvelin JS. Characterization of Enzymatically Induced Degradation of Articular Cartilage Using High Frequency Ultrasound. Phys Med Biol 44, pp. 2723-2733, 1999.

VanvBuskirk, W. C. and Ashman, R. B., The elastic moduli of bone, in Mechanical Properties of Bone , Joint ASME-ASCE Applied Mechanics, Fluids Engineering and Bioengineering Conference, Boulder, CO, 1981

Wu J. Z. and Herzog W. "Elastic anisotropy of articular cartilage is associated with the microstructures of collagen fibers and chondrocytes", J Biomech, 35(7), pp. 931–42, 2002.

Yang L, 2008. Mechanical properties of collagen fibrils and elastic fibers explored by AFM, PhD Thesis, University of Twente, Enschede, The Netherlands.

CHAPTER THREE

3 DEVELOPMENT OF A SOLID MODEL OF THE FOOT

3.1 INTRODUCTION

The anatomical study of the foot allow to develop with more accuracy the solid model of a particular anatomical site. In this thesis a detailed model of the hindfoot is proposed. This choice is due to the great importance of the hindfoot in the gait cycle and in all the movements of the foot, as seen in the kinematic analysis in chapter one. The solid model is built up starting from biomedical images (DICOM) and with a threshold method based on Hounsfield scale of grey levels some 3D masks are applied on each area representing a bone component. This technique allow to extract a solid body for each bone from DICOM images. The solid body obtained needs to be smoothed of errors due to discrete division in pixels and gray levels. The skeletal structure of the foot was then reconstruct as a composition of all solid bone. The structure obtained was checked for what concern morphology and some anatomical measures that are clinically taken into account to define if a foot is pathologic or normal. Cartilage was, instead, developed starting from the surface of each bone head. This was fundamental to allow a perfect adhesion of cartilage to bone head. The basic surface was chosen in consideration with anatomical data present in literature. The surface of cartilage was then extruded to obtain a thickness comparable with a physiological mean thickness of an adult person. It is important to notice that in this work cartilage is built up as a two-faced-layers and not as a whole body fulfilling the space between two bone heads.

This asked a more complicated numerical model, since the space between two cartilage layers should be considered as a space fulfilled with sinovial fluid and it was necessary to bound the sinovial fluid and to define the numerical contact between the bone heads.

3.2 *DEVELOPMENT OF A SOLID MODEL OF THE FOOT AND IN PARTICULAR OF THE HINDFOOT*

The first step in the creation of a finite element model is to represent its geometry. The numerical rapresentation can be achived either two dimensionally (2D) or three dimensionally (3D). With regard to the problem to be investigated, the numerical model of the structure under study can be described with a three dimensional model. The development of the geometry of a 3D virtual solid model is a process closely related to the ultimate objective of the model. The sequence of operations described bellow is applied to represent the morphometry of some bone and soft tissue identified by data from CT and MRI, respectively. The procedure adopted is a guideline, that does not impose standards or processing parameters set for all cases. Each model is defined by subjective evaluations and reaches a good compromise between an acceptable level of accuracy and a regular surfaces (De Souza V.A., 2007; Korioth and Versluis, 1997; Vannier et al., 1997).

3.2.1 Biomedical images for the development of the numerical model

Medical imaging is a branch of the medical field which involves the use of technology to take images of the inside of the human body. The goal of medical imaging is to provide a picture of the inside of the body in a way which is as non-invasive as possible. These images are used in diagnostics and in routine healthcare for a variety of conditions. There are a number of different types of technology used in medical imaging, however some of the most famous types of diagnostic imaging are the x-ray, the x-ray computed tomography and the magnetic resonance imaging (Stytz et al., 1991; Ayache , 1995).

The reconstruction of the virtual solid models, which is made with different processing techniques, requires the acquisition of images from computed tomography or magnetic resonance imaging. On the one hand, the reconstruction of the skeletal structure of the foot should be obtained from acquiring and processing images from CT, in which the bone tissue are highly distinct from other tissues. On the other hand, for the reconstruction of the soft tissues is necessary to use images from MRI which distinguish, with different gray levels, the different soft tissues that make up the anatomical portion studied (Rosenberg et al., 2000; Reach et al., 2007,

Matteoli et al., 2010).The digital processing techniques adopted have enabled a wide variety of analysis and improvements (Figure 3.1), until the development of models that faithfully reproduce the geometry and properties of anatomical structures (Cavalcanti et al., 2002).

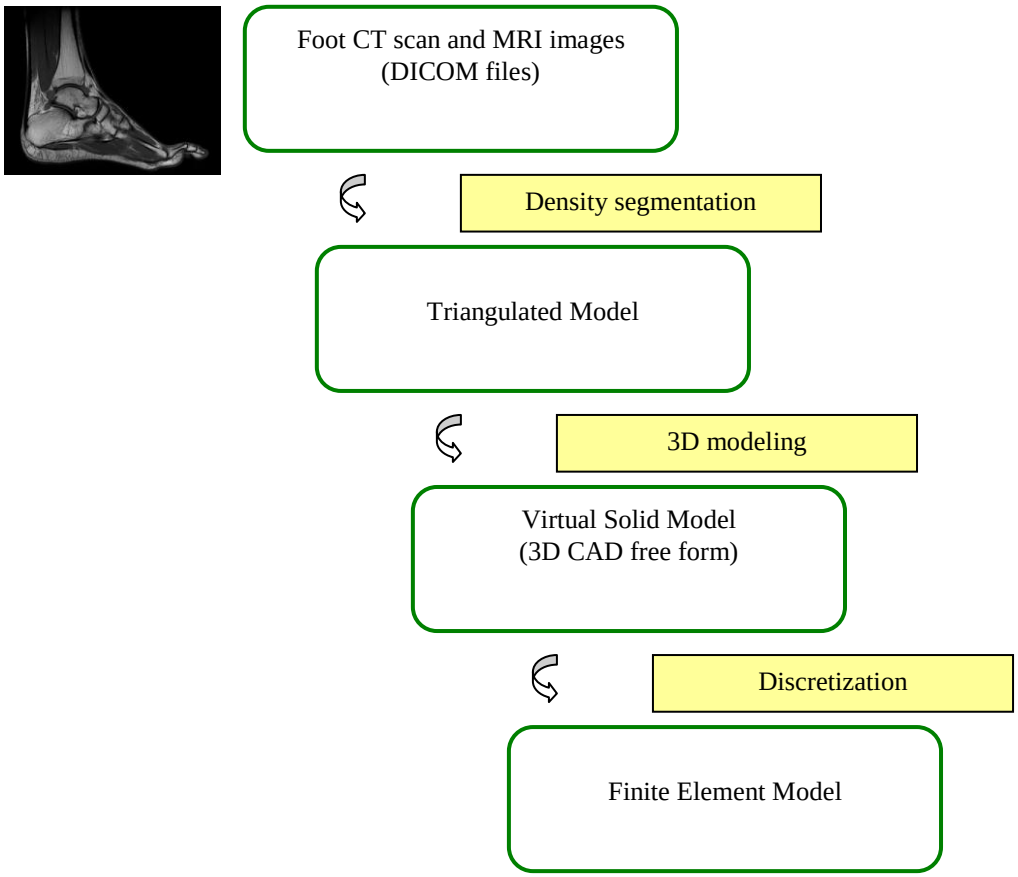

Figure 3.1: Modeling methodology

The sequence of collecting tomographic scans and magnetic resonance imaging of the patient is available in files sorted by type DICOM (Digital Imaging and Communications in Medicine), a standard communication protocol created by the National Electrical Manufacturers Association (NEMA). The DICOM standard has been introduced to define a mode of communication, storage and management of medical information, with particular attention to the images.

The reconstruction of the primary 3D anatomical structures is obtained by the use of a specific medical imaging density segmentation software. The DICOM image files generated in the CT and MRI are constituted by pixels with different gray intensities.

The different intensity fields correspond to different material densities presented at the anatomical structures (Antunes et al.,2010).

The reconstruction of the virtual solid model of the plantar tissue was allowed by the acquisition of 16 DICOM file, in the transverse direction, and 16 DICOM files in the sagittal direction. The software allows direct import of data generated by the MRI slice. Initially, it is necessary to impose the proper axial orientation to imported images. Then appears the main screen which is divided into two parts. The left side has four panels, representing the plane frontal, transverse and sagittal and one additional space for the subsequent viewing of the selected structure in 3D. The right side is the Project Management where is reported a list of all objects created, which can be viewed or modified.

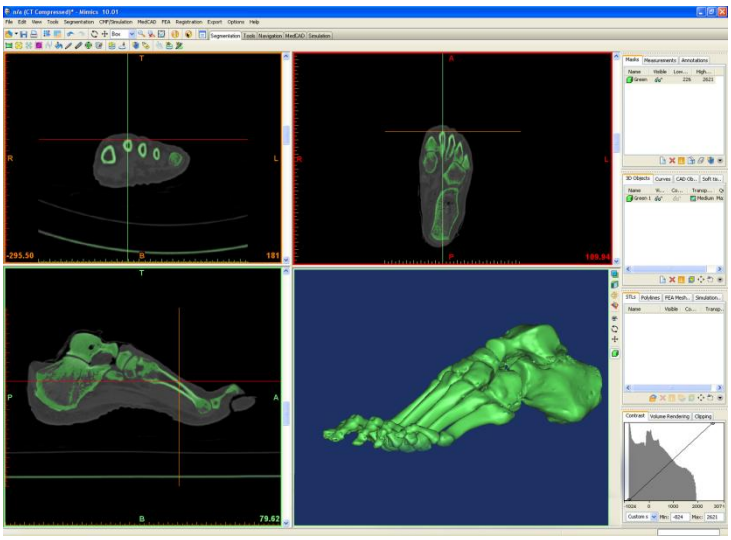

Figure 3.2: The main screen of the software of medical imaging elaboration.

The procedure makes the use of two module, Tools and Segmentation, for assessing the portion of the image of interest. With the a thresholding procedure, it is possible to select a range of gray values, based on the Hounsfield scale, which delimits the studied tissues. In the case of bone tissue was chosen as the bottom level 255 and as the top level 1365 in the scale of Hounsfield. It is important to observe that the gray scale is discretized and also the MRI files are discretized in slices, so the selection of a region can include spurious pixels or miss some pixels.

When a collection of all pixel is highlighted with same gray level it is possible to remove isolated points or areas that do not belong to the area of study. A procedure

allorw to limit the region of interest, then the selected area can be edited, deleted or redesigned. This operation allows to define the boundary surfaces for solid models.
The virtual reconstruction of solid models of foot bones was obtained from CT images. The software allows for the direct analysis of tomographic slices generated by the lower limb. To distinguish and highlight the bone tissues, the procedure adoptes the Segmentation Module, and in particular the command Thresholding. The program sets the default interval of gray levels in Hounsfield scale for selection of different tissues from CT images. In particular, the bone tissue of an adult has the gray levels between 226 and 3071 of the Hounsfield scale (Figure 3.3). In order to obtained a reliable selection of the bone components, subsequent oparetions, such as reported for soft tissues, are necessary.

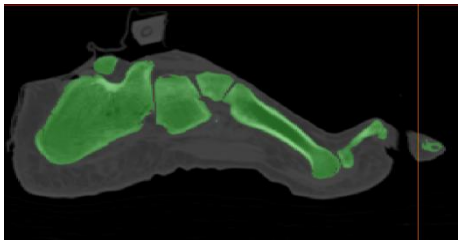

Figure 3.3: selection of bone tissues from CT scan obtained with a specific software.

The Project Management permits to create the virtual soli model of the selected tissue, as an encloosed volume delimited by a 2D triangular mesh (De Souza, 2007). During this operation, it is possible to choose the accurancy and the level of image quality to be implemented.
The virtual solid model of the soft tissue and of the bone components must be saved in .STL format to guarantee the subsequent importation into the processing software.
In the following paragraph a more detailed representation will be given for bone components.

3.2.2 Image processing for the reconstruction of bone components

The file formats. STL are imported by the modeling software, where a shell is registered in the project window. The shell is defined as an enclosed volume delimited by 2D triangular elements, usually related to each other, which form a polygon mesh. Working with a mesh is advantageous because of the speed of processing and the multiple control functions. The disadvantages relate to the

approximation with which the surfaces are represented, which are formed by small triangles. These traingles must be define by a description of the spatial coordinates of the vertices and the unit vectors normal to planes defined. Accordingly, these geometries not allow the control of the complete mathematical changes.

In order to obtain a virtual solid model which describes the real configuration of the biological structures, the calculations on the primitive model are intended to make the shape as smooth and clean as possible. At the same time, its pourpose is to join to reality without omitting details, although some approximations in procedure are inevitable.

With the process of segmentation previously described, the virtual solid model obtained is characterized by an irregular surface, with gaps, scattering and in some cases a constant trend in steps (stairstep) due to the stratification of the medical images. The software allows to select, by specific commands, such as paint brush and freehand polyline, the regions of the entire shell which present the major defects and must be corrected (Figure 3.5).

At this pourpose, the first stage pertains the regularization of the surface, starting from the operation of smoothing that solves the most minor defects, while maintaining the overall shape. This operation can be made a smooth global or local and can set the method of intervention (laplacian, loops or bends), the weight and the number of passes. The defects of surface often cannot be resolved completely with the only smoothing. A powerful tool that applies in these cases is Defeature, usually applied to small regions with the aim to not deform the overall surface. In these cases, the area selected is automatically deleted and replaced with a regular shape which follows the trend of the surroundings region.

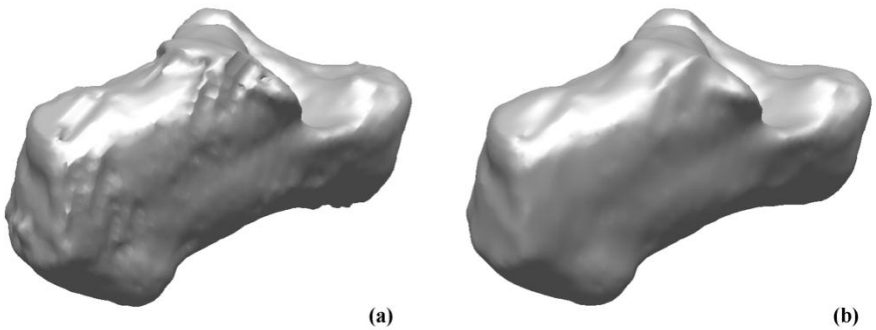

Figure 3.4: Triangulated model of calcaneum before (a) and after (b) the operation of modeling.

It is possible to select and delete the areas which present errors and discontinuity. With the use of the command fill it is possible to reconstruct and close of the cavity created in a continuous way. The command can be used with one hole or with all holes together and permit to shut with a flat, smooth or curved shape. There is also the command bridge hole which permit to create links between the contours of a large cavity, so as to reduce the extension to two smaller gaps and allow the next stage of closing to follow a precise pattern of the form.

Figure 3.5: Triangulated model of bone structures of the foot.

Other commands allow to deform and transform, with traslation and rotation, the shell obtained. For example, it is possible to create a reticle around the selected section of the shell and allows the deformation by moving the balls placed at the top and along the sides of the reticle.

In the tools menu there is also the function of remesh with which is possible to re-triangulated the overall surface, transforming all triangles into equilateral triangles.

3.2.2.1 Definition of the virtual solid models

From the description of rough tessellated geometry subsequently is obtained an exact mathematical model (Antunes et al., 2010).

The mathematical representation is called NURBS (Non-Uniform Rational B-Splines). The NURBS curves are piecewise polynomial curves that approximate the boundaries of free-form. The NURBS curves have the advantage of representing arbitrary shapes with mathematical precision, while maintaining control over the shape of the curves through their nodes and control points, which can be directly manipulated. The procedure uses a fitting algorithm, which consists of a series of patches that fit the discrete data, such as point cloud formed by the vertices of all

triangles. The patches are usually of the same mathematical nature, such as B-Spline grade 3, and are linked together by the conditions of tangency or curvature.

The software permit to obtain a mathematical surface directly from the tesselated surface (Figure 3.6). Before starting the automatic surfacing it is possible to set some parameters, such as the total number of surfaces created and the number of control points of the surface. Finally, it is useful to enforce certain conditions to the process: the generation of a uniform surface, the adhesion of the created patches to the original surface, removal of the roughness and the possibility of changing the boundaries of the patch after the execution. With an higher number of chosen areas, the resulting model is clearly more accurate. This operation is limited only by the computational capacity of computers, which can take a long time.

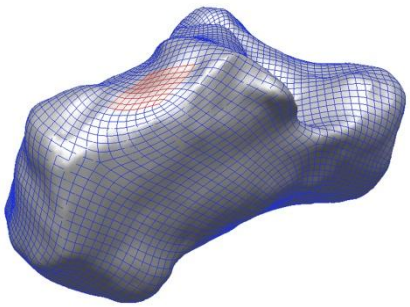

Figure 3.6: Triangulated model (gray solid) and CAD model free form (blue and red lines) of calcaneum.

To share the geometries with the software Unigraphics (UGS NX3, UGS Corporate, Plano, TX) all the surface must be exported as file IGES (Initial Graphics Exchange Specification). This operation increases the degree of approximation of mathematical models of the surfaces. In reference to solid models developed, it is necessary to make changes to portions of the surface that the command autosurface not been able to rent correctly. With the modelling package, the freeform surfaces created can be modify and correct.

In order to complete the procedure, the function of sew allows the connection of all the surface and the creation of a solid body. Solid models of the different components are exported in Parasolid format to be discretizaed in finite element models.

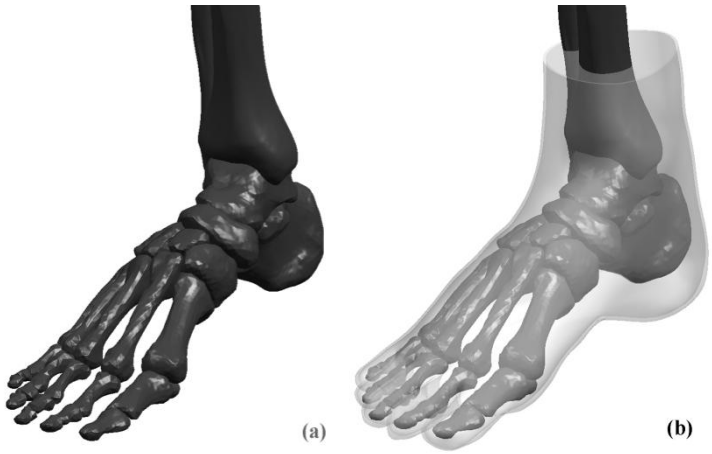

Figure 3.7: (a-b) CAD model free form of the bone structures, the soft tissues and the skin of the foot.

3.2.3 Anatomical images study for the reconstruction of cartilage components

The high complexity of hindfoot due to the presence of two important joints for the stability of human body in addition to the capability to develop a high number of movements during gate cycle and human activities. In particular the ankle joint is an incongruent articulation at light load with incomplete and separate contact areas, but high loads cause the transition from incongruence to complete congruence, allowing the joint to with stand large pressures (Huch et al., 1997, Wynatsky and Greenwald 1983, Greenwald and Matejczyk 1978).

3.2.3.1 Morphometric evaluation of the cartilage with respect to contact areas and thikness.

The tibiotalar articulation (or talocrural articulation)at the proximal level is formed by the articular surfaces of the distal tibial and fibular epiphyses and distally by the talus in its superior, lateral and medial aspect (see Figure 3.8 by de Leeuw and Golano 2010).

The morphology of these surfaces forms a hinge-type synovial joint, with a single axis of movement (bimalleolar axis) that allows dorsiflexion (flexion) and plantar flexion (extension) of the ankle and foot in the sagittal plane. Because of this configuration and the fact that it is a load-bearing joint, the intraarticular space is very narrow.

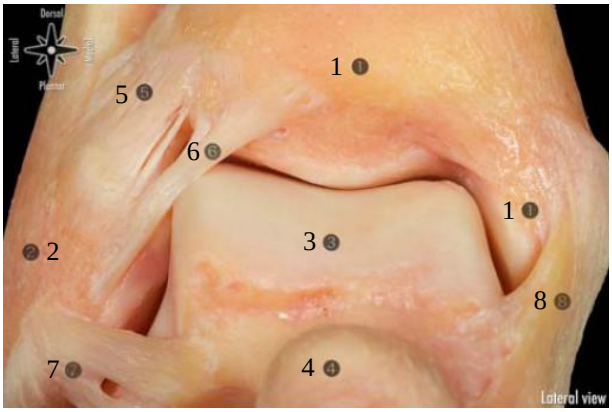

Figure 3.8: Anatomica view of the anterior subtalar joint. 1 Tibia and medial malleolus. 2 Lateral malleolus. 3 Talus. 4 Head of the talus. 5 Anterior tibiofibular ligament. 6 Distal fascicle of the anterior tibiofibular ligament. 7 Anterior talofibular ligament. 8 superficial and deep layers of the medial collateral ligament.

Hence there are some important aspects to be considered in modelling cartilage: bone's area covered by cartilage and involved in the contact during different articular movements; cartilage thickness that is fundamental to understand mechanical response during compression, and that is also a parameter to define if a cartilage is healthy or damaged; the presence of synovial capsule.

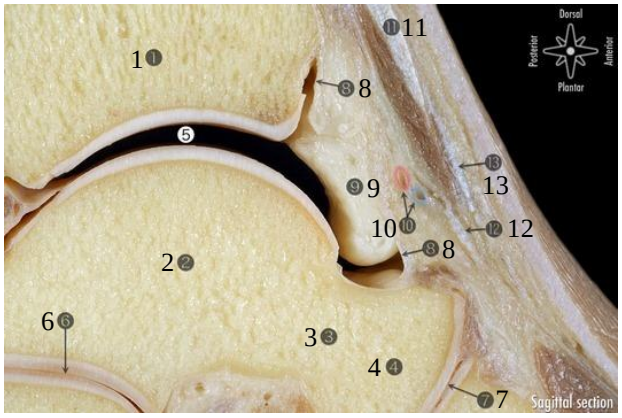

Figure 3.9: Sagittal section of the ankle showing the most relevant anatomical structures. 1 Tibia. 2 Talus. 3 Neck of the talus. 4 Head of the talus. 5 Tibiotalar working area. 6 Posterior subtalar joint. 7 Talonavicular joint. 8 Capsule. 9 Intracapsular but extrasynovial fatty tissue. 10 Anterior tibial artery and vein painted with Adobe Photoshop (the deep peroneal nerve has not been identified). 11 Extensor hallucis longus. 12 Deep layer of inferior extensor retinaculum. 13 Superficial layer of inferior extensor retinaculum.

For what concern literature, there are some works regarding the morphometry of tibio-talar joint. In particular the interest was on the thickness of the cartilage layer (Welsch (2008), Wan (2007), Millington (2006), Sugimoto (2005), Tang (2006), El-Khoury (2004), Kuettner (2004), Al-Ali (2002), Shepherd and Seedon (1999), Athanasiou (1997), Athanasiou 1995), Muller- Gerbl (1995), Schmitz (1985), Stockwell (1971)) and on the bone area covered by cartilage (Li (2008), Hewitt (2008) , Millington (2006), Corazza (2005), Al-Ali (2002), Bertsch (2001), Kura (1998)).

A mean value is defined considering the range of age used in the different work in order to give more importance to those with ankle from adult healthy subjects. In the table below are reported the mean values obtained for talar cartilage and tibial cartilage. There is also the value for talo-fibular cartilage, but very few works are present for that cartilage (Millington (2006)).

Joint considered	**Bone surface**	**Mean contact area (cm^2)**	**Mean thickness value (mm)**
Talo-fibular joint		3.67	0.9
Tibio-talar joint	**Distal tibia**	10.2	1.2
	Proximal talus	13.2	1.2
Sub-talar	**Distal talus**	6.97	1.1
	Proximal calcaneus	6.4	0.8

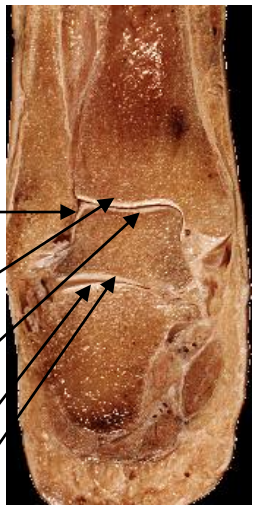

Figure 3.10: Section of a foot along sagittal plane, where it is possible to see cartilage layers of sub-talar joint, talo-fibular joint and talo-calcanear joint.

Synovial capsule has an important role in keeping the synovial fluid between tibia and talar bones.

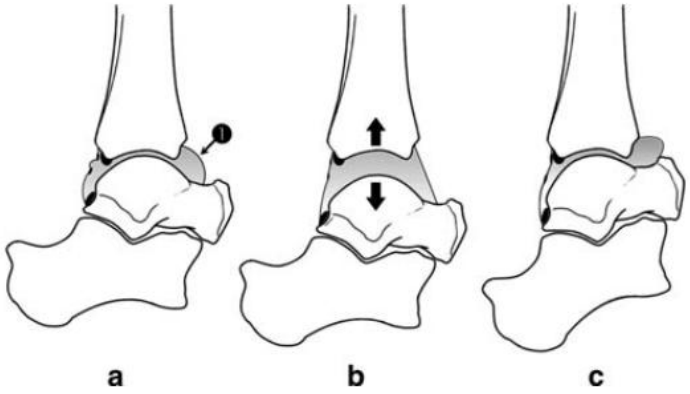

Figure 3.11: Schematic view of the ankle joint in the neutral ankle position a); capsular tension reduces the possibility of distraction during intrarticular work b); anterior working area is protected by synovial capsule during dorsiflexion c).

3.2.3.2 Solid model of cartilage layers

The definition of the solid model for cartilage layers is particularly complex since the layer should exactly be just appose on bone surface and the thickness should be chosen taking into account of anatomical peculiarity of the subject, the values given in literature. Moreover the cartilage layers here proposed are not simply a fulfilment of the space between the bone heads, but are two separate layers, with a morphological accordance to anatomical reports.

At first a curve delimitate the space of the cartilage. The curve is chosen following anatomical books and from the collaboration with the Department of Anatomy of the University of Padova.

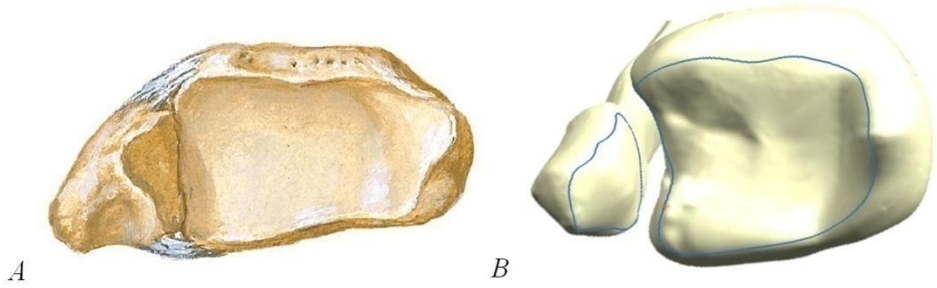

Figure 3.12: Image of a true tibia and fibula from the distal view with the cartilaginous area in evidence a); reconstruction of cartilage bounds on bone surface following anatomical images b).

The curve is then extruded for the length necessary to obtain a correct thickness, then the upper cap of the solid was obtained from the surface of the bone. In this way it is

possible to obtain a solid that is exactly just appose to the bone head and preserve the irregularity of the bone surface.

3.2.3.2.1 Tibia and fibula cartilage

The tibia and the fibula are both involved in tha tibio-talar articulation lot of articular surfaces since it is the centre of all the movements of the foot.

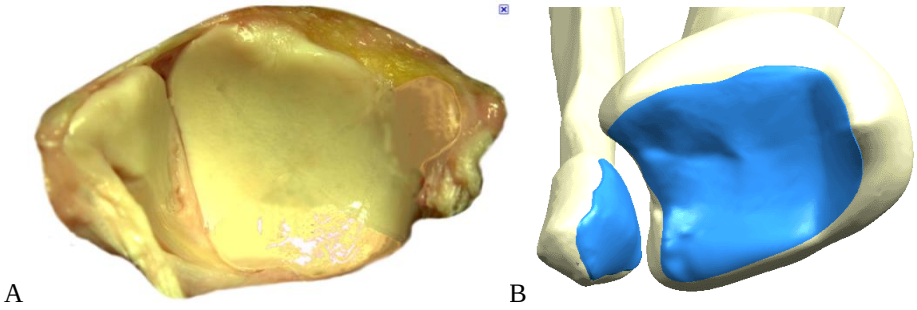

A B

Figure 3.13: Comparison between an anatomical image from anatomical atlas A) and the solid model with cartilage layer B).

3.2.3.2.2 Talar cartilage

In the talus there are a lot of articular surfaces since it is the centre of all the movements of the foot. More complex is the reconstruction of the talar cartilage. First because the convexity and the concavity of talar surfaces are more evident and this make it more difficult to extrude the curve and to reconstruct properly the bone surface.

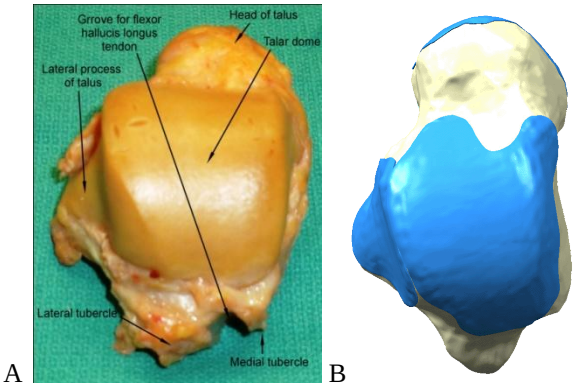

A B

Figure 3.14: Top view of the talar cartilage of tibio-talar joint from anatomical image a) and solid model image b).

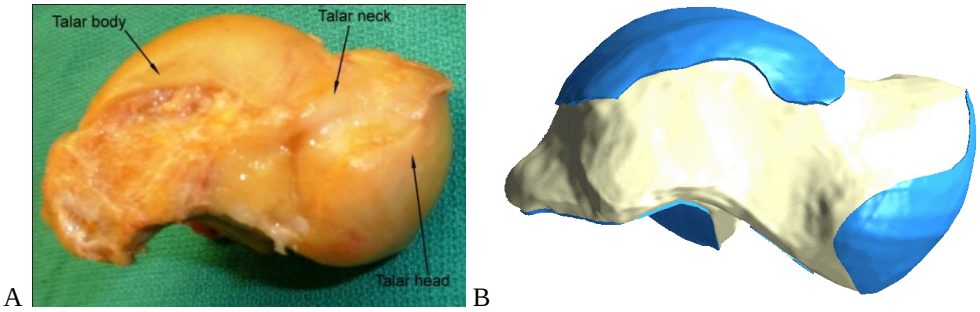

Figure 3.15: Medial view of the talar cartilage of tibio-talar joint from anatomical image A) and solid model image B).

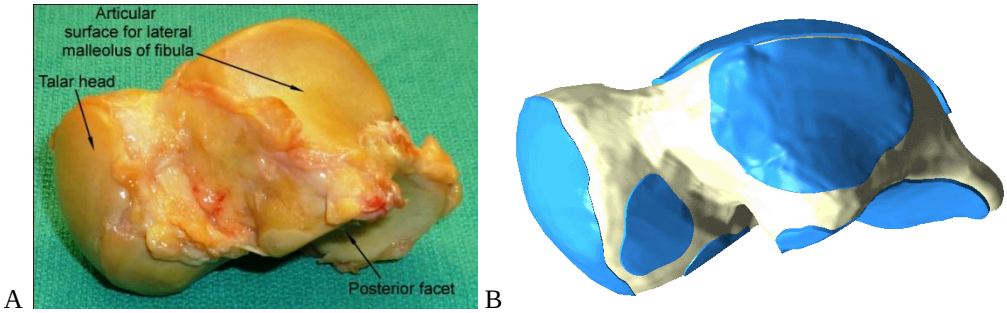

Figure 3.16: Lateral view of the talar cartilage of tibio-talar joint from anatomical image A) and solid model image B).

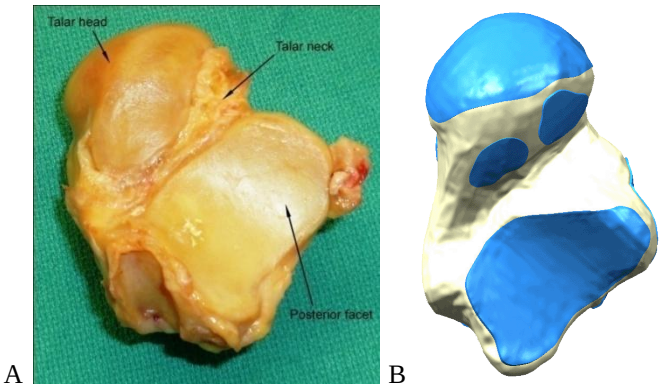

Figure 3.17: Bottom view of the talar cartilage of tibio-talar joint from anatomical image A) and solid model image B).

Once that both cartilage layers of tibia and talus are reconstructed, the two portion of the solid model are putted together and the ankle tibio-talar joint is completed.

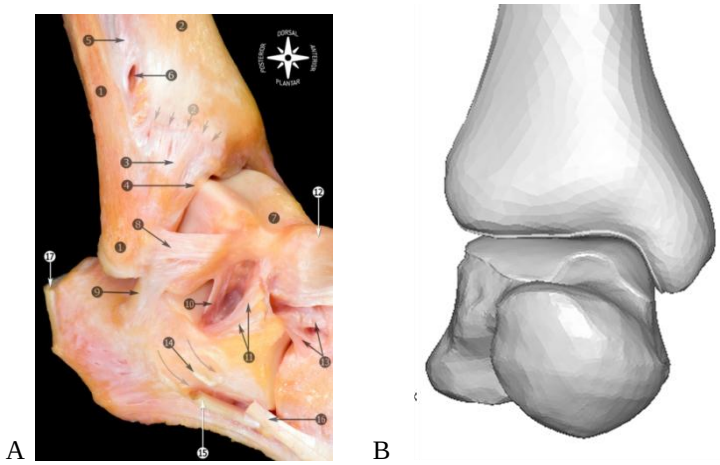

Figure 3.18: anatomical image A) Solid model of the tibio-talar joint complex B).

Moreover it is important to consider that between the two bone heads there is the synovial fluid constrained in a capsule.

The reconstruction of the capsule is made considering that the capsule should allow the movements of the joint and cover completely the cartilage layers. A true image of ankle synovial capsule is proposed in the following image.

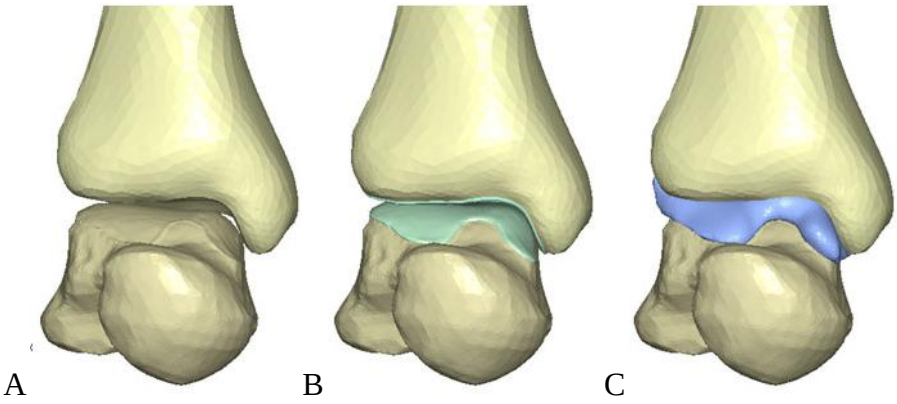

Figure 3.19: The full sub-talar model from frontal view with bones A); bones and cartilage B); bones, cartilage and synovial capsule C).

3.2.3.2.3 Calcaneal cartilage

In the calcaneus there are articular surfaces for sub-talar joint and calcaneo-cuboid joint.

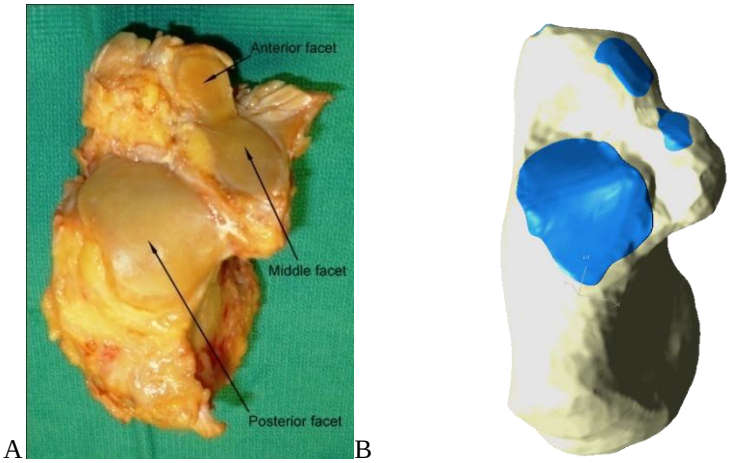

Figure 3.20: Top view of the calcaneus cartilage of sub-talar joint from anatomical image A) and solid model image B).

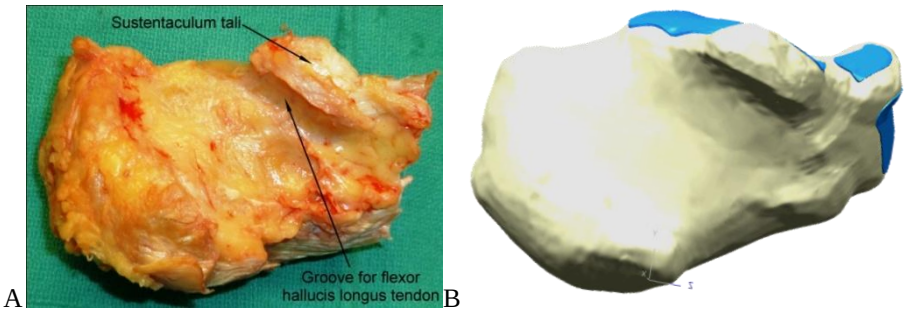

Figure 3.21: Medial view of the calcaneus cartilage of sub-talar joint from anatomical image a) and solid model image b).

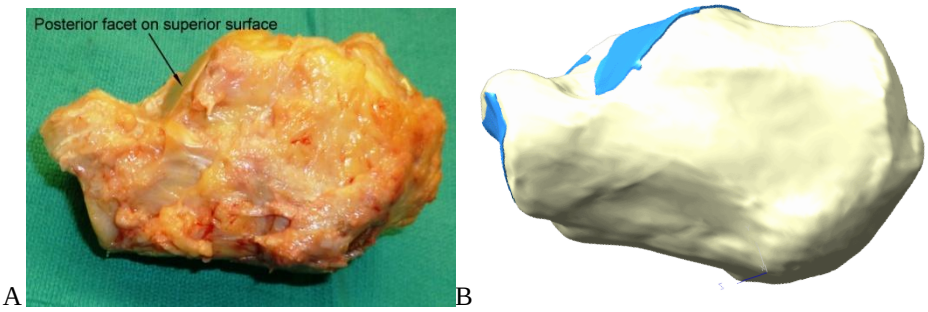

Figure 3.22: Lateral view of the calcaneus cartilage of sub-talar joint from anatomical image A) and solid model image B).

A 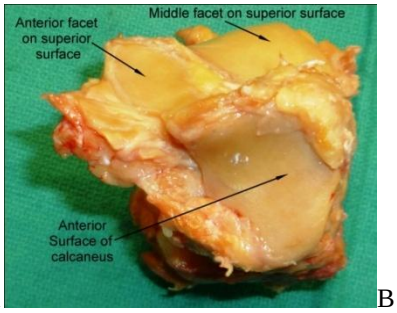

B 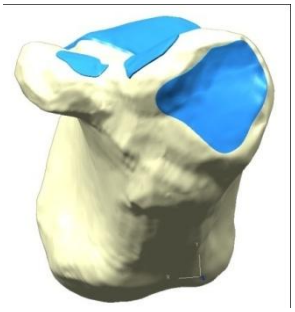

Figure 3.23: Front view of the calcaneus cartilage of sub-talar joint from anatomical image A) and solid model image B).

3.2.3.2.4 Navicular and cuboid cartilages

The naviculars has an articular surface for the talo-navicular joint, while the cuboid has an aricular surface for calcanues. They both have other articular surfaces with the bones of the medial foot (cuneiform bones) and of the forefoot (metatarsal bones), but here they are not represented, since the work is focused in particular on the hindfoot.

The thickness for the navicular and cuboid cartilages is reconstructed on the basis of a study by Al-Ali et al. (2002).

Joint considered	**Bone surface**	**Mean thickness value (mm)**
Talo-navicular joint	Talus	0.63
	navicular	0.57
Calcaneo-cuboid joint	Calcaneus	0.68
	Cuboid	0.64

Table 3.1: The table resumes the mean thickness values reported in literature for cartilages of talo-navicular and calcaneo-cuboid joint.

The solid model obtained are reported in the following images and compared with true anatomical images, in order to evidence the complex morphometry of each bone and of bone articular surfaces to be covered with a proper cartilage layer.

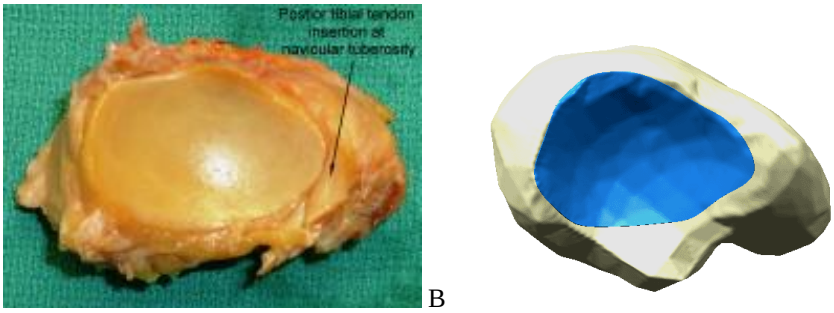

A B

Figure 3.24: Front view of the navicular cartilage of talo-navicular joint from anatomical image A) and solid model image B).

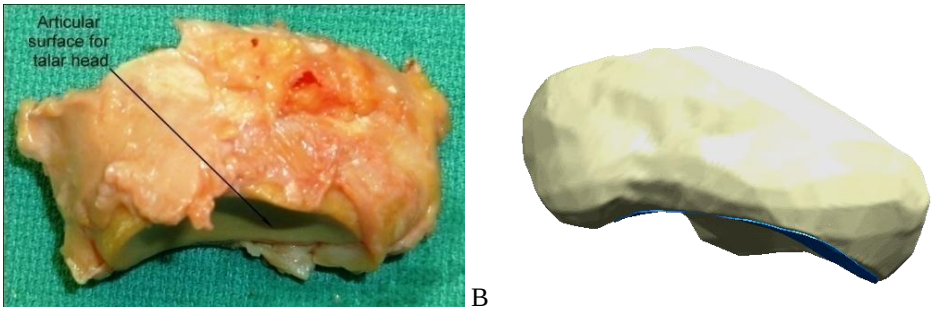

A B

Figure 3.25: Top view of the navicular cartilage of talo-navicular joint from anatomical image A) and solid model image B).

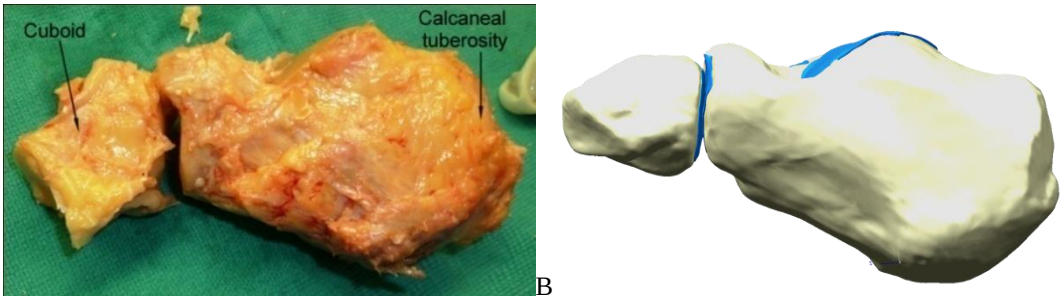

A B

Figure 3.26: Lateral view of the calcaneus cuboid joint from anatomical image A) and solid model image B).

3.3 NUMERICAL MODEL OF THE FOOT

3.3.1 Finite element discretization

The creation of the numerical model is perfromed by the finite element discretization of virtual solid models imported, using a specific software (Patran, MSC.Software Corporation, Santa Ana, CA). In order to obtain a numerical model with a properly and accurate discretization, firstly it is necessary to proceed with the discretization of the surfaces of solid virtual models with triangular elements.

These elements are defined by three nodes, with side length of about 2 mm. With this procedure the 2D mesh of all solid models is obtained. After this operation, the area of interaction between the models is modified to make them congruent. This operation is achieved by removing some triangular finite elements and defining new ones. On obtaining the different numerical models which are consistent with each others, it is necessary to define the 3D (Figure 3.27) mesh using tetrahedral elements.

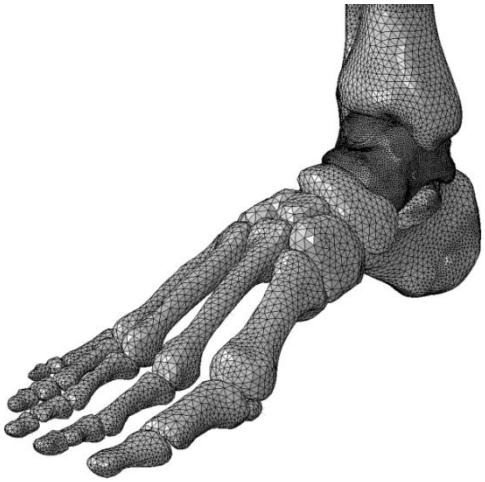

Figure 3.27: Finite element model of the bone structures.

It is important to notice that in relation to the presence of ligaments entheses and cartilage layers, the mesh density of bone components differs.

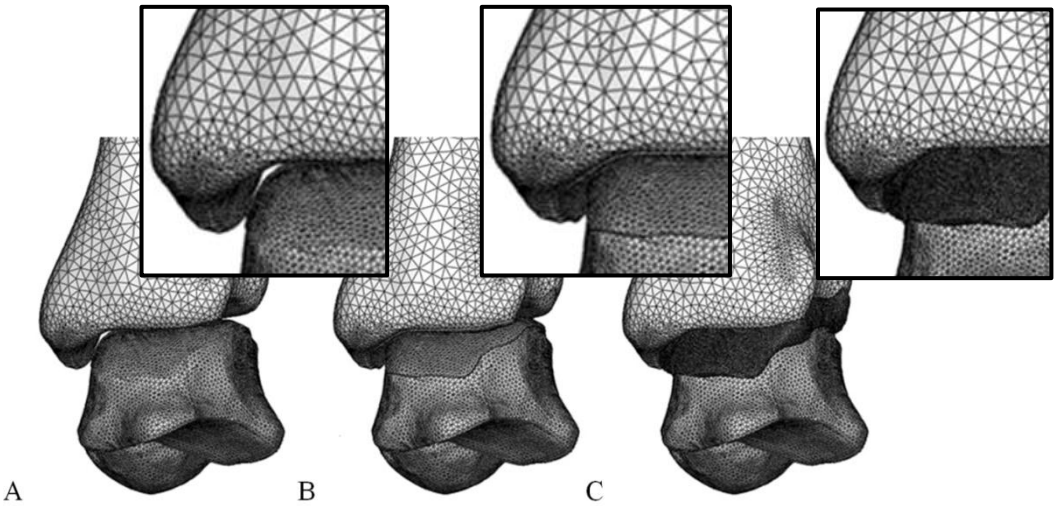

Figure 3.28: Numerical model of tibio-talar joint: A) only bones, B) bones and a double layer cartilage, C) bones and the synovial capsule surrounding cartilage. Details are reported to put in evidence the different dimension od mesh elements

The different mesh density is necessary to ensure a good approximation of the elements in contact and to observe the morphometry of each element. A detail of the numerical model of cartilage is reported in the previous Figure.
It is possible to notice the different mesh density between the talar and tibial bone. This is due to the fact that the talus is in contact with many different articular surfaces and therefore with cartilage layers of different thickness. In particular to have detailed results for tibio-talar joint a more dense mesh is created. On the tibia there is a more detailed mesh in correspondence to the articular cartilage layer but also in correspondence to ligament insertions. Herein the attention is set on cartilaginous tissue and in particular to hindfoot cartilage layers, therefore ligaments are not reported.

3.4 CONSTITUTIVE MODEL FOR CARTILAGE

Biological tissues are usually composed of fibrous elements (such as collagen) embedded in an isotropic and almost incompressible ground matrix and can be considered as composite materials. In particular in cartilage the ground matrix is a fluid that interacts with the GAGs charge. Moreover the local distribution of fibres is organized in different zones from surface to deep. In a first approach to the problem, non-linear behaviour can be analysed by hyperelastic models. This choice is foundamental since in this way many functional aspects of cartilage are taken into account (non linear geometry, elastic non-linear response and the particular comprimibility). Since the numerical model is slightly complex the constitutive model should represent correctly all the mechanical properties of cartilage but with a computational effort as low as possible.

3.4.1 State of the art of constitutive models porposed in literature

In the following paragraph a state of the art for constitutive formulation on articular cartilage tissue is proposed. The aim is to evidence the constitutive models proposed in literature with the relation to the mechanical properties due to cartilage histologic organization. Moreover, it is important to observe that to define constitutive parameters experimental tests are necessary, but for some particular aspects it is difficult to have a direct validation of the constitutive parameters obtained. Finally it

is important to highlight that when constitutive models are used to investigate the behavior of anatomical site of cartilage tissue, their complexity dramatically drop down to linear elastic model, probably due to computational costs.

3.4.1.1 Biphasic models

The first constitutive model for the articular cartilage was a single-stage model that did not consider the time dependency of the behavior in compression. In order to evaluate time-dependent behavior of the liquid phase, has been structured a biphasic pattern.

The biphasic model consists of a solid phase, consisting of the extracellular matrix, collagen, proteoglycans, and chondrocytes, and a liquid phase, characterized by interstitial fluid, water and electrolytes. It was also suggested that:

- the solid phase is homogeneous, isotropic, linearly elastic and permeable, while the liquid phase is not viscous;
- the solid matrix and interstitial fluid is incompressible;
- the leading cause of energy dissipation and the flow of interstitial fluid;
- the resistance of the tissue is proportional to the speed of application of stress.

A study by DiSilvestro et al. (2001), analyzes the ability of biphasic linear poroelastic (BPE), linear poroviscoelastic (BPVE), and linear viscoelastic (LVE) models to predict the reaction force and lateral deformation shown by cartilage joint during stress relaxation in unconfined compression tests.

The linear poroelastic model assumes that the solid phase is elastic, while in the poroviscoelastic model is assumed to be viscoelastic. The linear viscoelastic model considers that the viscoelastic behavior of articular cartilage is completely controlled by the intrinsic viscoelastic nature of the solid matrix, so regardless of the flow of interstitial fluid.

The biphasic poroelastic pattern (BPE), introduced by Mow et al. (1980) assumes that the solid phase is elastic, linear, with constant Poisson's ratio. The poroviscoelastic model (BPVE), introduced by Mak (1986), considered in addition to BPE model the intrinsic viscoelasticity of the solid phase of cartilage tissue and its dependence on the flow of interstitial fluid.

Moreover a comparison between these two models and the linear viscoelastic (LVE) model is performed. The comparison highlight the different capability of the three models in describing different mechanical aspects. The BPE model accurately describes the lateral displacement of the fabric but not the reaction force, the LVE model describes well only the performance of the reaction force, while the model BPVE accurately describes both the trends.

In a subsequent study, conducted DiSilvestro (2001), it was analyzed how different simulation models provided by the BPE and BPVE to vary the load applied in an unconfined compression test. The analysis of experimental data shows that the BPVE model approximates with a good degree of accuracy the viscoelastic behavior of cartilage tissue, while the BPE model was able to estimate the complete viscoelastic response in the case of a slow application of load, estimating only the final part of the deformation when stress is applied rapidly.

3.4.1.2 Biphasic Fibril-reinforced models

3.4.1.2.1 Fibril-reinforced poroviscoelastic

Articular cartilage can be described as a fibril-reinforced composite material consisting of a solid matrix and interstitial fluid (see chapter two). The main components in the solid matrix are two structural macromolecules, i.e. PGs and collagen. Cells (chondrocytes) are responsible for the synthesis of PGs and of collagen. The fluid phase contains water and solutes.

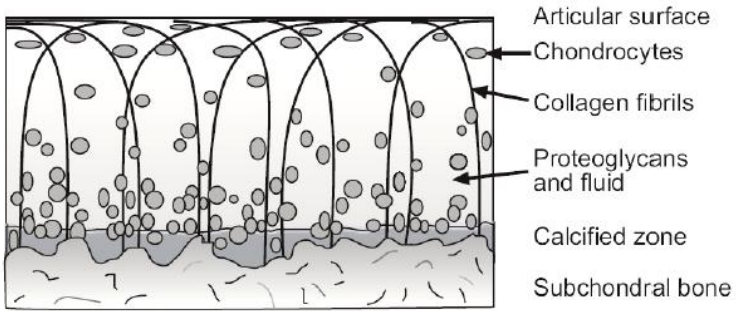

Figure 3.29: Schematic representation of cartilage main constituent.

In the fibril-reinforced models of cartilage, the tissue is assumed to be biphasic, and the solid matrix is divided into a fibrillar and non-fibrillar part. The fibrillar part mimics collagen fibrils, while the non-fibrillar part describes mainly PGs (Li et al

2000, Wilson et al 2005, Julkunen 2008). A swelling effect due to negative charges in cartilage are also included in some fibril-reinforced model (Julkunen 2008).

The fibril-reinforced poroviscoelastic (FRPVE) models consider the non-fibrillar matrix linearly elastic, defined by the Young's modulus E_m, and Poisson's ratio ν_m. The fibrillar matrix is instead assumed non-linear viscoelastic, depending on direction and location. In particular the fibrillar matrix is defined by Young's modulus E_f and the permeability k, both are considered to be depth dependent. Furthermore, E_f and k are dependent on strains: E_f=0 if the fibril strain is compressive, otherwise E_f increases with the fibril strain; k decreases when the compression of the matrix increases.

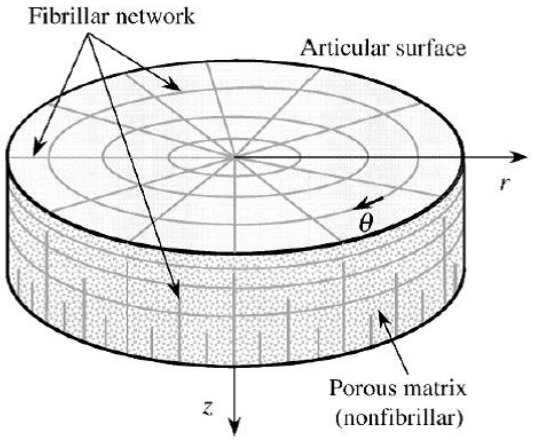

Figure 3.30*: Schematic representation of a nonhomogeneous fibril-reinforced poroelastic model of cartilage.*

In the fibril-reinforced model proposed by Li et al. 2000 it is assumed that the directional differences along θ are negligible despite their presence in the superficial zone (for example the tensile stiffness in a horizontal layer are studied by Mizrahi et al., 1986; Woo et al., 1979). Variations of material properties are also not considered. The elastic parameters of the drained non-fibrillar matrix are considered to be independent of strain, but to vary with the cartilage depth z. With regard to the different family of fibers some additional approximation are considered. The compressive modulus for the fibrils is taken to be zero as a first approximation. Indeed the axial fibrils are inactive in unconfined compression and only the horizontal fibrils (in the radial and circumferential directions) are necessarily considered. The fibrillar tensile modulus increases with the tensile strain (Pins et al.,

1997; Roth and Mow, 1980), and decreases with the depth. Therefore, in this model theYoung's modulus of the horizontal fibrils is taken to be strain dependent.

Regarding to the fluid part some consideration on hydraulic permeability are assumed. In detail the hydraulic permeability decreases with the depth, as the fixed charge density increases. However, an inverse trend may apply to the surface layer due to close packing of the collagen fibrils thereby offering a greater resistance to flow (Maroudas and Bullough, 1968; Muir et al., 1970; Setton et al., 1993; Torzilli et al., 1983). Then the permeability is taken to be strain dependent according to Lai and Mow (1980) and furthermore to vary with the depth.

The volume of the "voids" is assumed to be equal to that of water, the content of which does not change very much along the depth. The content can make up to as much as 85% of the total mass by wet weight in the most superficial (25% of the cartilage), and decreases to about 70% at the subchondral bone in normal adult cartilage (Lipshitz et al., 1976). For confined compression, no fibrils are in tension and thus the stiffness is actually contributed by the nonfibrillar matrix only.

The fibril reinforcement is adopted in a microstructural model to analyze the elastic behavior of cartilage. A fibril-network is introduced into the biphasic model (Mow et al., 1980) with the aim to simulate the strong load relaxation in unconfined tests (Soulhat et al., 1999). In unconfined compression the nonlinear fibril-reinforced poroelastic model (Li et al., 1999c) is able to describe the nonlinear load variations in addition to the strong relaxation pattern. The fibril reinforcement is also considered in a hyperelastic model used for the annulus fibrosus (Klisch and Lotz, 1999). These models employed different constitutive laws but all recognized the distinct role of the fibrils from that of the other solid matrix.

3.4.1.2.2 Fibril-reinforced biphasic viscohyperelastic

Another model, proposed by Garcia and Cortes (2007), is the fiber-reinforced biphasic viscohyperelastic model.

This formulation is able to describe the intrinsic viscoelasticity of the fibrillar component and of the solid phase, non-linear stress-strain response to tension or compression loads.

This model is also characterized by a good correlation between the curves that express the reaction force during a compression load and the lateral deformation with and without the intrinsic viscous effects of the extracellular matrix.
This biphasic pattern and fiber-reinforced viscohyperelastic finite element is therefore able to simultaneously evaluate the non-linear action of a stress-pressure, the intrinsic viscous effects of both solid components (fibrillar and non-fibrillar) of the biphasic pattern and the non-linear stress-strain relationship.

3.4.1.2.3 Fibril-reinforced poroviscoelastic swelling

Julkunen (2008) investigate the possibility of introducing osmotic swelling.
Due to the higher concentration of charges in articular cartilage than in the surrounding fluid, the excess of ions cause a pressure gradient called the Donnan swelling pressure gradient ($\Delta\pi$), which depend on π_{int} and π_{ext}. These variables are the internal and external osmotic pressures, which are dependent on the concentrations of the internal cations ($c+$) and anions ($c-$), on the external salt concentration (c_{ext}), on the internal (φ_{int}) and external (φ_{ext}) osmotic coefficients, on the gas constant R (8.314 J/(K mol)) and on the absolute temperature T (310K).
The Fibril-reinforced poroviscoelastic swelling (FRPVES) model combines viscoelastic fibrils with an inhomogeneous collagen architecture, neo-Hookean non-fibrillar matrix, osmotic swelling and chemical expansion. This model considers that, despite the prevalence of biphasic theory and its general acceptance, the cartilage is not just a set of elastic solid components and water. The negative charges present on the proteoglycans, which constitute the largest component of the solid matrix, introduce an osmotic pressure in the tissue affecting the mechanical properties, such as stress, strain, stress resistance, and electrical charge. Indeed, it was found that the electrical charge present on the proteoglycans affects the apparent increasing stiffness of the solid matrix and decreasing the effect introduced by the viscous fluid flow. In order to not underestimate these effects, three-phase model has been structured for the cartilage tissue.
In a study by Lu et al. (2009) is evaluated how the charge present on proteoglycans affect the response in creep indentation test. In this analysis, the cartilage has been structured according to a model characterized by three-phase: the solid-phase, The liquid phase and the two solutes. The first phase is incompressible, porous and

permeable by a liquid phase (water). The second phase is also incompressible. The third phase, or solute phase, consists of cations and monovalent anions. It is also assumed that the cartilage tissue is isotropic and homogeneous, the porous and permeable solid matrix is linear elastic. In order to focus on the effects on the mechanical behavior of tissue from the fixed charge present on the proteoglycans were not considered the solid matrix effects on permeability, stress-dependent, non-linearity of the relationship and tension-compression.

Another FPVES model that includes the complex structure of the collagen network, the chemical and osmotic swelling properties of articular cartilage is proposed by Wilson et al. (2005). This model showed to appropriately fit confined compression, swelling, unconfined compression and indentation experiments with a single set of material parameters.

This theory is particularly interesting since allows to analyze the link between the collagen network and the swelling properties of articular cartilage. This can be used to study cartilage physiology and pathology. Furthermore, the effect of loss of proteoglycans or collagen damage can be studied with this model. This model can be a useful tool for the analysis of the mechanical behavior and damage mechanisms of articular cartilage, but in complex numerical models the FPVES has high computational costs.

3.4.2 Hyperelastic fiber-reinforced model

The models proposed in literature are capable to describe with high detail the properties of cartilage, from a mechanical point of view and considering all the components involved in the mechanical response. However, when facing a numerical model of high complexity and detail, it is necessary to find a good compromise between the description of the mechanical properties of cartilage and the computational costs of the model. Moreover, some of the models present in literature have parameters that are not compared with experimental tests. Therefore, the constitutive model choose in this work is the fiber-reinfoced hyperelastic model.

The high presence of fibers in cartilage, as described in chapter 2, and the high organization of fibers parallel and riadially distribute on cartilage surface, lead to the necessity of an hyperelastic fiber-reinforced model. The strain-energy potential for

incompressible material is described in the following equation and is in the form of the Holzapfel-Ogden-Gasser model (2006):

$$W = \frac{1}{D}\left(\frac{J^{2}-1}{2} - \mathbf{ln}\, J \right) + C_{10}\ \tilde{I}_1 - 3\ + \frac{k_1}{2k_2}\sum_{\alpha=1}^{N}\ \mathbf{exp}\left[k_2\ \bar{E}_{\alpha}^{\ 2} \right] - 1 \tag{3.1}$$

where

C_{10} is related to the tangential stiffness of the matrix $2C_{10}=G$

D is related to the initial bulk modulus $K_v=2/D$

J is the volume ratio and is assumed J=1.

k_1 is related to the initial stiffness of the fibers

k_2 is related to the initial crimped conformation of the fibers

and $\bar{E}_{\alpha}$ is a structure tensor described as follow:

$$\bar{E}_{\alpha} = \chi(\tilde{I}_1 - 3) + (1 - 3\chi)(\tilde{I}_4 - 1) \tag{3.2}$$

$\bar{E}_{\alpha}$ depends on the variable χ , that allows to describe the dispersion of fibers in the tissue and its variation leads to of different levels of anisotropy for the model.

The existence of a density function ρ(M) is introduced as an orientation density function (Lanir et al. 1996), which characterizes the distribution of fibres with respect to the referential orientation M. The vector M is an arbitrary unit vector located in three dimensional Eulerian space. Thus |M|=1. By characterizing M in terms of two Eulerian angles $\Theta \in [0, \pi]$ and $\Phi \in [0,2\pi]$ it is possible to obtain

$$M(\Theta,\phi) = \sin\Theta\cos\phi e_1 + \sin\Theta\sin\phi e_2 + \cos\Theta\phi e_3 \tag{3.3}$$

where {e1, e2, e3} denote the axes of a rectangular Cartesian coordinate system.

The density function ρ(M) is defined such its derive in dΘdΦ represents the normalized number of fibres with the same orientations in the range [(Θ,Θ+dΘ), (Φ,Φ+dΦ)], and it has to obey the symmetry requirement

ρ(M) ≡ρ(-M).

In addition, it is assumed that ρ(M) is normalized, to obtain

$$\frac{1}{4\pi}\int_{\omega} \rho\ \ M(\Theta,\phi)\ d\omega = 1 \tag{3.4}$$

where ω is the unit sphere and $d\omega=\sin d\Theta d\Phi$. Subsequently, $\rho(M)$ is limited to general orthotropic distributions, where, without loss of generality, the preferred directions of the distribution are assumed to coincide with the axes $\{e_1, e_2, e_3\}$ of the underlying Cartesian coordinate system.

Therefore, given fibres family distributed with rotational symmetry about a mean preferred direction, say a_0 (a unit vector), so that the family contributes a transversely isotropic character to the overall response of the material. Without loss of generality, the preferred direction a_0 is considered to be parallel to the surface of the cartilage layer. Then with the use of equation (3.3) and (3.4) the generalized structure tensor **H** can be defined. The Green-Lagrange strain-like quantity $\bar{\mathbf{E}}\alpha$ is introduced. $\bar{\mathbf{E}}\alpha$ characterizes the strain in the direction of the mean orientation a_{0i} of the family of fibres. Considering the relation

$$\bar{\mathbf{E}}_{\alpha} = \mathrm{H_i}: \bar{\mathrm{C}} - 1 \tag{3.5}$$

$\bar{\mathbf{E}}_{\alpha}$, which is an alternative measure of the fibre distribution, can be written as the equation 3.3 where χ is defined as

$$\chi = \frac{1}{4}\int_0^{\pi} \rho\ \theta\ \sin^3\theta d\theta \tag{3.6}$$

The lower limit of the dispersion parameter, χ=0, describes the ideal alignment of collagen fibres. In this case, the Dirac delta function characterizes the density function, and the (3.2) reduces to:

$$\bar{\mathbf{E}}_{\alpha} = (\tilde{I}_4 - 1) \tag{3.7}$$

The upper limit of the dispersion parameter, χ=1/3, describes the isotropic distribution of the collagen fibres. In this case the density function is constant, $\rho \equiv 1$, and the generalized structure tensor **H** reduces to **I**.

Assuming that a_0 lies in the principal plane it is possible to consider a radial family of fibers all parallel to the surface of the cartilage but radially organized.

In the following figure a schematic representation of the primary and the secondary fibril direction is reported.

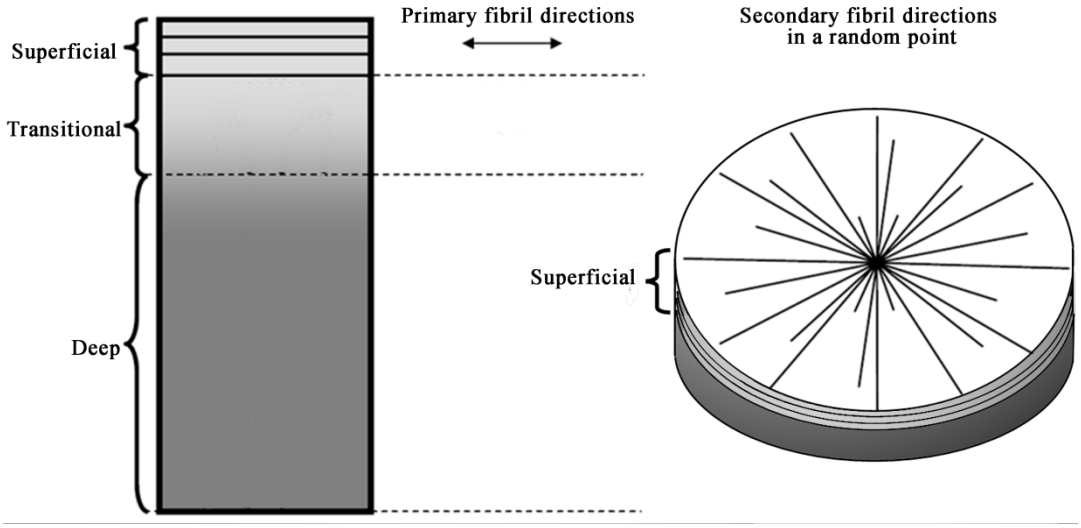

Figure 3.31: Schematic presentation of the collagen architecture in the fibril-reinforced model. In the superficial zone, the collagen fibrils are aligned parallel to the cartilage surface, secondary fibrils represent the collagen network at any given point of the superficial tissue.

On the basis of histological observation and experimental results the biomechanical behavior of cartilage are described ad hyperelastic fiber-reinforced model.

3.5 REFERENCES

Antunes P.J., Dias G.R., Coelho A.T., rebelo F., Pereira T., 2010.Non-linear finite element modeling of anatomically detailed 3D foot model, http://www.materialise.com.

Ayache N., 1995. Medical computer vision, virtual reality and robotics, Image and Vision Computing, vol. 13(4), pp. 295-313.

Cavalcanti M.G.P., Ruprecht A., Vannier M.W., 2002. 3D volume rendering using multislice CT for dental implants, Dentomaxillofacial Radiology, vol. 31, pp. 218-223.

De Leeuw Peter A. J., Pau Golano Joan A. Clavero, C. Niek van Dijk, Anterior ankle arthroscopy, distraction or dorsiflexion?, Knee Surg Sports Traumatol Arthrosc, 18:594–600, 2010.

De Souza V.A., 2007. Design of insole using image base analysis, PhD Thesis, The University of Tokyo, Graduate School of Frontier Sciences.

García JJ, Cortés DH. 2006, A biphasic viscohyperelastic fibril-reinforced model for articular cartilage: formulation and comparison with experimental data, J Biomech. 2007;40(8):1737-44.

Gasser T. Christian, Ogden Ray W and Holzapfel Gerhard A, Hyperelastic modelling of arterial layers with distributed collagen fibre orientations, J. R. Soc. Interface 2006, 3, 15-35

Greenwald A.S., Matejczyk M.B., Articular cartilage contact areas of the ankle, Ann. Rheum. Dis, 37, p: 482, 1978

Huch K., Kuettner K.E., Dieppe P., Osteoarthritis in ankle and knee joints, Semin. Arthritis Rheum. 26 (4), pp 667-674, 1997.

Korioth T.W.P., Versluis A., 1997. Modelling the mechanical behaviour of the jaws and their related structures by finite element (FE) analysis, Critical review in Oral Biology & Medicine, vol. 8(1), pp. 90-104.

Li L. P. and Herzog W. Strain-rate dependence of cartilage stiffness in unconfined compression: the role of fibril reinforcement versus tissue volume change in fluid pressurization. J Biomech, 37(3):375–82, 2004.

Li L. P., Buschmann M. D. and Shirazi-Adl A. Strain-rate dependent stiffness of articular cartilage in unconfined compression. J Biomech Eng, 125(2):161–8, 2003.

Li L. P., Herzog W., Korhonen R. K. and Jurvelin J. S. The role of viscoelasticity of collagen fibers in articular cartilage: axial tension versus compression. Med Eng Phys, 27(1):47–53, 2005.

Li L.P., M.D. Buschmann, A. Shirazi-Adl "A "bril reinforced nonhomogeneous poroelastic model for articular cartilage: inhomogeneous response in uncon"ned compression" Journal of Biomechanics 33: 1533-1541, 2000.

Lu X. L., Miller C., Chen F. H., Guo X. E. and Mow V. C. The generalized triphasic correspondence principle for simultaneous determination of the mechanical properties and proteoglycan content of articular cartilage by indentation. J Biomech, 40(11):2434–41, 2007.

Matteoli S., Corvi A., Wilhjelm J.E., 2010. Modeling the human heel pad, Simpleware Users' Meeting, Solihull, 3 June 2010.

Mak, A. F., 1986, ''The Apparent Viscoelastic Behavior of Articular Cartilage—The Contributions From the Intrinsic Matrix Viscoelasticity and Interstitial Fluid Flows,'' ASME J. Biomech. Eng., 108, pp. 123–130.

Mow, V.C., Kuei, S.C., Lai, W.M., Armstrong, C.G., Biphasic creep and stress relaxation of articular cartilage: theory and experiment. ASME Journal of Biomechanical Engineering 102, pp. pp. 73–84, 1980.

73Ð84.Reach J.S., Amrami K.K., Felmlee J.P., Stnley D.W., Alcorn J.M., Turner N.S., Carmichael S.W., 2007. Anatomic compartments of the foot: a 3-tesla magnetic resonance imaging study, Clinical Anatomy, vol. 20, pp. 201-208.

Rosenberg Z.S., beltran J., Bencardino J.T., 2000. MR Imaging of the Ankle and Foot, Radiographics, vol. 20, pp. S153-S179.

Stytz M.R., Frieder G., Frieder O., 1991. Three-dimensional medical imaging: algorithms and computer systems, ACM Computing Surveys, vol 23(4), pp. 421-499.

Vannier M.W., Hildebolt C.F., Conover G., Knapp R.H., Yokoyama-Crothers N., Wang G., 1997. Three-dimensional dental imaging by spiral CT, Oral surgery, Oral Medicine, Oral Pathology Oral and Maxillofacial Radiology , vol. 84(5), pp. 561-570.

Wilson W., van Donkelaar C. C., van Rietbergen B., Ito K. and Huiskes R., 2004, Stresses in the local collagen network of articular cartilage: a poroviscoelastic fibril-reinforced element study. J Biomech, 37:357–66.

Wilson W., van Donkelaar C. C., Van Rietbergen B., Ito K. and Huiskes R., (2005), "A fibril-reinforced poroviscoelastic swelling model for articular cartilage", Journal of Biomechanics 38(10) 1195–1204.

Wynarsky G.T., Greenwald A.S., Mathematical model of the human ankle joint, J. Biomech. 16 (4), pp 241-251, 1983.

CHAPTER FOUR

4 CONSTITUTIVE MODEL AND EVALUATION OF CONSTITUTIVE PARAMETERS OF CARTILAGE TISSUES

4.1 INTRODUCTION

In this chapter a general view is given on the experimental tests used to characterize the constitutive formulation of bone tissue and cartilage tissue. Moreover the optimization method is introduced defining the cost function that represent the distance between experimental and numerical results and that is minimize with a stochastic method, simulating annealing, coupled with a deterministic method, Nelder-Mead. This optimization method consent to define a set of parameters that minimizes the distance between a set of experimental data and a numerical result obtained with an analytical model. The experimental tests considered are in-vitro indentation test on cartilage with subchondral bone. The set of data that best fit the experimental test should be verified with additional comparison between experimental and numerical results. The constitutive model fully characterized with the selected set of constitutive parameters is used to describe the biomechanical behavior of cartilaginous tissue, and in particular is used in hindfoot joints numerical model. The numerical results obtained for tibio-talar joint are validated with in-vivo tests on ankle joint. In particular the numerical results for strain field distribution on talar articular surface is compared with the strain distribution proposed in the experimental test present in literature. Further consideration on minimum principal stress values obtained are based on data poresent in literature.

4.2 EXPERIMENTAL DATA FOR THE EVALUATION OF CONSITUTIVE PARAMETERS

4.2.1 Cartilage indentation test

It is well known that the mechanical properties of articular cartilage vary significantly both across a normal joint, and between joints depending on factors such as age and the predominating mechanical environment (Brown et al. 2007, Broom & Flachsmann 2003; Swann & Seedhom 1993; Yao & Seedhom 1993; Kempson 1982).

To model complex loading geometries of articular cartilage the most important technique is finite element (FE) method. The indentation test described by Mak et al. (1987) for an unconfined configuration is reproduced considering the biphasic configuration of cartilage. In fact, from a mechanical point of view, articular cartilage is a biphasic material consisting of two distinct phases: a solid phase and a fluid phase. The solid phase is composed of non-fibrous structural macromolecules, fibrous structural macromolecules such as type II collagen, and chondrocytes. In the fully hydrated state, the fluid phase comprises ~80% of the total tissue weight. Attention, as underlined in the second chapter, should be given to the micro-structural organization with type II collagen fibrils of the solid phase organized parallel and radially in the superficial zone. This is made at first with a simple model of an indenter on a cartilage layer above a subcondral bone. This simple model is the basis to define a set of constitutive parameters, that are to be validated with results from *in-vivo* experimental tests.

The indentation test method is the most often used method to determine the in-situ mechanical properties (Mak et al 1987). In the test proposed a total displacement of -0.6 mm corresponding to a strain of 33 % is imposed on a square cartilage layer with subchondral bone of 2 mm in thickness, 20 mm in side. The cylindrical indenter is 4 mm in diameter and is considered frictionless, rigid, and plane-ended as the boundary conditions considered by Brown et al. (2007). The strain rate considered is 0.1 /s.

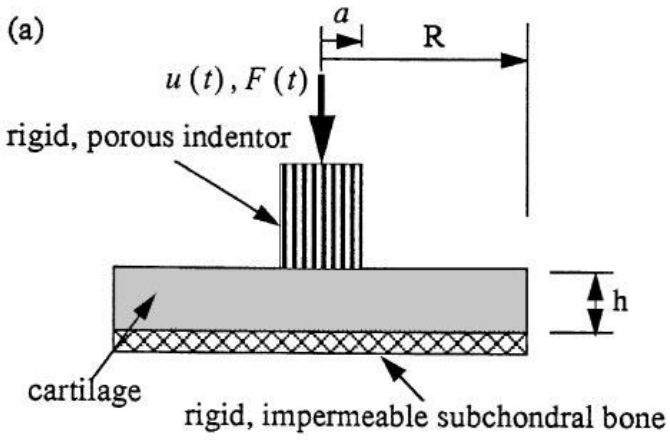

Figure 4.1: Schematic representation of the indentation test set from Brown et al. 2007.

Experimental results obtained with the previously reported experimental set-up are represented in the following figure.

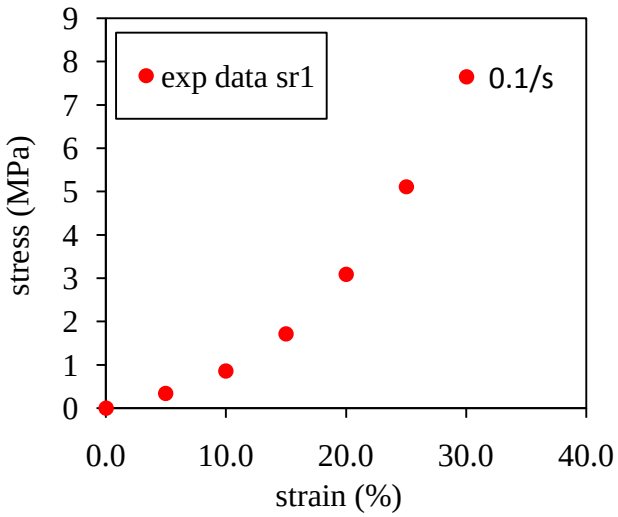

Figure 4.2: Experimental results obtained by Brown et al. 2007 for an indentation test with a strain rate of 0.1/s.

Cartilage shows a non linear response and in particular an hyperelastic behavior, this is due to the complex microstructural composition and organization, as evidenced in chapter two. The experimental curve obtained is to be compared with the numerical results obtained with the hyperelastic fiber-reinforced model proposed in chapter 3.

4.3 MINIMIZATION PROCEDURE FOR THE EVALUATION OF CONSTITUTIVE PARAMETERS

The determination of parameters that govern the constitutive equations of biological materials is a challenge that becomes difficult to face when the number of parameters is significant. Such a case occurs when anisotropic materials and refined nonlinear laws are considered (Araújo A.L. et al., 1996; Grédiac M. et al., 2002). The usual approach consists of the inverse analysis of constitutive models. Inverse analysis assumes that stress-strain history is given by experimental procedures and it attempts to estimate parameter values that would yield the best fit to the given stress-strain history (Lei F. and Szeri A.Z., 2006). Constitutive parameters are consequently evaluated using experimental data, corresponding analytical model results and optimization techniques. Mechanical tests should be performed on geometrically simple specimens and appropriate boundary conditions should be adopted to generate the most homogeneous stress-strain fields possible. Indeed, simple experimental tests can be described using analytical formulations. For more complicated situations, numerical methods must be adopted. Analytical formulations are comparatively less expensive than numerical assessments, enabling cheaper computation for the development of optimization procedures. Furthermore, experimental data should explore several different deformation modes in order to provide the necessary information for the characterisation of the generic stress-strain behaviour of the tissue and the univocal definition of constitutive parameters (Natali A.N. et al., 2006).

4.3.1 Definition of the cost function

The procedure adopted for the definition of the constitutive parameters requires the minimization of the discrepancy between experimental and analytical or numerical model results through a specific cost function.

The cost function depends on the accuracy of the input data (such as experimental data), the quantity of data at disposal and the weight that each data is associated with. There are several cost function proposed in literature (Praagman et al. 2006, Cash et al 2005, Stokes et al. 2001, Kyriacou and Davatzikos 1998, Crowninshield and Brand, 1981). With regard to the biomechanical contest, the formulation used (Natali

et al., 2009a, 2010) is reported in the following equation, where the weight of each data in the output is related with the ratio between the experimental data and model results:

$$\Omega\ \alpha\ = \frac{1}{n}\sqrt{\sum_{i=1}^{n}\left[2-\frac{P_{ii}^{mod}\ \alpha,\lambda_i^{exp}}{P_{ii}^{exp}}-\frac{P_{ii}^{exp}}{P_{ii}^{mod}\ \alpha,\lambda_i^{exp}}\right]^2} \tag{4.1}$$

where α is the set of constitutive parameters, n the number of experimental data, λ_i^{exp} the i^{th} experimental input datum, P_{ii}^{exp} the i^{th} experimental output value, and P_{ii}^{mod} the i^{th} model output result corresponding to the constitutive parameters α and the experimental input λ_i^{exp}. The function Ω is a measure of the overall difference between experimental and model results when constitutive parameters α are adopted. The optimization problem entails evaluation of the set of constitutive parameters α_{opt} that minimizes Ω.

Some limitations on constitutive parameters may be necessary, such as the imposition to tendency of the hyperelastic strain energy function to increase strictly with strain. These conditions may be difficult to be defined by boundaries on parameters domain and should be more easily implemented by penalty contributions to the cost function (Boukari D. and Fiacco A.V., 1995):

$$\Omega\ \alpha\ = \frac{1}{n}\sqrt{\sum_{i=1}^{n}\left[2-\frac{P_{ii}^{mod}\ \alpha,\lambda_i^{exp}}{P_{ii}^{exp}}-\frac{P_{ii}^{exp}}{P_{ii}^{mod}\ \alpha,\lambda_i^{exp}}\right]^2}+\frac{1}{n}\sum_{i=1}^{n}\Theta_i\ \ \alpha,\lambda_i^{exp},P_{ii}^{exp},P_{ii}^{mod} \tag{4.2}$$

where the penalty term Θ_i assumes a reasonably high value when the model result P_{ii}^{mod} does not satisfy a specified criterion.

4.3.2 Implementation of the stochastic-deterministic procedure

If the adopted constitutive model is strongly non-linear, the cost function is often characterised by multimodal behaviour (i.e. the function presents a global minimum and further local minima). Solving the optimization problem by deterministic methods (Stoer J. and Bulirsch R., 1992) may result in the definition of only one of the local minima, without generating the optimal solution. On the other hand a stochastic algorithm performs well in the presence of a very high number of variables. It is based on random evaluations of the cost function, in such a way that

transitions out of a local minimum are possible but it does not guarantee to exactly reach the global minimum, but only to move close to the minimum itself.

It becomes necessary, therefore, to perform the optimization using a new algorithm that is formulated by coupling a stochastic and deterministic methods. A specific simulated annealing procedure (Kirkpatrick S. et al., 1983; Corana A. et al., 1987) and Nelder-Mead (Begambre 2009; Lagarias, J.C, 1998) method can be adopted for this purpose.

The new procedure explores all minima, evaluates the region where the global minimum is located and after returns the exact position of the global minimum itself. In detail the computation begins from an initial set of constitutive parameters that is recorded in the vector α_0. According to SA technique, applying random moves new candidate points α' are generated around the current point α_i. A new point α' is accepted or rejected according to the Metropolis criterion (Metropolis N. et al., 1953) leading to a new current position α_{i+1}. The best point reached, that corresponds to the set of constitutive parameters that mainly minimizes the cost function, is recorded as α^*_{opt}. The solution is used as input to NM method that returns a new point α^{**}_{opt} that is compared with the previous α^*_{opt}. The best of them is recorded as α_{opt} until no more useful cost function improvement can be expected. The procedure returns the set of constitutive parameters associated with the best solution.

To evaluate the efficiency and the reliability of the described procedure, a test is used that refers to the Rosenbrock function, which minimization is a classical test problem that is extensively adopted to evaluate the performance of different optimization algorithms (Hillstrom et al., 1977; Begambre et al, 2009). Results of the comparison between the performance of the suggested algorithm and the SA procedure are reported by Natali et al., 2009.

4.4 DEFINITION OF THE CONSTITUTIVE PARAMETERS FOR CARTILAGE AND COMPARISON WITH NUMERICAL RESULTS

The mechanical behaviour of articular cartilage has been traditionally characterized with elastic, viscoelastic, biphasic or triphasic models. For the sake of simplicity, most analytic models consider cartilage as linear elastic, homogenous and isotropic material. Poroviscoelastic, transversely isotropic biphasic and fibril reinforced

poroelastic models have also been introduced to simulate more realistically the complex structure of articular cartilage and to capture accurately the time-dependent mechanical behavior under loading. But considering a more complex structure, such as a full and anatomically precise tibio-talar joint, it is necessary to choose an adequate constitutive model so as to have reliable numerical results, with a reasonable computational cost. When considering the presence of articular cartilage in complex anatomical site, the cartilaginous tissue is often modeled as a volume between two bone heads. The two different layers are not considered (Gefen 2002, Cheung et al. 2003, Chen et al. 2003, Antunes et al. 2010) and when considered there is no synovial capsule (Anderson et al. 2006). Some example of constitutive formulation used to characterize cartilage in recent numerical model of complex anatomical site, in particular of the foot and the ankle, are presented in the following table:

Year	**Author/s**	**Constitutive formulation for numerical model**
2002	Gefen	linear elastic, isotropic, homogeneous
2003	J.T. Cheung et al.	linear elastic, isotropic, homogenous
2003	Wen-Pin Chen et al.	linear elastic
2006	Anderson et al.	linear elastic
2007	Lin et al.	linear elastic
2008	Ledoux et al.	linear elastic
2010	Antunes et al.	linear elastic, isotropic

Table 4.1: The table resumes some work present in literature with the FE model of the ankle or of a foot joint and the constitutive model proposed for cartilage.

Herein a hyperelastic fiber-reinforced model is considered with one family of fibers, that are parallel to the cartilage surface and radially oriented.

4.4.1 Description of the characteristics of the numerical model for indentation test

The indentation test described in the previous paragraph have been analyzed with a solid model. The solid model consist of a cartilage sample with the shape of a disk

2mm thick and with dimensions sufficient to contain a square of 20mm in side (since the specimen tested by Brown was a 20mm square). The plate ended cilyndrical indentor has the diameter of 4mm as proposed by Brown et al. (2007). Since the indenter is considered frictionless and exactly justapposed to the sample surface avoiding any incongruency, in the solid model it is represented with a group of nodes with an imposed compressive displacement of 0.6mm.

The displacement is applied with a strain rate of 0.1/s. Elements used to model the cartilage specimen are tetrahedral elements with eight nodes. Since the disk is symmetrical only results for a quarter of disk are presented.

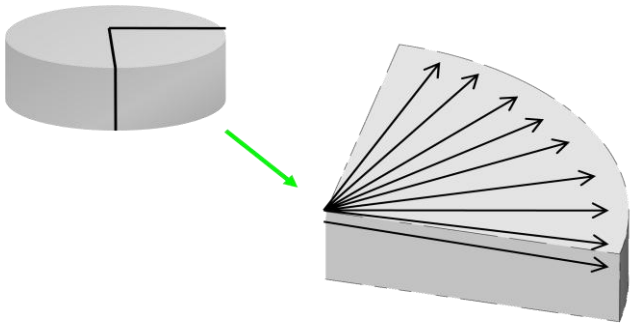

Figure 4.3: Schematic representation of the numerical disk sample with fibers direction.

In the model fibers are parallel to the cartilage surface and in the constitutive model this can be obtained defining χ=0.

The parameters to be defined are: C_{10}, D, k_1, k_2. Where the first parameter is C_{10} is due to the iso-volumetric behaviour of the matrix and it is related to the tangential stiffness of the matrix with the relation $2C_{10}=G$; D describes the volumetric behabior of matrix and is related to the initial bulk modulus $K_v=2/D$. Whereas k_1, k_2 are due to fibers properties and in particular the first is related to the initial stiffness of the fibers, the second is related to the initial crimped conformation of the fibers.

4.4.2 Comparison between numerical and experimental results

Numerical and experimental results are compared and proposed in a graph that represents the stress (MPa) vs strain (%).

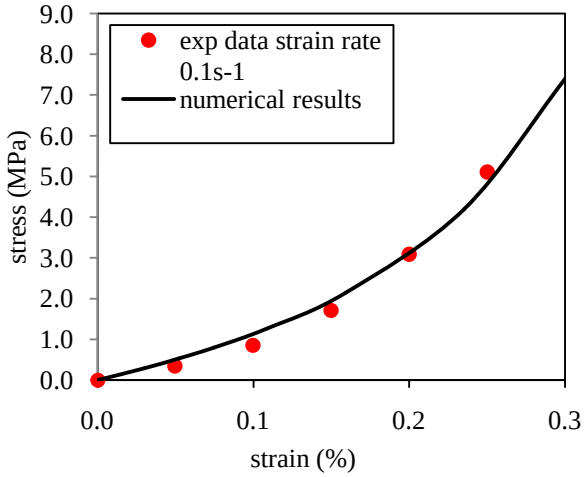

Figure 4.4: Results of hyperelastic fiber-reinforced model compared with experimental data obtained by Brown et al. 2007.

This preliminary analysis is foundamental to define a proper model and a starting set of mechanical parameters to use in the more complex model of the sub-talar joint. Parameters of hyperelastic fiber-reiforced model are the following table:

Constitutive model parameters			
For matrix		**For fibers**	
C_{10} (MPa)	0.01	k_1 (MPa)	33.0
D	0.22	k_2	2.1

Table 4.2: Set of parameters defined for fibro-reinforced hyperelastic model.

The contour of numerical results obtained are given for displacement field in mm as a sequence of frames. Frame A is related to the first contact between the indenter and the cartilaginous disk, frame B is a taken when half deformation is imposed and frame C refers to the fully deformed condition. It can be noticed that at first only the region of contact between the indenter and the cartilage disk layer is involved in the deformation, with the increasing of strain imposed the deformation involves more the deep peripheral area of the disk.

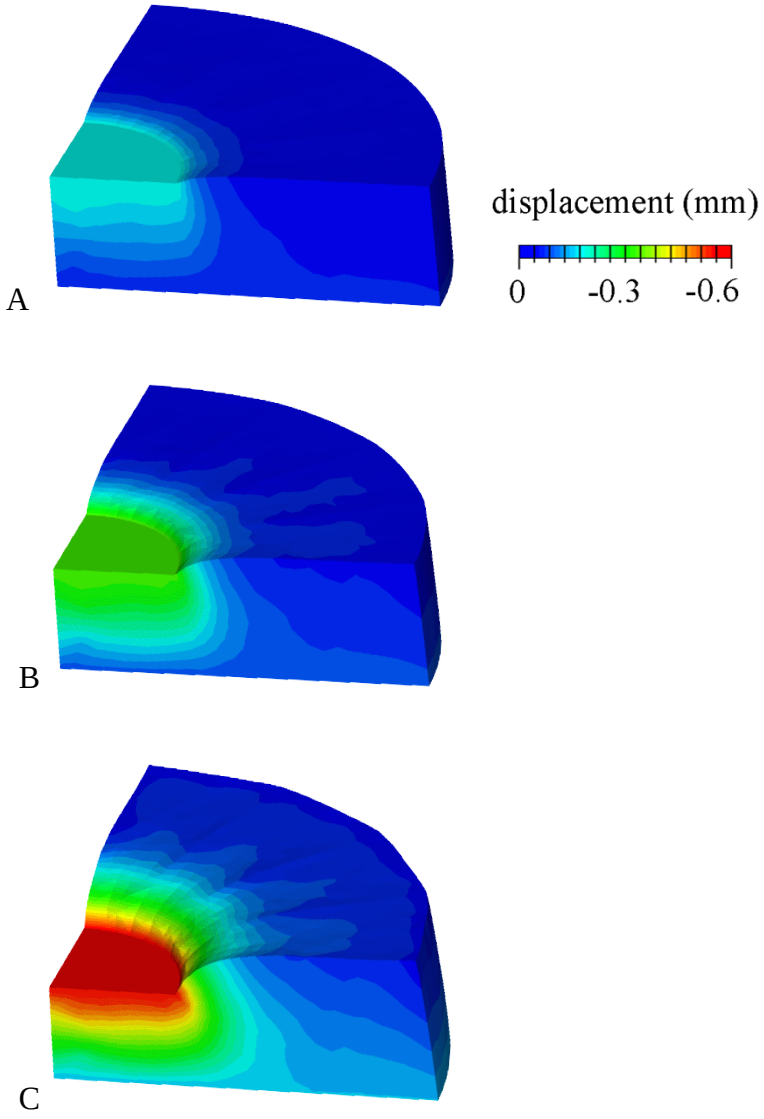

Figure 4.5: Results of different frames of the numerical results model.

A first analysis on the set of parameters obtained is developed considering the relations: $2C_{10}=G$ and $K_v=2/D$ and the relations between bulk modulus and tangential stiffness with the aggregate modulus and the Poisson's ratio.

Using the relations proposed the following mechanical properties are defined:

G= 0.02 MPa tangential stiffness

K_v=9.09 MPa bulk modulus

H_a=3.05 MPa aggregate modulus

ν=0.49 Poisson's ratio

These are in congruence with values present in literature for the aggregate modulus Li and Shirazi 2000 porposed a renge between 0.4 and 4 MPa, while for the Poisson's ratio Anderson et al. 2006 proposed 0.42, Li and Shirazi 2000 porposed a 0.49, Mow et al. 1988 proposed 0.39.

The parameters obtained for the hyperelastic fiber-reinforced formulation are the starting point for more complex analysis in the tibio-talar numerical model. This step is foundamental also for the validation of the numerical results with the proposed set of parameters, since the experimental data used are taken from tests made on cartilage froma a bovine patellae. To validate the set of parameters an *in-vivo* test on tibio-talar joint will be used.

4.5 COMPARISON BETWEEN NUMERICAL RESULTS OF TIBIO-TALAR JOINT DEFORMATION AND IN VIVO COMPRESSION TESTS

The results obtained with the constitutive formulation and the set of parameter defined are in good agreement with indentation tests. This kind of experimental test is performed on disks of cartilage harvested from bone articular surface, then it is important to verify if the hyperelastic fiber-reinforced model and the set of parameters defined are adequate to describe mechanical response of human articular cartilage and in particular of foot joints.

4.5.1 Description of the characteristics of the sub-talar joint numerical model

With the Finite Element Method, the solid model is discretized, for the numerical analysis of tibio-talar joint. The elements used in the numerical model are tetrahedral with 8 nodes. Hyperelastic fiber-reinforced formulation is used to describe the biomechanical behaviour of cartilage, while synovial fluid is considered as a material with very low Young modulus and incompressible, as if it was a liquid.

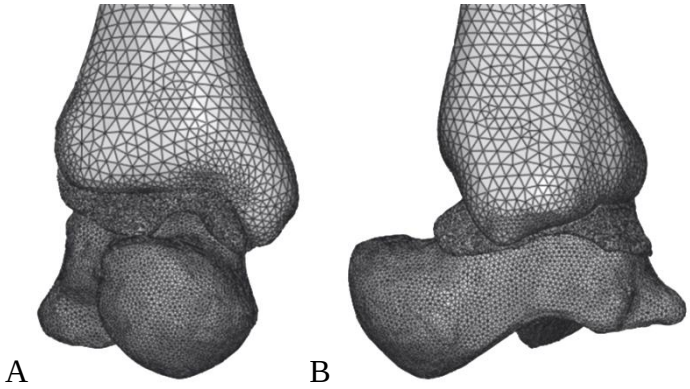

Figure 4.6: Numerical model of tibiotalar joint A) in frontal view, B) sagittal view. It is possible to see the sinovia around the joint.

4.5.2 Description of the sub-talar joint compression test

In living human subjects, it is impossible to accurately scan joint under loading conditions, especially under body weight. The time dependent biphasic behavior of the cartilage causes continuous cartilage deformation during loading and the MR imaging always takes minutes to scan the joint.

In a study by Li et al. (2008) it is proposed the deformation of srticular cartilage of human ankle joints using a combined dual-orthogonal fluoroscope and MR imaging technique. The *in-vivo* position of the ankle was recorded at different time intervals. Subsequently the *in-vivo* bones and joint positions at different time intervals under the controlled loading conditions were used to calculate the *in-vivo* cartilage deformation response as a function of time.

The most interesting aspect in this procedure is that the *in-vivo* ankle positions with time were reproduced using the 3D ankle joint model and the captured fluoroscope images. Even though MR imaging techinique has been widely used to investigate cartilage deformation under various loading conditions, the study by Li et al. is one of the few to report 3D real-time cartilage deformation in response to a physiological loading history and *in-vivo*. In a parallel work by Wan and Li et al. (2007) a strain field distribution was reconstructed for talar surface.

4.5.3 Comparison between numerical and experimental results

The hyperelastic fiber-reinforced formulation and parameters are then used in the more complex solid model of the sub-talar joint. A compression load with a

physiological magnitude of 765 N is applied on the tibia. The strain distribution along the talar surface, at the end of the load, is compared with the one obtained in the study by Wan et al. (2007).

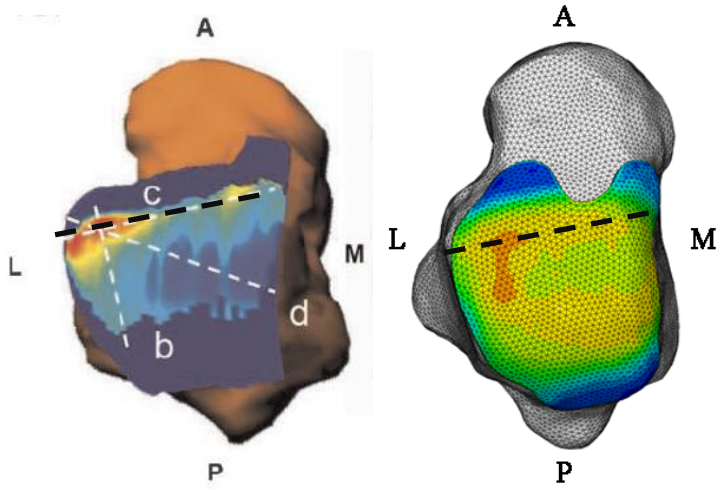

a) b)

Figure 4.7: Strain distribution on the talar cartilage surface of one typical subject in Wan et al. a); Strain distribution on the talar cartilage surface of one typical subject in the present work b).

In more detail, results proposed by Wan et al. for the strain % along the latero-medial line are compared with the strain % results obtained in the numerical model along a latero-medial line that is comparable with the one porposed by the author.

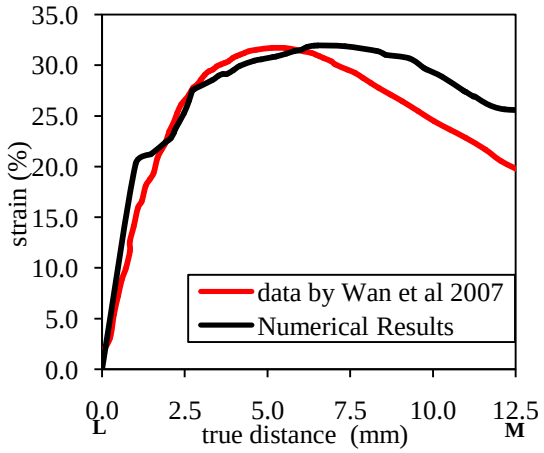

Figure 4.8: Strain distribution on the talar cartilage surface along latero-medial line for one typical subject in Wan et al. (red line) compared with numerical results obtained along latero-medial line (black line).

Differences are due to intersubject differences, in fact even if the analyzed modals are developed starting from healty subject exists an intersubject variability in talar cartilage thikness and surface. For example Tang evidence an intersubject variability in talar cartilage thickness of 1.80±0.06 mm in talus cartilage thickness obtained evaluating an average root mean square (RMS) considering four repeated measurements in each of four specimens. Also Al-Ali (2002) evidenced an average root mean square (RMS) of 44.0±0.38 μm for the talus cartilage thickness intersubject variability. Moreover a possible morfometric difference can exist beween two subject even if both healty.

A deformation up to 30% of cartilage thickness on the surface of human articulation is in agreement also with unconfined compression tests on cartilage by Gore et al (1983).

The so characterized model will be used in the following chapter in the investigation of different tibio-talar loading and the investigation of a full model of the hindfoot.

4.6 NUMERICAL ANALYSIS OF THE HINDFOOT DEFORMATION CONSIDERING THE OSTEOARTHRITIC CARTILAGE

Osteoarthritis (OA) afflicts more than 20 million people in the United States and about 10% of adults over the age of 50 years. It has been demonstrated that 2.0% of women and 1.4% of men per year develop radiographic OA, although only approximately half of these cases lead to symptomatic disease (Felson et al. 1995). In the UK osteoarthritis is the most common form of arthritis, affecting an estimated 8.5 million people. This pathology lead to important socio-economical consequences, due to the longer perspective of life and to the fact that nowadays it is normal to have an active social and working life over 50 years old. .

4.6.1 Pathology and degradation of cartilage a case study of OA cartilage

OA is one of the leading causes of disability and dysfunction in the elderly population; it has been estimated that the total cost for arthritis, including OA, is over 2% of the United States gross domestic product. In end-stage disease, clinical characteristics including various degrees of joint pain, stiffness, dysfunction, and deformity as well as the radiographic manifestations of joint space narrowing,

subchondral sclerosis, and osteophyte formation, are easily recognized. The osteoarthritic ankle loses the smooth cartilage lining which normally allows for low friction and pain free weight bearing However, signs and symptoms in earlier stages, when treatment may alter disease course, are more elusive.

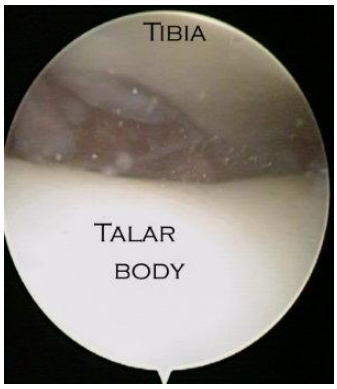

Figure 4.9: Laparoscopic image of ankle joint with cartilage affected by OA, on the left side of tibia distal surface degradation of cartilage can be easily identified.

Understanding the basic science of cartilage and the changes that occur in OA is imperative to develop novel strategies to diagnose and treat this disorder.

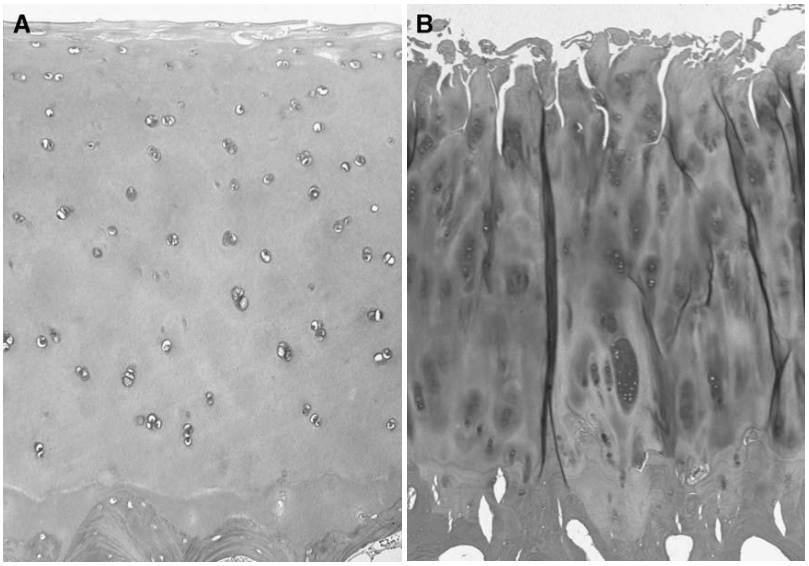

Figure 4.10: Histologic section with hematoxylin and eosin staining of articular cartilage in (A) healthy adult and (B) early OA, demonstrating cartilage clefts, chondrocyte cloning, and chondrocyte necrosis.

Typical absorbance profiles, showing the distribution of proteoglycans over the depth of the normal and degraded cartilage samples are presented in the following figure (Brown et al. 2007). The aim of the authors was to study if it was possible to recreate

the OA degraded condition with trypsin treatment, here also the trypsin curve is reported.

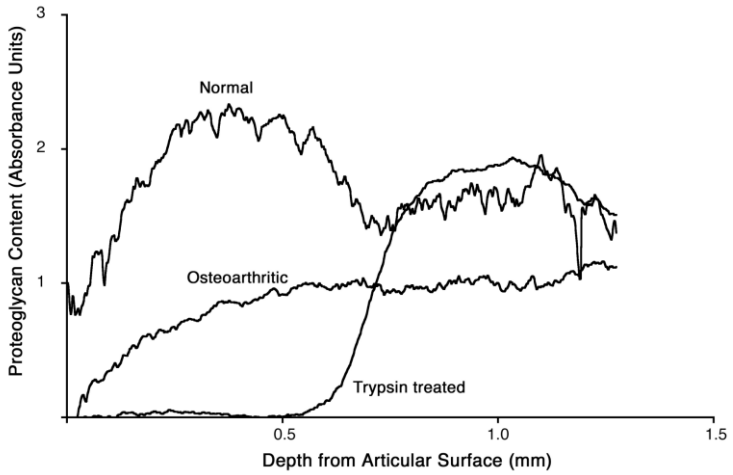

Figure 4.11: The concentration of proteoglycans by absorbance value for normal, trypsin treated and osteoarthritic samples.

The results evidence that normal samples followed similar patterns, while trypsin treatment produced a wavefront of proteoglycan (PG) depletion on the surface. Samples from osteoarthritic joints were characterised by a more uniform depletion of proteoglycans over the depth of the tissue. The difference between the proteoglycan present on the surface of healty cartilage versus OA cartilage is evident. In addition the distribution of proteoglycan on the whole cartilage depth is strongly different. An high presence of proteoglycans is evident in healty cartilage and in particular on the superficial zone, while OA cartilage shows a close-to-zero presence of PG on the very superficial area. Then osteoarthritic specimens are characterized by a uniform loss of proteoglycan over the depth of the cartilage matrix but on the surface disruption of PG is more evident.

Moreover, in OA cartilage a higher percentage of nonarranged proteoglycan exists. Reducing the length of proteoglycans the formation of normal macromolecular complex is inhibited (Mankin 1982). This breakdown of proteoglycan architecture leads to a more permeable solid matrix resulting in a significan diminuition of the hydraulic pressure in early OA cartilage (Pearle et al. 2005). This lead to larger zones filling out the matrix space between several cell cluster. Broom (1984) analyzed the microstructure of OA cartilage and evidenced that the consequence of this rupture of

macromoleculae was associated with a series of fibrous arrays with a waveform or crimp configuration.

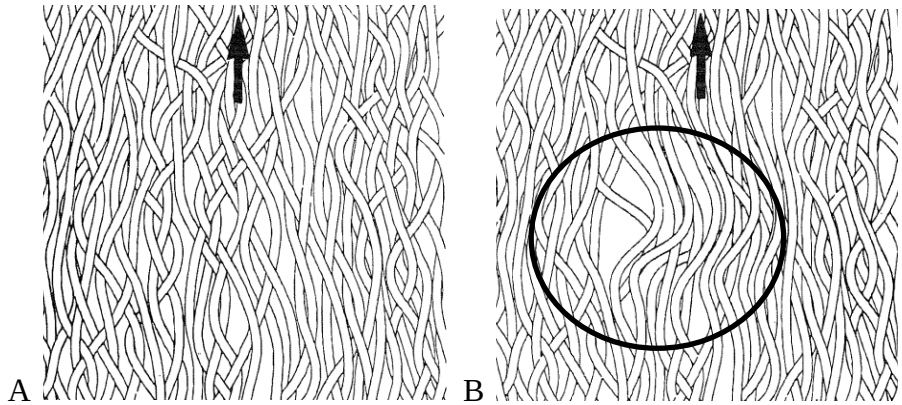

Figure 4.12: Schematic representation of collagenous network in middle region of normal articular cartilage A) and degrade cartilage B). Arrows indicate radial direction.

The degenerative process involves a loss of tensile strength of the individual collagen fibrils and a modified inter-fibril crosslinking of the principally radial arrays of fibers.

4.6.2 Definition of constitutive parameters

The experimental tests used to identify parameters is the indentation test developed by Brown et al. (2007) on a disk of cartilage harvested from bovine patellae degraded due to OA. With the same procedure introduced for healty cartilage a set of constitutive parameters is defined for the hyperelastic fiber-reinforced model.

To define the set of parameters (D, C_{10}, k_1, k_2) according to literature evidence on OA cartilage composition, only the parameters related to the bulk modulus (D) and the initial crimped configuration of fibers are changed (k_2) (Pearle et al 2005, Broom 1984). The set of parameters that best fit the experimental data are:

Constitutive model parameters			
For matrix		**For fibers**	
C_{10} (MPa)	0.01	k_1(MPa)	33.0
D	0.66	k_2	3.2

Table 4.3: Set of parameters defined for fibro-reinforced hyperelastic model for cartilage affected by OA.

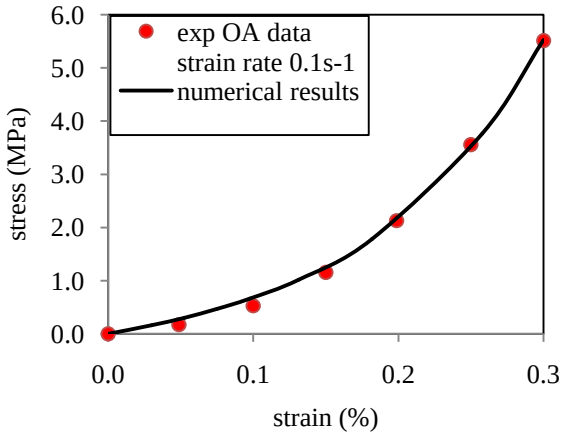

Figure 4.13: Comparison between experimental results and numerical results for the indentation test of a disk of cartilage characterized with OA set of parameters.

It is possible to notice that according to literature the new set of parameters microstructurally describes the cartilage as formed by collagen in a more comped configuration (higher k2) and with a small bulk modulus (D is higher) that lead to a reduced aggregate modulus Ha (Pearle et al. 2005) In fact, from the parameters obtained it is possible to deduce the following mechanical properties:

tangential stiffness G= 0.02 MPa

bulk modulus K_v=3.03 MPa

aggregate modulus H_a=1.03 MPa

Poisson's ratio ν=0.49

The numerical results for a disk of OA cartilage loaded with an indenter are reported in comparison with numerical results obtained for healty cartilage.

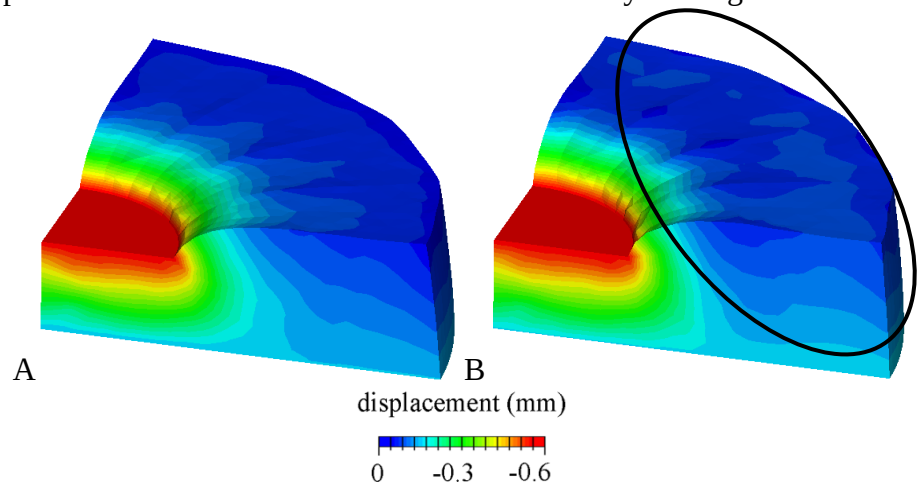

Figure 4.14: Comparison between numerical results for healty cartilage A); and for OA cartilage during the indentation test.

It is interesting to notice that the cartilage affected by OA showa a displacement field larger than healty cartilage. The displacement involves an higher area of tissue even in the peripheric zone of the disk.

Further, analyzing the stress numerical results it is possible to see that the stress il less distributed, that is related with the reduced capability of redistributing loads in OA cartilage.

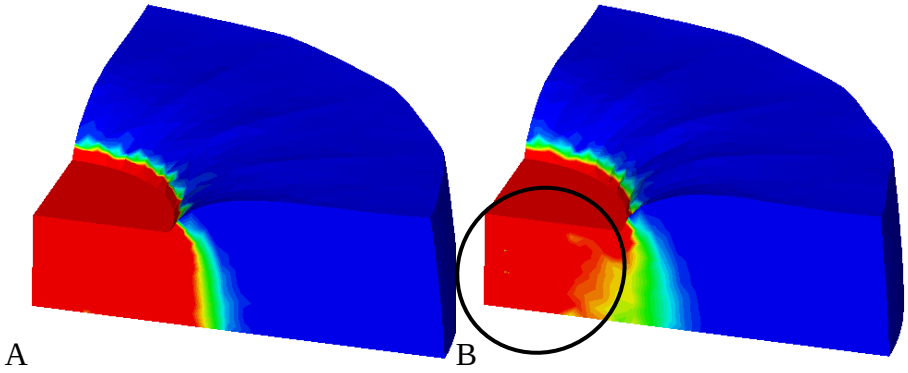

Figure 4.15: Comparison between numerical results for healty cartilage A); and for OA cartilage during the indentation test (Min Principal Stress range 0-4MPa from blue to red).

The overload on a smaller area even of ohysiological load can lead to the death of more cells and therefore to the distruption of more propteoglycan moleculare, and as a result the tissue is damaged without the possibility of recovering its function (Repo and Finlay (1977).

4.7 REFERENCES

Al-Ali D, Graichen H, Faber S, Englmeier KH, Reiser M, Eckstein F. 2002 Quantitative cartilage imaging of the human hind foot: precision and inter-subject variability, J Orthop Res. Mar;20(2):249-56.

Antunes P.J., G.R. Dias, A.T. Coelho, F. Rebelo, T. Pereira Non-Linear Finite Element Modelling of Anatomically Detailed 3D Foot Model, http://www.materialise.com

Araújo A.L., Mota Soares C.M., Moreira de Freitas M.J., 1996. Characterization of material parameters of composite plate specimens using optimization and experimental vibrational data, Composites: Part B, vol. 27, pp. 185-191.

Begambre O., Laier J.E., 2009. A hybrid particle swarm optimization – simplex algorithm (PSOS) for structural damage identification, Adv. Eng. Softw, vol.40(9), pp. 883-891

Boukari D., Fiacco A.V., 1995. Survey of penalty, exact-penalty and multiplier methods from 1968 to 1993, Optimization, vol. 32, pp. 301–334.

Broom, N. D. & Flachsmann, R. 2003 Physical indicators of cartilage health: the relevance of compliance, thickness, swelling and fibrillar texture. Journal of Anatomy 202, 481-494.

Brown, Cameron P. and Crawford, Ross W. and Oloyede, Adekunle, 2007. Indentation stiffness does not discriminate between normal and degraded articular cartilage. Clinical Biomechanics 22(7):pp. 843-848.

Cash D.M., Miga M.I., Sinha T.K., Galloway R.L., and Chapman W.C., 2005, Compensating for Intraoperative Soft-Tissue Deformations Using Incomplete Surface Data and Finite Elements, Ieee transactions on medical imaging, 24 (11), 1479-91.

Cheung JT, Zhang M, Leung AK, Fan YB., 2005, Three-dimensional finite element analysis of the foot during standing--a material sensitivity study, J Biomech. May;38(5):1045-54.

Corana A., Marchesi M., Martini C., Ridella S., 1987. Minimizing multimodal functions of continuous variables with the "Simulated Annealing" algorithm, ACM Transactions on Mathematical Software, vol. 13, pp. 262-280

Crowninshield R. D. and Brand R. A., 1981, A physiologically based criterion of muscle force prediction in locomotion," J. Biomech., vol. 14, pp. 793–801.

Grédiac M., Toussaint E., Pierron F., 2002. Special virtual fields for the direct determination of material parameters with the virtual fields method. 1 – Principle and definition, International Journal of Solids and Structures, vol. 39, pp. 2691-2705.

Kempson, G. E. 1982 Relationship between the tensile properties of articular cartilage from the human knee and age. Annals of th Rheumatic Diseases 41, 508-511.

Kirkpatrick S., Gelatt C.D., Vecchi M.P., 1983. Optimization by simulated annealing, Science, vol. 220, pp. 671-679.

Kyriacou S.K. and Davatzikos C., 1998, A biomechanical model of soft tissue deformation, with applications to non-rigid registration of brain images with tumor pathology, Lecture Notes in Computer Science, Volume 1496, 531-538

Lagarias, J.C., J.A. Reeds, M. H. Wright and P. E. Wright, 1998. Convergence properties of the Nelder Mead simplex method in low dimensions, Siam J. Optim. vol. 9, pp. 112-147.

Ledoux William R, Evan DW Dengler and Michael J Fassbind, A finite element foot model for simulating muscle imbalances, J Foot Ankle Res. 2008; 1(Suppl 1): O45.

Lei F., Szeri A.Z., 2007. Inverse analysis of constitutive models: biological soft tissues, Journal of Biomechanics, vol.40 (4), pp.936-940.

Li G, Wan L, Kozanek M, 2008, Determination of real-time in-vivo cartilage contact deformation in the ankle joint, J Biomech.;41(1):128-36.

Metropolis N., Rosenbluth A., Rosenbluth M., Teller A., Teller E., 1953. Equation of state calculations by fast computing machines, Journal of Chemical Physics, vol. 21, pp. 1087-1090.

Natali A.N., Carniel E.L., Pavan P.G., Dario P., Izzo I., 2006. Hyperelastic models for the analysis of soft tissue mechanics: definition of constitutive parameters, proceedings of BioRob2006, Pisa (I), pp. 1-4.

Natali A.N., Forestiero A., Carniel E.L., 2009, Parameters identification in constitutive models for soft tissue mechanics, Russian Journal of Biomechanics, V.13 N. 4 (46): 29-39.

Praagmana M., Chadwick E.K.J., van der Helm F.C.T., Veegera H.E.J., 2006, The relationship between two different mechanical cost functions and muscle oxygen consumption, Journal of Biomechanics 39, 758–765

Stoer J., Bulirsch R., 1992. Introduction to numerical analysis (second edition), Springer-Verlag, New York.

Stokes I.A.F., Gardner-Morse M., 2001, Lumbar spinal muscle activation synergies predicted by multi-criteria cost function, Journal of Biomechanics, 3, pp 733–740

Swann, A. C. & Seedhom, B. B. 1993 The stiffness of normal articular cartilage and the predominant acting stress levels. British Journal of Rheumatology 32, 16-25.

Wu L., Nonlinear finite element analysis for musculoskeletal biomechanics of medial and lateral plantar longitudinal arch of Virtual Chinese Human after plantar ligamentous structure failures, Clin Biomech (Bristol, Avon). 22(2), 2007, pp. 221-9.

Yao, J. Q. & Seedhom, B. B. 1993 Mechanical conditioning of articular cartilage to prevalent stress. British Journal of Rheumatology 33, 16-25.

CHAPTER FIVE

5 NUMERICAL ANALYSIS AND RESULTS OF HINDFOOT BIOMECHANICAL BEHAVIOR

5.1 INTRODUCTION

The numerical model developed in chapter 3 is fully characterized with a constitutive model for each biological tissue involved and each constitutive model is fully characterized with specific parameters obtained in chapter 4. It is important to underline that the constitutive model proposed is chosen to fit adequately the biomechanical properties of bone tissues and cartilage layers, in consideration of the particular physiological loads of the anatomical site here studied, the foot. In consideration of the high complexity of the numerical model, the attention is focused on the joints of the hindfoot and in particular numerical analysis of tibio-talar joint and subtalar joint in different loading condition are developed. The particular conditions to be studied are:standing position, dorsiflexion. Standing position is also called neutral position and is comparable with the configuration in stance phase of gate cycle.It consists of a physiological load applied on the tibia axis. Dorsiflexion is one of the main foot configuration during heelstrike phase. In this phase cartilage layers role is particularly important. In fact, during the heel strike phase of the gate cycle the hindfoot joints can bear 1.15 times the whole body weight and cartilage plays an important role in redistributing load over articular surface and trsmitting load to mid-foot bones.

In the last paragraph of this chapter the procedure developed for healty cartilage is the starting point in the analysis of osteoartritic cartilage. A specific set of parameters for the fiber-reinforced hyperelastic constitutive model is defined for OA cartilage, and the parameters are changed according to experimental and clinical evidence on the effects of OA on cartilage microstructure. Numerical results obtained from the numerical model with OA cartilage in standing position are compared to those obtained for healty cartilage.

5.2 NUMERICAL ANALYSIS OF HIND-FOOT JOINTS IN DIFFERENT PHYSIOLOGICAL CONFIGURATIONS

5.2.1 Numerical analysis of standing configuration

In this numerical analysis standing position is considered applying a load of 765N on the tibia axis. This condition is comparable with a one-foot standing position or with the stance phase of the gate cycle. The numerical model used is the one introduced in the previous chapter. Therefore cartilage is characterized with the fiber-reinforced hyperelastic model with the parameters that showed to give results comparable with *in-vitro* indentation test and with *in-vivo* results for strains (%) on talar articular surface. Herein, the results are given more in detail for tibia and talo. It is important to underline that results are proposed for an articulation with two cartilage layers and with synovial capsule.

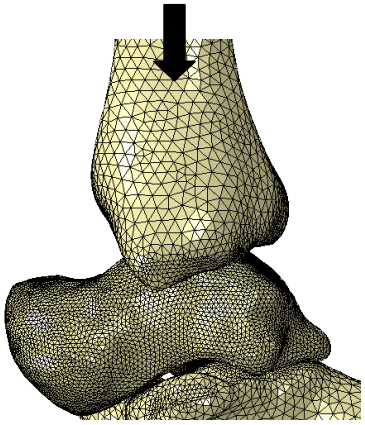

Figure 5.1 Lateral view of tibio-talar joint with the loading direction in evidence.

In the following figures are reported in detail of the numerical results for tibia and talo in the loaded condition.

Considering a section of the lateral view of foot numerical model it is possible to notice that synovial capsule deforms very little. Strain field involves mainly cartilage layers as expected, since synovia is a capsule fulfilled with a fluid that has the

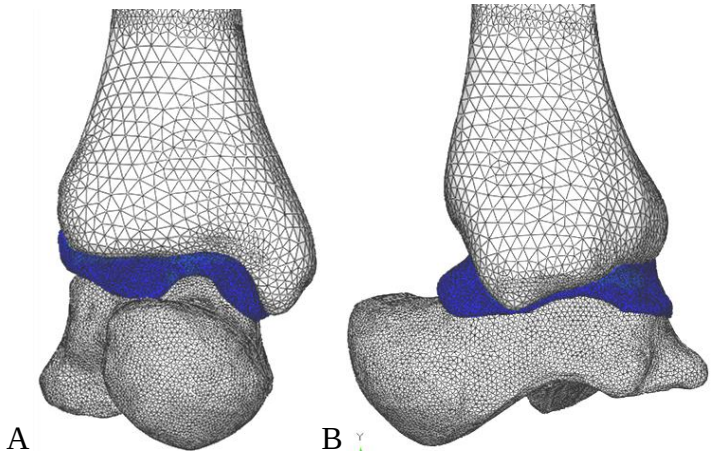

Figure 5.2 Front view A) and Lateral view B) of tibio-talar joint with synovial capsule in the numerical model after compression.

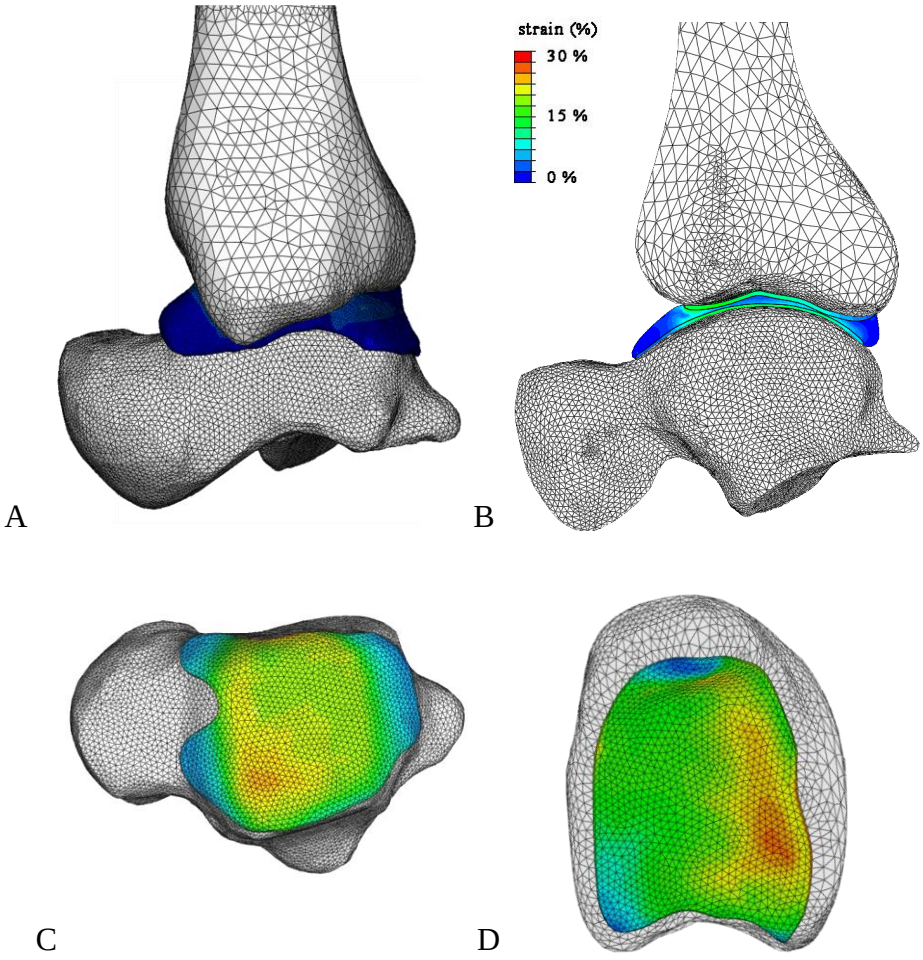

Figure 5.3 Lateral view of tibio-talar joint with synovial capsule for strain field numerical results in compression A); section of the same view B); talar articular surface C); tibia articular surface D).

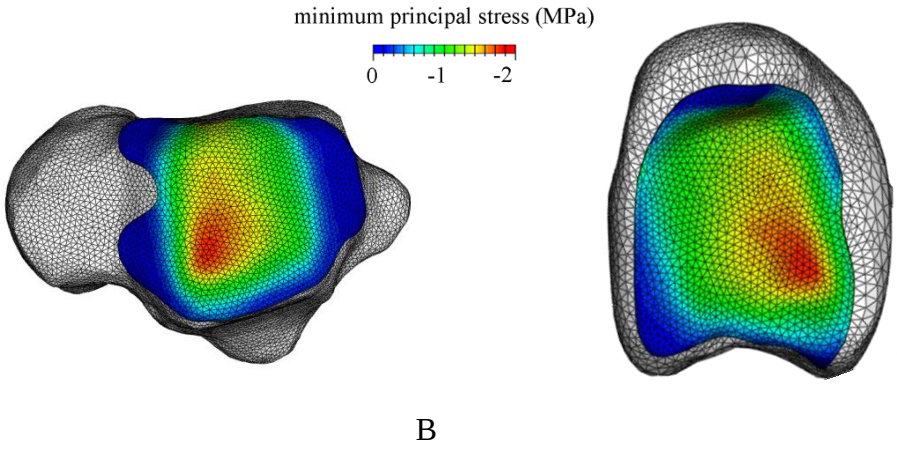

Figure 5.4 Detail of tibio-talar joint with synovial capsule for stress field numerical results for talar articular surface A) and tibia articular surface B).

Further a comparison is proposed for numerical results of stress field obtained in the tibio-talar joint with and without synovial. This analysis is aimed to evidence the role of synovial in the redistribution of stress during load.

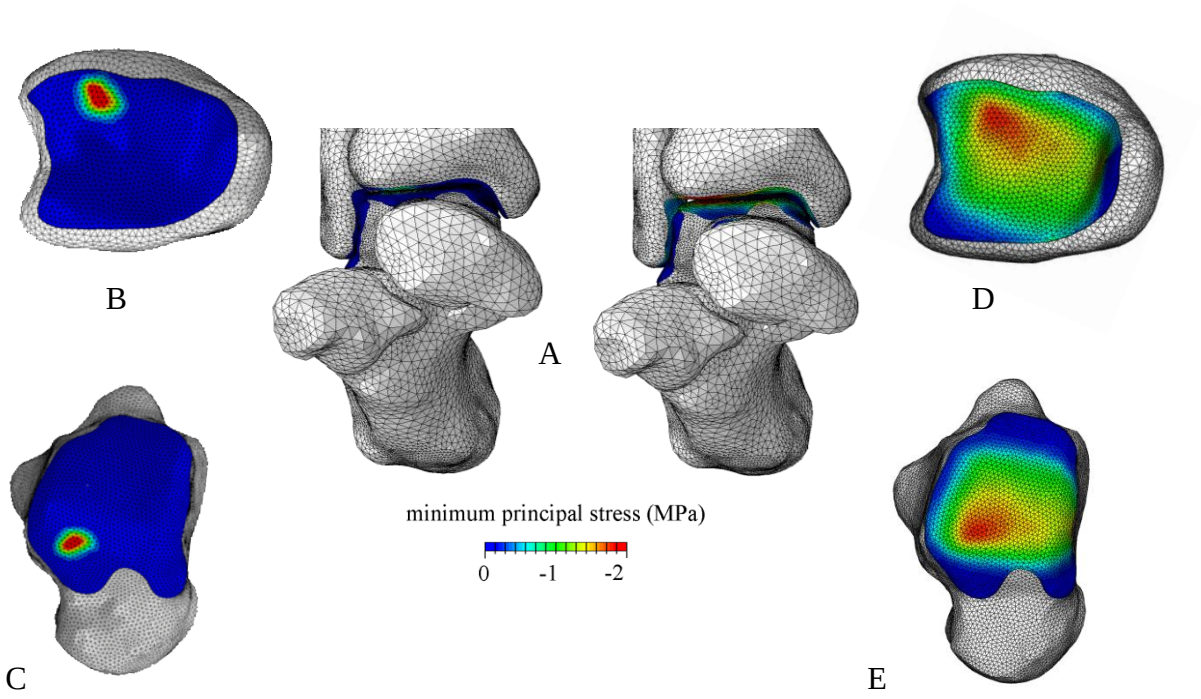

Figure 5.5 Frontal view of tibio-talar joint minimum principal stress field A) without synovial on the left and with synovial on the right; tibia articular surface without synovial B); talar articular surface without synovial C) ; tibia articular surface with synovial D); talar articular surface with synovial E).

It is possible to notice how the synovial allow to redistribute stresses on the surface of the talo, whether without synovial capsule only a small area bear the load applied.

In the following figure are reported the numerical results for other talar joints, and in particular for talo-navicular joint, talo-fibular joint and talo-calcanear joint.

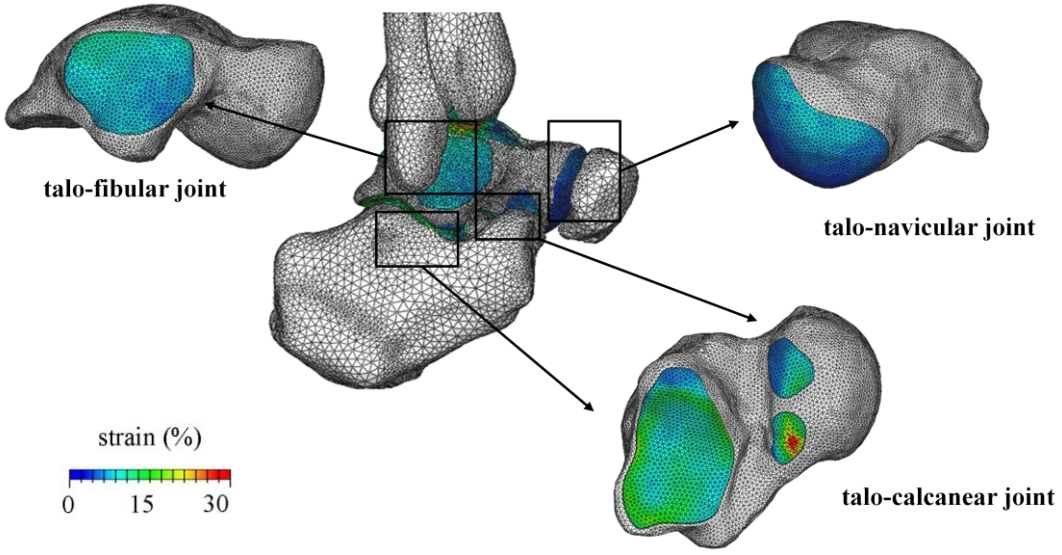

Figure 5.6: Representation of stance condition minimum principal strain in other joints of the hindfoot relataed to talar bone.

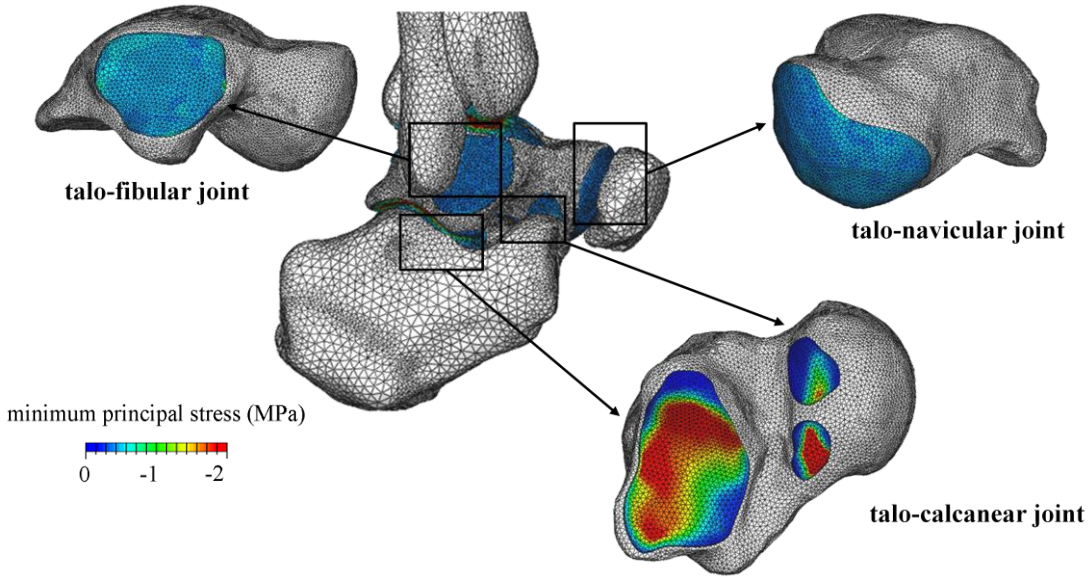

Figure 5.7: Representation of stance condition minimum principal stress in other joints of the hindfoot relataed to talar bone.

From numerical results it is possible to notice that the both strain field and stress field develop more in the talo-calcanear joints. Then it is interesting to analyze

differrent physiological conditions such as dorsiflexion and plantarflexion, to understand if the load in those cases is trasmetted to the forefoot.

5.2.2 Numerical analysis of dorsiflexion foot configuration

Numerical analysis for hind-foot considering a physiological dorsiflexion angle of 13° degrees is developed. With dorsiflexion it is meant that the angle between tibial axis and talo axis is reduced. The rotation is considered around the intermalleolar axis.

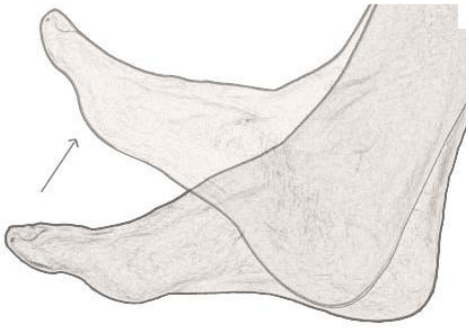

Figure 5.8: Schematic representation of dorsiflexion movement.

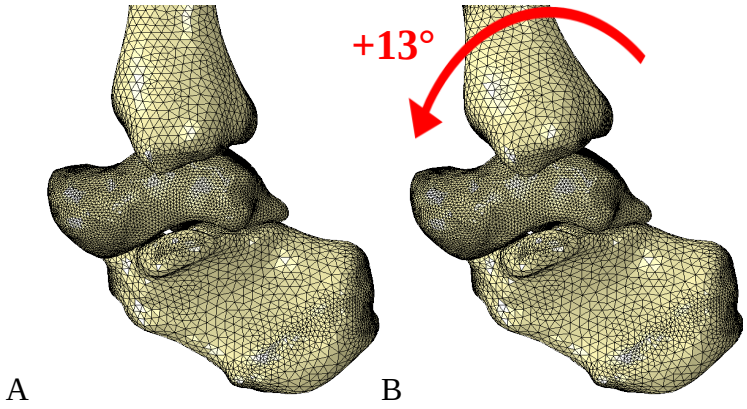

Figure 5.9: Schematic representation of hindfoot in normal configuration A) in dorsiflexion B) conditions as imposed in numerical models.

In the following figures are reported in detail of the numerical results for the hindfoot and in particular for tibia and talo in dorsiflexion condition.

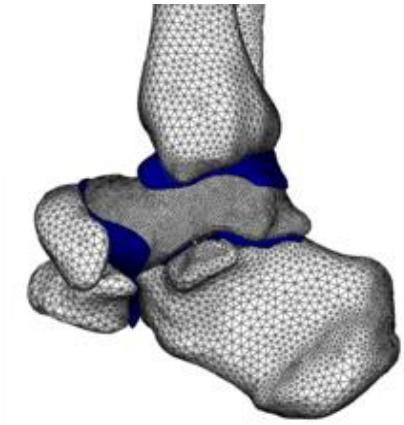

Figure 5.10: Lateral view of hindfoot joints with synovial capsule for strain field numerical results in dorsiflexion.

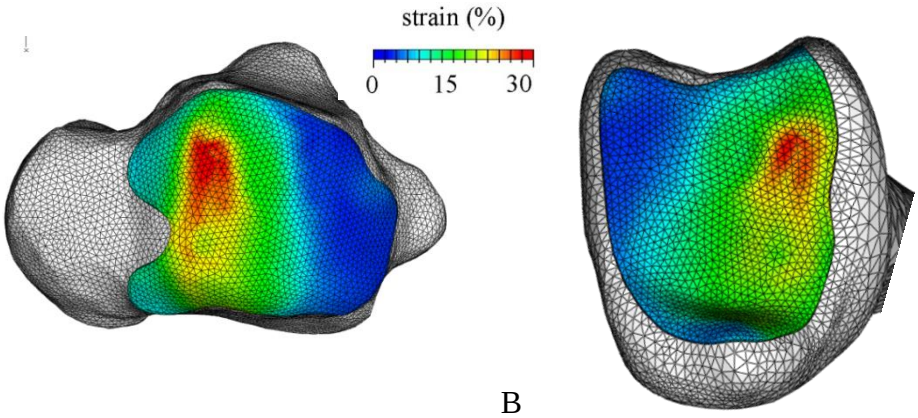

Figure 5.11: Detail of tibio-talar joint strain field numerical results in dorsiflexion: talar articular surface A); tibia articular surface B).

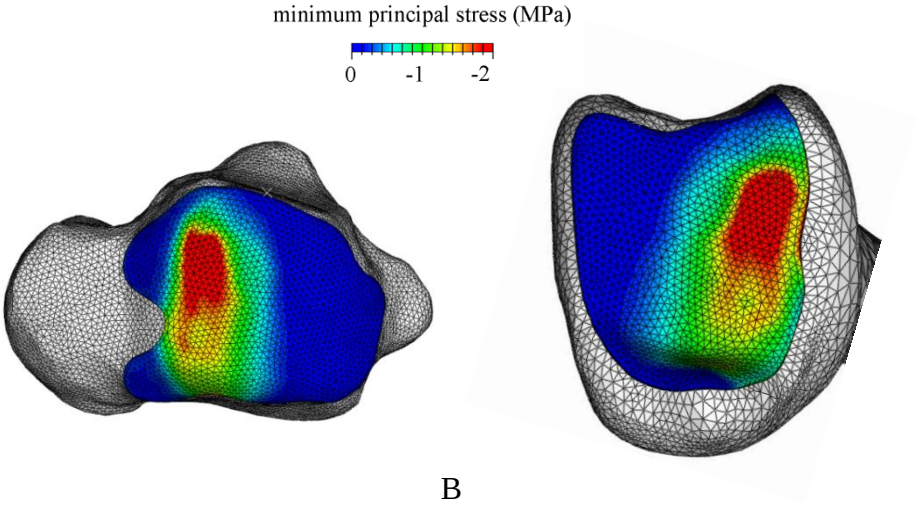

Figure 5.12: Detail of tibio-talar joint with synovial capsule for stress field numerical results for talar articular surface A) and tibia articular surface B).

Comparing the strain and the stress fields obtained in dorsiflexion analysis and in compression (or stance) analysis it is possible to see the change in the fields distribution. Both strain and stress develop more in the anterior area of the articulation.

Here for completeness, are reported the minimum principal stress results for other articular surface that involves the talus and in particular those of talo-navicular joint, talo-fibular joint and talo-calcanear joint.

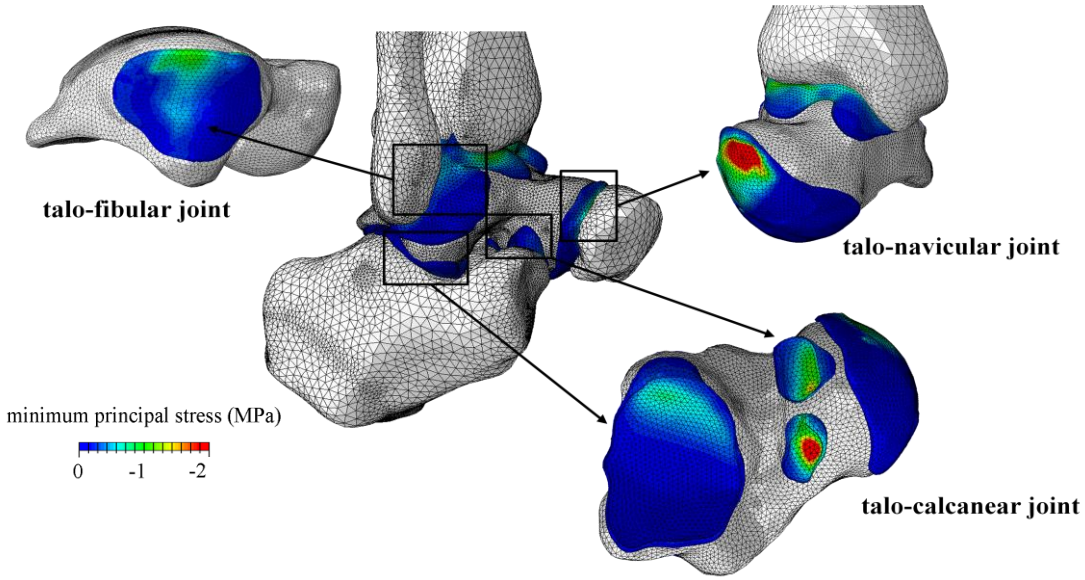

Figure 5.13: Representation of dorsiflexion condition minimum principal stress in other joints of the hindfoot.

The numerical results obtained evidence a concentration of minimum principal stress field in some articulation that are particularly involved in load transmission during the gate cycle, where the dorsiflexion configuration if physiologically present. These results are the starting for further investigation of other configurations that involve in particular the hindfoot, such as plantarflexion or adduction/abduction, but also of the whole foot, such as inversion/eversion or "en-pointe".

5.3 NUMERICAL ANALYSIS OF THE HINDFOOT DEFORMATION CONSIDERING THE OSTEOARTHRITIC CARTILAGE

A healthy joint is able to withstand the large forces associated with weight-bearing and joint motion over the lifetime of an individual. During pathologies such as

osteoarthritis (OA), however, joint degeneration is characterized by cartilage and bony changes that lead to deformities, impaired joint motions, pain, and disability. The goal of many studies of cartilage mechanics over the years has been to determine the relationships between composition, structure (micro and macro), and material properties of healthy articular cartilage and, perhaps more importantly, to determine changes in its material properties associated with degeneration (Mou and Guo 2002).
The numerical results obtained show a concentration of the stress field on tibio-talar joint and talo-navicular joint expecially in dorsiflexion and plantarflexion. These two movements are configuration prsent during the impact and the propulsive phase of gait and running. In fact, runners are often affected by Osteoarthritis on the tibio-talar joint and talo-navicular joint due to overuse or cyclic and intensive loading of articulation for a long period. In the following paragraph the procedure developed for healty cartilage tissue is proposed for OA affected cartilage and some additional consideration will be given with regard to OA.

5.3.1 Numerical analysis results

As previously reported a typical mean compressive stress levels up to 7 MPa may be seen in cartilage during daily activities, with higher stresses experienced in localized regions. In contrast to the above normal ranges of joint forces, stress and strain above the physiological range have the potential to damage the matrix and chondrocytes. Repo and Finlay (1977) have shown that at peak compressive stress levels 25 MPa (nominally 25 % strain) chondrocyte death and cartilage fissuring occur. In a work by Zimmerman et al. (1988) it was found that repetitive compressive stresses of 6.9 MPa (nominal strain rate of 250 %/s) are sufficient to produce accelerated fissuring in plugs of articular cartilage and subshondral bone. Articular damage can lead arthritis and subsequently to deformities of articulation and of the overall foot.
Acute trauma to the joint is known to increase the risk of osteoarthritis (OA) (Devis et al. 1989, Gelber et al. 2000), other mechanical influences that cause abnormal forces, such as joint laxity, obesity, and muscle weakness, are also linked to the progression of OA (Felson et al. 2000)
In vivo studies have shown that impact trauma can cause osteoarthritic changes. Radin et al. impacted patellofemoral joints of rabbits, causing damage to the bone

and cartilage and subsequently leading to OA-like degradation. Even impacts that do not appear to fracture the bone can result in cartilage degradation (Radin et al. 1972).
The subtalar and talonavicular joints are frequently affected by rheumatoid arthritis, leading to a flatfoot deformity as the static restraints are overcome by the forces of gait (Keenan 1990). Lesser tarsal joints may also be affected by RA and this may contribute to flatfoot in some patients.
Post-traumatic OA may affect any of the tarsal joints:

- Subtalar OA mainly after calcaneal fractures, but also ankle/subtalar ligament injuries and peritalar dislocations
- Talonavicular and calcaneocuboid OA mainly after midtarsal subluxations, some of which are quite subtle
- Tarsometatarsal OA mainly after Lisfranc and "subtle Lisfranc" injuries

Primary OA, often as part of generalised OA, is rarely commented on in textbooks, but is seen reasonably frequently in practice, especially in the TMT joints. Osteoarthritis may also occur in association with tarsal coalitions.
Subtalar joint pain is felt mainly in the lateral hindfoot on activity. If there is a valgus hindfoot or synovitis, there may be impingement pain felt mainly on lateral hindfoot deviation. Some patients complain of instability or locking, which may be described as being in the ankle.
Talonavicular pain is felt on the medial, dorsal or occasionally lateral midfoot. Patients often describe it as being in the ankle, and it is important to clarify exactly where "ankle" symptoms are felt. Dorsal osteophytes may present as painful lumps or be misinterpreted as ganglia.
Calcaneocuboid pain is felt on the lateral side of the hindfoot. It may be difficult to distinguish from peroneal tendon pain. Some patients complain of clicking or instability.
In fact according to numerical analysis on healty tissue revealed an higher concentration of loads on the joints of the foot more affected by OA. In the following part numerical analysis developed on the hindfoot with a tissue carachterized as osteoarthritic are reported and compared to numerical analysis on healty tissue.

5.3.1.1 Standing position

First configuration to be studied is the standing position. As previously reported a compressive load of 765 N is considered applied allined to tibia longitudinal axis.

In this pharagraph numerical results obtained for OA cartilage with the OA set of parameters for the fiber-reinforced hyperelastic model are compared with the numerical results obtained for healty cartilage.

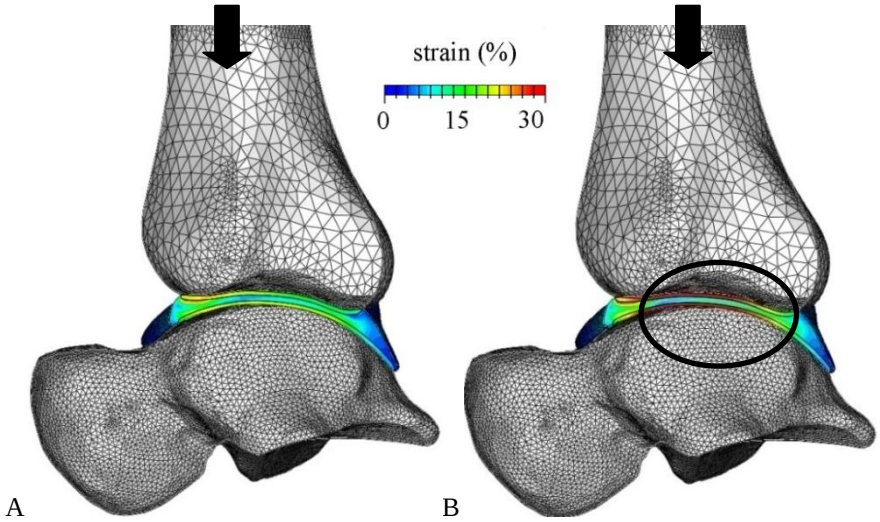

Figure 5.14: Comparison between numerical results of strain % for healty cartilage A); and for OA cartilage B) in a section of tibio-talar joint.

The properties of the synovia are the same, therefore variation on stress and strain fields are present only in cartilage response as can be seen in the section.

More detailed results are reported for talus and tibia. Numerical results of articular surface of talus and tibia evidence a high strain on the overall surface of the joint. This is probably due to the lower capability of articular cartilage affected by OA to link water moleculas with proteoglycans, since their number is reduced and teir structure is compromised and shorter.

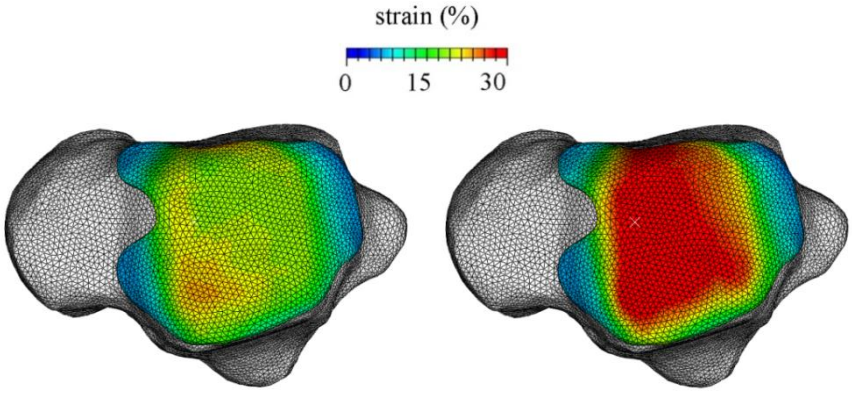

A *B*

Figure 5.15: Comparison between numerical results of strain % for healty talar articular surface A); and for OA cartilage B).

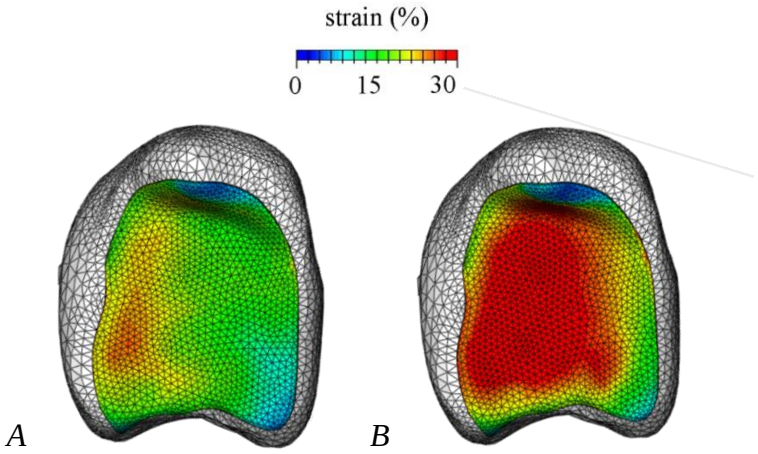

A *B*

Figure 5.16: Comparison between numerical results of strain % for healty tibial articular surface A); and for OA cartilage B).

Stress field evidence the lower capability of OA cartilage to distribute loads as can be seen in the following figure for talar and tibial articular surface.

In particular it is possible to notice that the pathology reduces the capability of the tissue in redistributing loads on the articular surface, therefore the stress field reaches its peak value in a smaller area then in the case of healthy cartilage. This phenomenon can be the cause of overload on cartilage cells components and can lead to their deadh and, as a consequence, to the reduced capability of cartilafge in renewing its structure and its superficial layer, which is the most important for joint mobility. Then this could be the cause of degradation of articular surfaces both in mechanical properties and in smoothness.

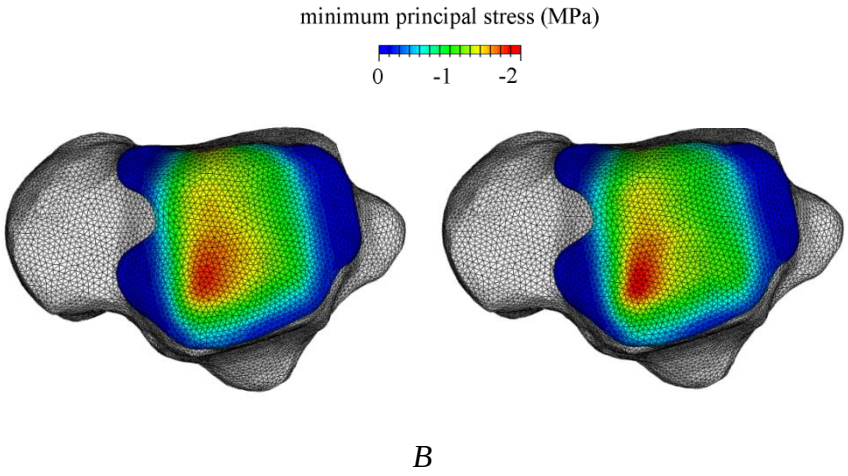

Figure 5.17: Comparison between numerical results of stress (MPa) for healty talar articular surface A); and for OA cartilage B).

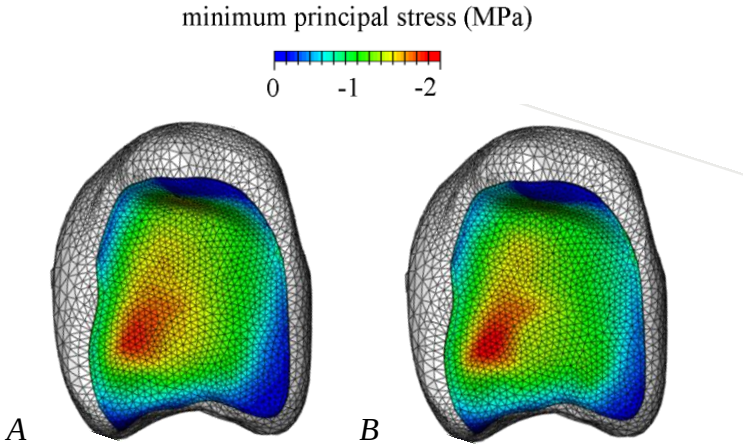

Figure 5.18: Comparison between numerical results of stress (MPa) for healty tibial articular surface A); and for OA cartilage B).

Results are in congruence with what is clinically observed and reported in literature.

Briefly are reported the minimum principal strain results for other articular surfaces that involves the talus and in particular talo-navicular joint, talo-fibular joint and talo-calcanear joint for cartilage carachetized with the fribril-reinforced hyperelastic model and the OA cartilage set of constitutive parameters.

As can be noticed in the following Figure, the articular surface of the talus involved in the sub-talar joint presents a wider area of strain if compared with the one presented for healty cartilage in standing condition. This observation is in congruence with what observed now-on and with what reported in literature.

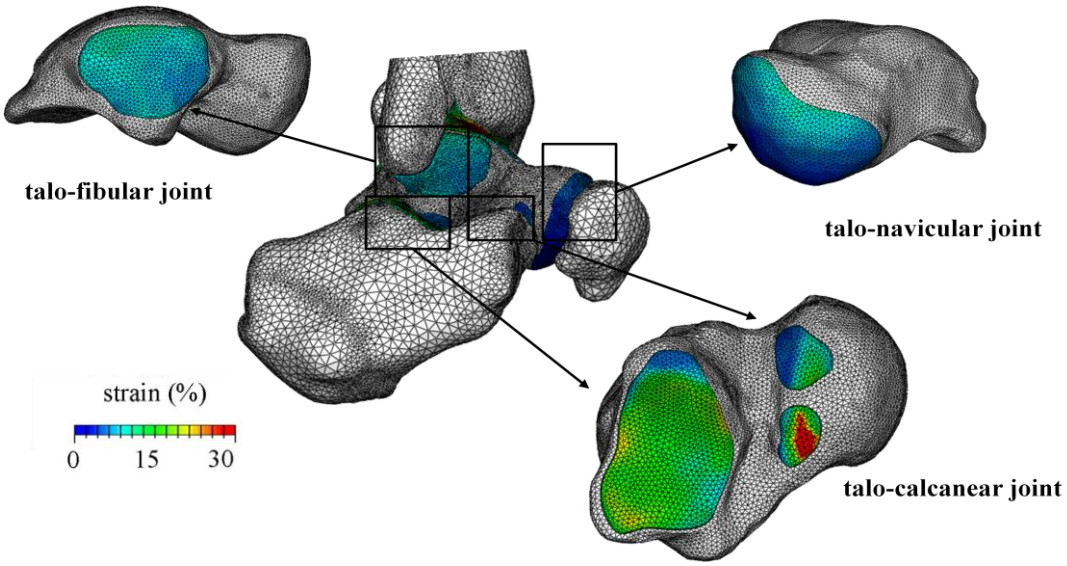

Figure 5.19: Representation of stance condition minimum principal strain in other joints of the hindfoot for OA cartilage.

For the minimum principal stress are reported the other talar articular surfaces involved in talo-navicular join, talo-fibular joint and sub-talar joint.

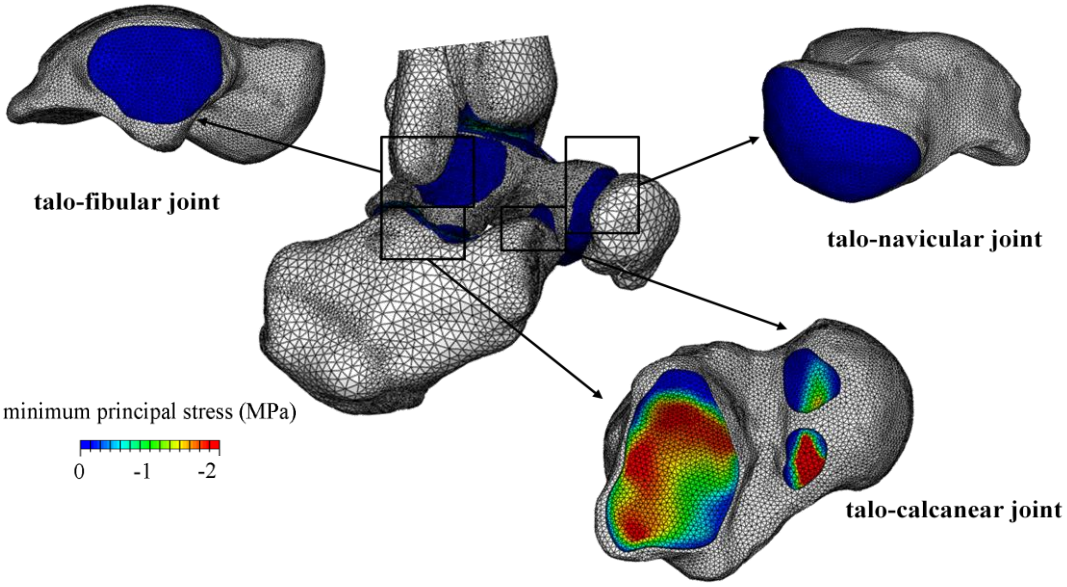

Figure 5.20: Representation of stance condition minimum principal stress in other joints of the hindfoot for OA cartilage.

Since the results proposed are related to stance condition, as expected, the minimum principal stress field results show that tibio-talar joint and the sub-talar joint present higher values.

5.4 REFERENCES

Akizuki S, Mow VC, Muller F, Pita JC, Howell DS, Tensile properties of human knee joint cartilage. II. Correlations between weight bearing and tissue pathology and the kinetics of swelling. J. Orthop. Res. 5:173–86, 1987.

Armstrong CG, Mow VC. 1982. Variations in the intrinsic mechanical properties of human articular cartilage with age, degeneration, and water content. J. Bone Joint Surg. Am. Vol. 64:88–94, 1982.

Davis M. A., Ettinger W. H., Neuhaus J. M., Cho S. A. and Hauck W. W. (1989) The association of knee injury and obesity with unilateral and bilateral osteoarthritis of the knee. Am. J. Epidemiol. 130: 278–288, 1989.

Felson D. T., Lawrence R. C., Dieppe P. A., Hirsch R., Helmick C. G., Jordan J. M. et al. Osteoarthritis: new insights. The disease and its risk factors. Ann. Intern. Med. 133: 635–646, 2000.

Gelber A. C., Hochberg M. C., Mead L. A., Wang N. Y., Wigley F. M. and Klag M. J., Joint injury in young adults and risk for subsequent knee and hip osteoarthritis. Ann. Intern. Med. 133: 321–328, 2000.

Gore, D.M., Higginson G.R., Minns R.J., "Compliance of articular cartilage and its variation through the thickness", Physics in Medicine and Biology, 28, 233-247, 1983.

Guilak F, Ratcliffe A, Lane N, Rosenwasser MP, Mow VC, Mechanical and biochemical changes in the superficial zone of articular cartilage in canine experimental osteoarthritis. J. Orthop. Res.12:474–84, 1994.

Mankin H.J., The response of articular cartilage to mechanical injury. J Bone Joint Surg Am, 64 (3), 460-466, 1982.

Mankin HJ, Mow VC, Buckwalter JA. 2000. Articular cartilage repair and osteoarthritis. In Orthopaedic Basic Science: Biology and Biomechanics of the Musculoskeletal System. ed. JA Buckwalter, TAEinhorn,SRSimon. Rosemont, IL: Am. Acad. Orthop. Surg.

Mow Van C. and Guo X. Edward, Mechano-electrochemical properties of Articular cartilage: their inhomogeneities and anisotropies, Annu. Rev. Biomed. Eng. 4, 175–209, 2002.

Newberry W. N., Garcia J. J., Mackenzie C. D., Decamp C. E. and Haut R. C., Analysis of acute mechanical insult in an animal model of post-traumatic osteoarthrosis. J. Biomech. Eng. 120: 704–709, 1998.

Pearle A.D., Russel F.W., Scott A.R., Basic science of Articular cartilage and Osteoarthritis, Clin Sports Med 24, 1-12, 2005.

Repo, R.U., Finlay, J.B., Survival of articular cartilage after controlled impact. Journal of Bone and Joint Surgery [Am] 59-A, 1068–1076, 1977.

CONCLUSIONS

The aim of this work is to develop a procedure to investigate articular cartilage tissue from a biomechanical point of view and with regard to the functions that it performs. In particular the attention is focused on hindfoot joints for the important function that they cover in human movements such as walking and running.

The study of such complex joints required some steps, that involve different aspects of a biological structure: the investigation of cartilage histology, the analysis of the biomechanical behavior with a subsequent constitutive formulation capable to describe the mechanical response paying attention to histological considerations, the morphological investigation to develop a detailed solid and numerical model of the anatomical site of interest and in particular of hindfoot joints.

The mechanical experimental tests on cartilage disks evidenced an hyperelastic behavior, in addition the peculiar hystological composition and organization showed that in cartilage biomechanics the most important family of fibers is parallel to cartilage surface and radially distributed. These findings lead to the definition of a fiber-reinforced hyperelastic constitutive model. The procedure to identify the set of constitutive parameters consists in the minimization of the discrepancy between experimental data and numerical results. This procedure allow to define a set of parameters that is congruent with cartilage mechanical properties proposed in literature. Moreover, numerical results with that specific set of parameters showed to be in agreement with the *in-vitro* indentation experimental results.

The solid model of the foot and in particular of hindfoot joints, is studied in different physiological configuration: standing and dorsiflexion. The standing configuration for tibio-talar joint is compared with an *in-vivo* test present in literature. The results of numerical model and in particular for the strain field distribution of talar cartilage, showed to be in good congruence with the *in-vivo* experimental results, even if there are discrepancy attributed to intersubject variability. This result confirms the reliability of the procedure for the definition of the set of constitutive parameters and the suitability of the constitutive formulation propsed. It is interesting to notice that the value of minimum principal stress peak obtained are also congruent with what is reported in literature for physiological load on hindfoot joints.

In addition, for what concearn dorsiflexion configuration, the numerical results obtained evidence the transmission of load to the forefoot, in particular through the talo-navicular joint which is considered often affected by osteoarthritis (OA) in runners due to overuse. This lead to the interest in studyng cartilage affected by OA.

The procedure developed for healthy cartilage is the basis for the definition of a specific set of costitutive parameters for OA cartilage. The fiber-reinforced hyperelastic model characterized with the OA parameters is used in the numerical model of the hindfoot to compare the standing configuration for cartilage affected by OA and for healty cartilage. The comparison evideces how OA cartilage has higher level of minimum principal strain and these are spread on a wider area of the articular surface, while stress field reach higher peak in OA cartilage but the area involved is lower. This is in congruence with what is experimentally highlighted in the analisys of patients with foot joints affected by OA and is one of the cause of cartilage surface flaking, possible contact between bones and bone lesions or bone union, these events lead to joint pains, deformations and, in severe OA, immobilization of joints.

This work provides a procedure for the study of complex biological structure with different biological tissues involved. Results here presented for hindfoot joint are the basis for further study of articular joints and in particular for the definition of cartilage as a multilayer tissue with different family of fibers. Moreover the problem of degraded cartilage need additional study in relation to different causes of degeneration and to different foot configurations. In addition the foot solid model presented can be improved with the definition of cartilage layers also for forefoot joints and as a consequence for the study of push-off and toe-off phases of the gait cycle.